

Department of Physics and Astronomy

University of Heidelberg

Master thesis

in Physics

submitted by

Elsa Wilken

born in Hamburg

2018

# **Retrieval Advances of BrO/SO<sub>2</sub> Molar Ratios from NOVAC**

This Master thesis has been carried out by Elsa Wilken  
at the  
Institute for Environmental Physics, University of Heidelberg,  
Germany  
under the supervision of  
Prof. Ulrich Platt

## **Optimierte Bestimmung des Molaren BrO/SO<sub>2</sub> Verhältnisses aus NO-VAC Daten**

Die Messung der absoluten Menge und des Verhältnisses von Vulkanischen gas Emissionen geben Einsicht in magmatische Prozesse. Das Network for Observation of Volcanic and Atmospheric Change (NOVAC) verfügt über ein System an automatisierten UV-Spektrometern, welche die Gas Emissionen der Vulkane aufzeichnen. Der Ausstoß von BrO und SO<sub>2</sub> kann mithilfe von Differenzieller optischer Absorptionsspektroskopie (DOAS) aus den aufgenommenen Spektren bestimmt werden wobei die optische Absorption in der Fahne mit einem Hintergrundspektrum verglichen wird. Dies setzt voraus, dass das Hintergrund Spektrum nicht durch Vulkanische Gase beeinträchtigt ist. Typischerweise wird das Hintergrund Spektrum für einen Scan ein Höhenwinkel gewählt welcher als außerhalb der Fahne liegend identifiziert wird. Es hat sich jedoch gezeigt, dass auch diese Spektren noch durch Vulkanische Emissionen verunreinigt sein können. Als alternative Referenzspektren könnten 1) ein theoretisches Solar Atlas Spektrum oder 2) ein nicht verunreinigtes referenz Spektrum des selben Messgeräts dienen. Option 1) hat den Nachteil einer verringerten Messgenauigkeit, da Instrumenteneffekte hier modelliert werden müssen. Option 2) setzt voraus, dass das Referenzspektrum unter ähnlichen Wetter- und Strahlungsbedingungen aufgenommen wurde. Wir verwenden die erste Methode um Kontaminierung zu identifizieren und greifen für die Bestimmung der Gas Konzentration auf die zweite Methode zurück um eine hohe fit Qualität sicher zu stellen. Stellen unsere Methode für NOVAC Daten von den Vulkanen Tungurahua und Nevado Del Ruiz vor.

### **Retrieval advances of BrO/SO<sub>2</sub> molar ratios from NOVAC:**

Measurements of magnitude and composition of volcanic gas emissions allow insights in magmatic processes. Within the Network for Observation of Volcanic and Atmospheric Change(NOVAC) automatically scanning UV-spectrometers are monitoring gas emission at volcanoes. The emissions of BrO and SO<sub>2</sub> can be retrieved from the recorded spectra by applying Differential Optical Absorption Spectroscopy(DOAS) and comparing the optical absorption of the volcanic plume to the background. Therefore, the background spectrum must not be affected by volcanic influence. Classically, the background spectrum is taken from the same scan but from an elevation angle which has been identified to be outside of the volcanic plume. However, experience shows those background spectra can still be contaminated by volcanic gases. Alternatively reference spectra can be derived from 1) a theoretical solar atlas spectrum or 2) a volcanic-gas-free reference spectrum recorded by the same instrument. 1) comes with a drawback of reduced precision, as the instrumental effects have to be modeled and added to the retrieval. For 2), the alternative reference spectrum should be recorded at similar conditions with respect to meteorology and radiation. We use the first option to check for contamination and the second to evaluate the spectra to maintain a god fit quality. We present our approach and its results when applied on NOVAC data from Tungurahua and Nevado Del Ruiz.

# Contents

<b>1</b>	<b>Introduction</b>	<b>6</b>
<b>I</b>	<b>Theoretical background</b>	<b>9</b>
<b>2</b>	<b>Volcanism and volcanic chemistry</b>	<b>10</b>
2.1	Volcanism . . . . .	10
2.2	Volcanic gases and their impact on the climate . . . . .	10
2.3	Volcanic degassing . . . . .	12
2.4	Volcanic plume chemistry . . . . .	12
2.4.1	Sulphur species . . . . .	12
2.4.2	Bromine oxide . . . . .	13
2.5	Using the BrO/SO <sub>2</sub> ratio to study volcanic activity . . . . .	15
<b>3</b>	<b>Remote sensing of volcanic gases</b>	<b>20</b>
3.1	Differential Optical Absorption Spectroscopy (DOAS) . . . . .	22
3.1.1	Technical implementation of the DOAS approach . . . . .	23
<b>II</b>	<b>Evaluation of the data of Tungurahua and Nevado Del Ruiz</b>	<b>26</b>
<b>4</b>	<b>Network for Observation of Volcanic and Atmospheric Change</b>	<b>27</b>
4.1	Measurement routine . . . . .	29
<b>5</b>	<b>Evaluation routine</b>	<b>31</b>
5.1	Conventional evaluation routine . . . . .	31
5.2	Contamination problem . . . . .	34
<b>6</b>	<b>BrO Evaluation and its limitations</b>	<b>39</b>
6.1	BrO error dependence on external parameters . . . . .	39
6.1.1	Temporal difference . . . . .	40
6.1.2	Temperature . . . . .	45
6.1.3	Daytime . . . . .	47
6.1.4	Colorindex . . . . .	49
6.1.5	Elevation Angle . . . . .	51
6.1.6	Exposure Time . . . . .	55

6.2	BrO dependence on external parameters . . . . .	59
<b>7</b>	<b>Contamination based method</b>	<b>65</b>
7.1	Fit data . . . . .	66
7.2	Other approaches . . . . .	69
7.2.1	Nearest neighbor approach . . . . .	69
7.2.2	Iterative approach . . . . .	71
<b>8</b>	<b>Comparison with NOVAC evaluation</b>	<b>72</b>
8.1	Tungurahua . . . . .	74
8.2	Nevado Del Ruiz . . . . .	75
8.3	BrO/SO <sub>2</sub> time series . . . . .	75
<b>9</b>	<b>Issues of our method</b>	<b>80</b>
9.1	Contamination of the plume . . . . .	80
<b>10</b>	<b>Conclusion</b>	<b>82</b>
<b>III</b>	<b>Appendix</b>	<b>83</b>
<b>A</b>	<b>Lists</b>	<b>87</b>
A.1	List of Figures . . . . .	87
A.2	List of Tables . . . . .	91
<b>B</b>	<b>Bibliography</b>	<b>93</b>

# 1 Introduction

Volcanic activities on Earth have always shaped the earth surface and influenced atmospheric processes. Volcanoes are often particularly recognized by their dramatic consequences of a major volcanic eruption. But volcanoes influence our lives in more than this way. Volcanic gases can effect the weather (timescales of days to weeks) or the climate (timescales of months to years) Schmidt and Robock (2015). Examples are the lake eruption in Iceland (1783-1784) followed by a very hot summer and a cold winter in central Europa Thordarson and Self (2003) and the Tambora eruption, indonesia in 1815 which caused the "year without summer" in 1816.

Considering the plate tectonics of earth most volcanoes are caused by diverging or converging of the continental plates and therefore located at the margins of the continental plates. Another possibility for occurrence of volcanoes is the the interior of continental or oceanic shelves. Schmincke (2000)

The most abundant volatile species released during a volcanic eruption are water vapour ( $H_2O$ ; relative amount of the plume: 50%-90%) and carbon dioxide ( $CO_2$ ; relative amount of the plume: 1%-40%) Platt and Bobrowski (2015). But the short effects of those two gases are rather low since there effect on atmospheric composition is negligibly due to the high abundance of atmospheric  $H_2O$  and  $CO_2$ . But on timescales of the age of the earth the volcanic emission of  $H_2O$  and  $CO_2$  are the source of our current atmosphere. Schmidt et al. (2015)

A typically volcanic plume consists of many different gases alongside  $H_2O$  and  $CO_2$  sulfur dioxide ( $SO_2$ ) contributes with 1%-25% to the plume, hydrogen sulfide ( $H_2S$ ) with 1%-10% and hydrogen chloride with ( $HCl$ ) 1%-10%. Furthermore there are trace gases for example carbon disulfide ( $CS_2$ ), carbon sulfide ( $COS$ ) carbon monoxide ( $CO$ ) hydrogen fluoride ( $HF$ ) and hydrogen bromide ( $HBr$ ) Platt and Bobrowski (2015)

A decrease of stratospheric ozone ( $O_3$ ) has been observed after the eruption of El Chickon in 1982 and the eruption of mount Pinatubo 1991. A depletion stratospheric  $O_3$  results in ozone holes. The depletion comes from volcanic aerosols which serve anthropogenic chlorine/bromine into more reactive forms Solomon et al. (1998). Volcanic gases can alter the radiative balance of the earth in timescales relevant for climate change due to scatter and absorption of solar radiation Schmidt et al. (2015).

The gas composition of the volcano plume change with activity and could be a indication for the processes inside the earth.

In this work we are particularly interested in the ratio of  $BrO$  and  $SO_2$ . The halogen sulfur ratio is a proxy for volcanic processes. Therefore we make the assumption

that the ratio of BrO and SO<sub>2</sub> contains informations about its degassing source depth. A change in BrO/SO<sub>2</sub> prior to eruption was observed at Etna and Nevado del Ruiz.

To gain further knowledge about the volcanoes the Network for Observation of Volcanic and Atmospheric Change (NOVAC) was installed. NOVAC is a Network of DOAS Instruments located next to about 30 volcanoes in America, Africa and Europe. At every Volcano there are two to four DOAS Instruments installed, recording record back-scattered solar radiation spectra at different viewing angles.

NOVAC is a network which produces a large amount of data and we have the chance to evaluate long time periods which is a unique opportunity to study correlations of the trace gases.

Since the conditions at volcanoes are rough, the instruments need to be rather simple to keep the maintenance cheap and to assure a longer lifetime of the instruments. So we need to waive on temperature stabilization even at the expense of the quality of the data.

One possibility to measure the volcanic trace gases is to use Differential Optical Absorption Spectroscopy [Platt and Stutz \(2008\)](#). DOAS exploit the wavelength dependency of the absorption of light. Here the gas emissions can be retrieved from the quotient of the absorption signal of the volcanic plume and a reference region. This will be explained in a further chapter.

The reference region, is usually treated as free of volcanic trace gases. If the reference region is for any reason contaminated by volcanic trace gases, the reference spectrum has to be replaced by a volcanic-gas-free reference. Alternative spectra could be for example a theoretical solar atlas spectrum or a volcanic-gas-free reference spectrum recorded in the temporal proximity(eg. a day before) by the same instrument. The first option comes with the drawback of reduced precision, as the instrumental effects have to be modeled and added to the retrieval. The reduction in precision is acceptable for the SO<sub>2</sub> retrieval, but not suitable for a BrO retrieval because then most data would be below the detection limit. For the second option, the alternative reference spectrum should have been recorded at similar conditions with respect to meteorology and radiation as well as in the temporal proximity due to instrumental changes with time and ambient conditions. We combined both options in order to achieve both, enhanced accuracy but still maximum possible precision of the SO<sub>2</sub> and BrO retrievals. We present an algorithm which finds the optimal reference spectrum automatically. As first step, a possible SO<sub>2</sub> contamination of the standard reference is checked by a comparison with the theoretical solar atlas. If a contamination is detected, as second step, the algorithm picks a volcanic-gas-free reference (beforehand automatically checked for contamination) from another scan.

In this work we are mainly dealing with data from Tungurahua in Ecuador in the timespan of 01.08.2008 to 30.07.2009. Later on, we will also show the results of

Nevado del Ruiz a volcano located in Colombia.

# Part I

## Theoretical background

## 2 Volcanism and volcanic chemistry

### 2.1 Volcanism

The high thermal energy in the deep interior of the earth is mostly well separated from the earth's surface by the earth's crust. A volcano is geological structure that allows magma to reach the earth's surface. Such a phenomenon can occur in various ways. In the following paragraphs the different types of volcanoes are described.

**Mid-ocean ridge volcanism** The mid-ocean ridge volcanism can be traced back to tectonic processes of oceanic plates. The spreading of two plates, that are pulled apart, leads to a thinning of the oceanic earth crust. This way solid material from the upper mantel (lower than 100 km) can ascend to depths of approximately 50 km. As the pressure at this depth is much lower, the mantle material starts to melt to basaltic magma that fills the gap between the two plates.

**Continental rift zone volcanism** Similar to mid-ocean ridge volcanism continental rift zone volcanism results from two continental plate are pulled apart.

**Subduction zone volcanoes** Subduction zone volcanoes occur if an oceanic plate converges under another plate (oceanic or continental). This way the descending plate penetrate into the lower mantle. At a depth of 80-150 km the water of this plate evaporates and rises and causes the mantle material above to melt. The resulting water-rich magma mainly consists of andesite. Subduction zone volcanoes are known for their violent eruptions caused by the low viscosity magma.

**Hot-spot volcanoes** Hot-spot volcanoes occur on continental or oceanic plates. This type of volcanoes arises from a hot spot at the coremantle boundary inside Earth that leads to a plume in the mantle where solid material can rise. This material melts to basaltic magma at a depth of 100-150 km. Through a futher rise also other types of magma (e.g. rhyolitic, more-viscous magma) can arise.

### 2.2 Volcanic gases and their impact on the climate

Volcanoes emit various gases (see table 2.1) in the atmosphere. This can occur due to volcanic eruptions or due quiet degassing. Gas emitted by quiet degassing remains in the troposphere while eruptions can inject volcanic gases up to the stratosphere Robock (2000). The larger lifetime in the stratosphere and a larger sensitivity of



Figure 2.1: Influence of volcanic eruptions and quiet degassing on earth climate.  
Redrawn on the basis of [Robock \(2000\)](#)

the stratospheric chemistry to volcanic gases leads to an higher impact on the earth climate of these gases. Volcanic gases have a large influence on the earth climate especially CO<sub>2</sub> and SO<sub>2</sub> or more specific its oxidation product sulfur acid. The relevance of CO<sub>2</sub> for the climate is a subject of many discussions about the climate change compared to CO<sub>2</sub> in the atmosphere, the share of volcanic CO<sub>2</sub> is rather low.

Even though the SO<sub>2</sub> emissions during eruptive episodes are up to one order higher than during quite degassing episodes, Halmer et al. (2002) estimated that quiescent degassing contributes 40% of the accumulated SO<sub>2</sub> between 1972 to 2000.

Halmer et al. (2002) estimated the mean annual SO<sub>2</sub> emitted from volcanoes from 1972 to 200 as 7.5 to 10.5TgSyr<sup>-1</sup>, while the anthropogenic SO<sub>2</sub> amount for 2000 is estimated as 55TgSyr<sup>-1</sup> (IPCC, 2013). Despite the less SO<sub>2</sub> occurring from volcanoes the impact may be higher as the impact of the anthropogenic SO<sub>2</sub>. Graf et al. (1997) supposed that the volcanic SO<sub>2</sub> has a higher impact on the climate since it reaches up to the stratosphere while the anthropogenic SO<sub>2</sub> is mostly located in planetary boundary layer. In the lower troposphere sulphuric acid has a lifetime of about a week whereas the lifetime in the stratosphere is about a year (IPCC, 2013). Sulphuric acid in the atmosphere increases the earth albedo due to direct backscattering radiation. Additional the condensation on sulphuric acid particles leads to finer droplets thus to more stable and more white clouds this increases the albedo as

well (Twomey, 1974). volcanic particles can be surfaces for heterogeneous reaction. The result is a depletion of stratospheric Ozone, and thus a more high energetic solar flux on the earth surface. Large particles may backscatter IR radiation from the earth surface and the lower atmosphere, leading to a small reduction of the net cooling of the lower troposphere. In the upper troposphere or stratosphere absorption of IR or UV radiation results in a net heating in the stratosphere and a cooling at the earth surface. Figure 2.1 shows the above described effects and their localization in the atmosphere. The dominating radiative effect of volcanic gases is a cooling of the earth atmosphere due to more backscattered radiation, more diffusive scattering(Robock, 2000). IPCC (2013) records a volcanic radiative forcing of  $-0.11Wm^{-1}$  between 2008 and 2011. For comparison the radiative of CO<sub>2</sub> is estimated as  $1.68Wm^{-1}$ .

## 2.3 Volcanic degassing

## 2.4 Volcanic plume chemistry

Volcanoes are emitter of many gases and aerosols particles, which are rising and forming the volcanic plume. The Temperature where the gases and aerosols are emitted is approximately 500°C Gerlach (2004). Due to the high temperatures the gas raises, cools down and mix up with ambient air. This process leads to many chemical reactions. The large amount of aerosols catalyses heterogeneous reactions. The volcanic gases are listed in Table 2.1.

In the following the chemical reactions of the plume constituents BrO and SO<sub>2</sub> will be discussed. This are the gases observed in this thesis.

Species	H <sub>2</sub> O	CO <sub>2</sub>	SO <sub>2</sub>	H <sub>2</sub> S	COS	SC <sub>2</sub>	HCl	HBr	HF
% / vol	50	1	1	1	$10^{-4}$	$10^{-4}$	1		
	-	-	-	-	-	-	-	?	<
	90	40	25	10	$10^{-2}$	$10^{-2}$	10		$10^{-3}$
Tg / year	?	75		1.5	1	0.005	0.007	0.4	0.0078
				50	2.8	0.1	0.096	11	0.1
									6

Table 2.1: Volcanic gas constituents at the emission vent and global estimated source strength. Adapted from Textor et al. (2004)

### 2.4.1 Sulphur species

Sulphur species are the third most abundant gases in volcanic plumes, hereby contributes SO<sub>2</sub> with about 25% and H<sub>2</sub>S with 1 to 10%. Only H<sub>2</sub>O and CO<sub>2</sub> have a

larger share on the volcanic gases in the plume Table 2.1.

Outside of the volcanic plume the SO<sub>2</sub> amount is with approximately 1ppb negligible, in contrast the SO<sub>2</sub> amount inside the plume can easily reach 1ppm ? When H<sub>2</sub>S escapes from the volcano vent, it enters the oxidizing conditions in the atmosphere. The conversion of H<sub>2</sub>S into SO<sub>2</sub> starts with:



The SH radical goes through a series of reactions, leading to the SO<sub>2</sub> formation ? SO<sub>2</sub> is removed from the atmosphere by dry or wet deposition. At homogeneous reactions the lifetime is from 1-3 weeks Robock (2000). Heterogeneous reactions such as take place on particles or liquid phases leads to much faster depletions. But this was yet not observed by volcanic plume measurements.

Further discussions of the stability of SO<sub>2</sub> in the atmosphere can be found at Lübcke (2014).

However SO<sub>2</sub> can be seen as stable several ours after the release of the volcanic vent. The long lifetime alongside of the negligible amount of SO<sub>2</sub> in the atmospheric background makes SO<sub>2</sub> a good tracer of the volcanic plume. Therefore relatively to other trace gases SO<sub>2</sub> may be used to examine their evolution independent of the plume dispersion.

One attempt to use SO<sub>2</sub> to examine other trace gases was made by Bobrowski et al. (2007). They found a higher BrO/SO<sub>2</sub> ratio at the edges of volcano plumes (Mt. Etna on Sicily, Italy, in August–October 2004 and May 2005 and Villarica in Chile in November 2004) and concluded that the BrO amount is higher at the edges due to the insufficient mixing with ozone rich air inside of the plume (see 2.2).

In this thesis it is supposed that SO<sub>2</sub> is stable on time-scales occurring with ground based remote sensing measuring of about 20 minutes.

## 2.4.2 Bromine oxide

The amount of Bromine in volcanic plumes is rather low compared to SO<sub>2</sub>. The first time Bromine monoxid (BrO) was observed at a volcano was 2013 at the soufrière hills by Bobrowski et al. (2003). Since then many others were able to detect BrO using ground based remote sensing measurement techniques (DOAS: see Section 3.1) for example: Bobrowski and Platt (2007), Bobrowski et al. (2007), Vogel (2011) and Lübcke et al. (2014)

The main Bromine formation which is released from the volcano is HBr. BrO is formed due to mixing with the ozone rich atmosphere at ambient temperatures Bobrowski et al. (2007).

Due to the raising of hot air in the volcano vent , ambient air is pulled into the vent. There temperatures of 600°C to 1200°C prevent the formation of BrO. Only Br is formed. BrO occur after further cooling and mixing while rising. When the temperature cooles down to ambient conditions the so called "Bromine Explosion"

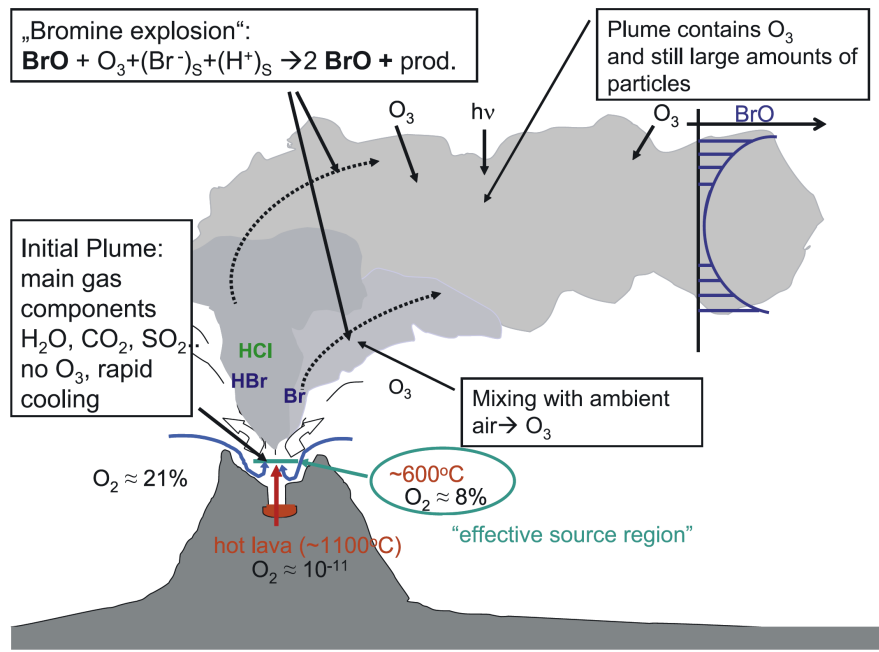
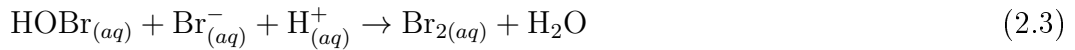


Figure 2.2: schematic sketch of a Bromine Explosion. Release of HBr at the volcanic vent. Mixing with ambient air in the effective source region leads to Br formation. This resulting Bromine species react to BrO with ozone from the plume. Adapted from Bobrowski et al. (2007)

causes a non linear formation of BrO. The "Bromine Explosion" is illustrated in Figure 2.4 and can be described with the following reaction cycle:



The gaseous HBr emitted by the volcano is split heterogeneously into  $\text{H}^+$  and  $\text{Br}^-$  (eq. (2.1)). Inside of an aerosol it forms with HOBr  $\text{Br}_2$  and  $\text{H}_2\text{O}$  (eq. (2.3)).  $\text{Br}_2$  evaporates to the gaseous phase and splits photolytically into 2Br. Including an ozone molecule ( $\text{O}_3$ ) the two Br react to 2BrO. The last step of the circle visualized in Figure 2.4 with blue lines is the reaction of a BrO with  $\text{H}_2\text{O}$  to an HOBr molecule condensing into the liquid phase and thus closing the circle. The non linear explosion occurs due to the formation of two BrO particles from one HBr from



Figure 2.3: BrO/So<sub>2</sub> ratio as a function of the distance from the volcanic vent with a constant wind speed of 10 m/s. From Lübcke (2014)

the volcano.

The BrO formation is slightly diminished due to self reaction of BrO molecules marked with the red lines in fig. 2.4. The 2BrO react with themselves and form Br<sub>2</sub> or may split photolytically into 2Br.

The BrO concentration reaches a maximum approximately 5 minutes after emission and then remains constant for the next 25 minutes Lübcke et al. (2014).

## 2.5 Using the BrO/So<sub>2</sub> ratio to study volcanic activity

Volcanic degassing is influenced by many factors, which can be exploited to study volcanic activity by using the gas composition of the volcano plume. Therefore remote sensing should be an additional tool for forecasting of volcanic activity next to classical monitoring techniques like seismographic and deformation measurements. Inside of volcanoes volatiles are in solution in magmatic melt. The Henry law Equation (2.10) describes the necessary conditions for gas formation:

$$P = K_H \cdot c \quad (2.10)$$

Here P is the partial pressure at equilibrium of the solute, c is the concentration and  $K_H$  is the Henry constant which is anti proportional to the solubility  $\alpha$  ( $\alpha = \frac{1}{K_H}$ ). If the partial pressure of the gas solute (in this case a magmatic gas constituent) exceeds the pressure of the surrounding solvent, a formation of gaseous bubbles occur. Otherwise, if the partial pressure of the gas in the solution is below the surrounding

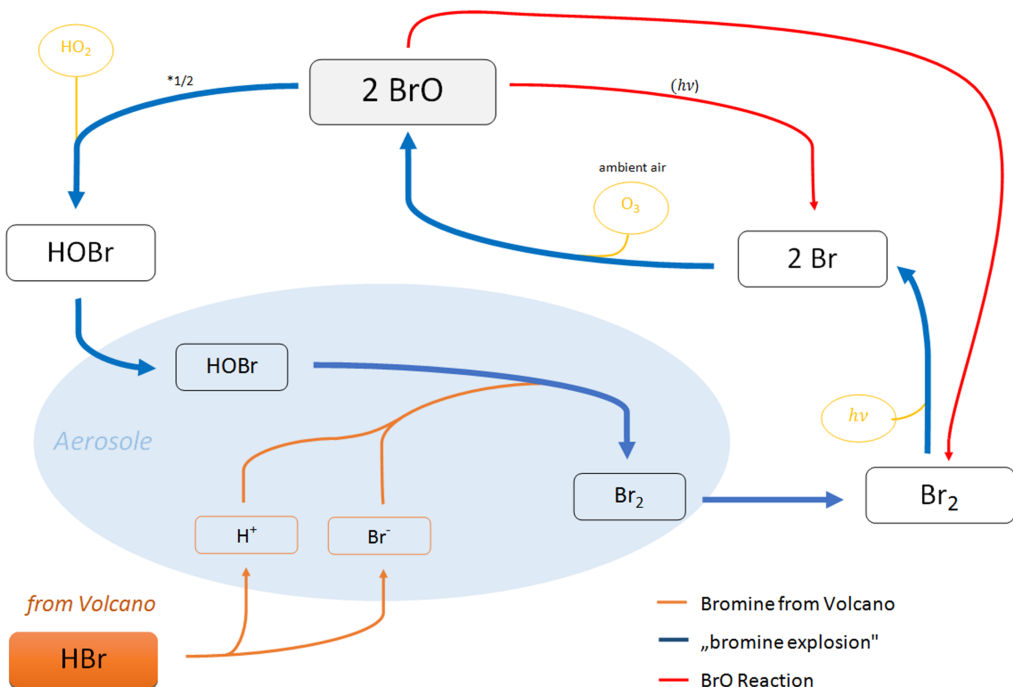


Figure 2.4: Bromine reactions inside of a volcanic vent. The release of HBr at the volcanic vent is drawn in orange. Inside of aerosols heterogeneous dissociation with HOBr forms Br<sub>2</sub>. Then Br<sub>2</sub> splits photolytically into single Br radicals. BrO results through a reaction with O<sub>3</sub> upon mixing with ambient air. Reactions with H<sub>2</sub>O forms HOBr creating an autocatalytic cycle. The reaction cycle along the blue lines are called Bromine explosion. From Warnach (2015)

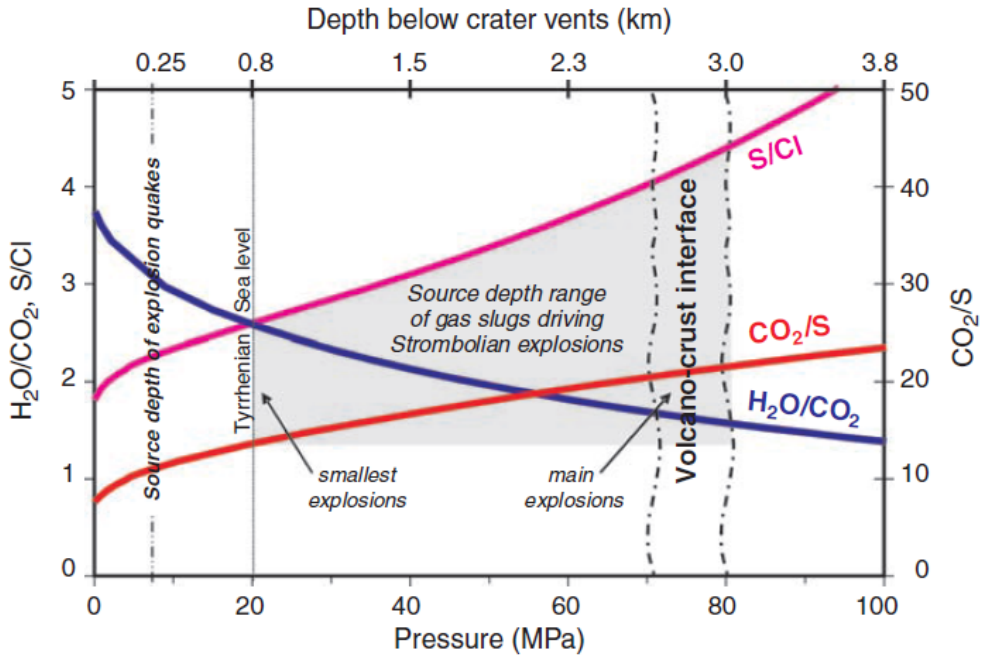


Figure 2.5: Dependency of the ratios of different volcanic trace gases on depth. Data originate from Stromboli volcano. From Lübcke (2014) reproduced from Burton et al. (2007)

pressure the formation of gas bubbles stops.

The solubility  $\alpha$  depends on the temperature, the chemical composition and on the solvent (here magma). Whereas the partial pressure of the constituent depends on the surrounding pressure. The pressure below the volcanic vent increases with depth, this leads to a correlation between the partial pressure of the constituents and the depth. The result is, that the gas starts exsolving at a certain depth depending on the partial pressure of the constituent. Thus the gas bubble formation increases with rising magma. But at a certain depth the percentage of solved gas is different for each volcanic gas. The result is, that the composition of the gases changes with depth. So gas ratios contain information about its originating source depth.

Prior to volcanic eruptions the magma starts raising since the gas is mostly less dense than the magma, it raises faster and could be therefore a indicator for its origin source depth thus a indicator for the volcanic activity.

Figure 2.5 shows the ratios of  $H_2O / CO_2, S/CL$ ,  $CO_2/S$  as a function of the pressure respectively on the depth. Noguchi and Kamiya (1963) found decrease  $Cl/S$  prior to eruptive periods Pennisi and Le Cloarec (1998) observed lower  $CL/S$  ratio during eruptive periods than not eruptive periods at Mt. Etna. Burton et al. (2007) found  $CO_2/SO_2$  and  $SO_2/hCl$  ratios 3-5 times higher during explosions compared to quiet degassing episodes. the authors compared these data to gas formation simulations for different degassing source depth they concluded that these eruptions were driven

by gas slugs from deeper levels where the ratios were higher while quiet degassing originates from shallow magma

Especially halogen-sulfur ratios are interesting as possible tracer for the volcanic activity since the ambient air concentrations are negligible BrO/SO<sub>2</sub> curves equivalent as in Figure 2.5 are yet not available due to lack of bromine solubility curve but the following observations were made: Changes of BrO/SO<sub>2</sub> were found by Bobrowski and Giuffrida (2006): multiple eruptions between 2006 and 2009 highest ratios 2-3 month before the eruptions the ratio then decreased and was lowest during eruptive phase. Therefore it could be concluded that bromine exsolves earlier, at lower depth than sulphur. Lübcke et al. (2014) found decrease of BrO 5 month prior to the eruption 2012 at Nevado Del Ruiz can also be attributed to an earlier exsolution of bromine during rising magma. Despite the lack of the solubility curve of BrO until now, the BrO/SO<sub>2</sub> has a great potential for investigations of the volcanic activity. The first reason is, that both gases can be measured with remote sensing by DOAS instruments. For examples ground based measurements by Bobrowski et al. (2007), Lübcke (2014) or satellite based measurement by ? or ?. The advantage of remote sensing techniques is the possibility of measuring during eruptions which is with in situ measurements not always possible. Secondly due to the NOVAC network (See 4) continues measurements are possible.

Another reason for the research on BrO/SO<sub>2</sub> ratios at volcanoes is the constance of the ratio from 5 to at least 30 minutes after release (Bobrowski et al., 2007);(Lübcke, 2014). As well as the constance from 5 to 20 km off the volcano see 2.3. This ensures that the data measured from different positions or at different conditions are comparable.

This chapter motivated the research on the BrO/SO<sub>2</sub> ratio as a tracer for volcanic activity.

## Tungurahua

Tungurahua is a steep-sided andesitic-dacitic subduction zone volcano located in the Ecuadorian Andes (Lat: 1.467°S; Long: 78.442°W). 2014 Tungurahua was one of the most active volcanoes in southern America, since then the activity was decreasing. Tungurahua is 5023m high and is one of the defining volcanoes of the eastern volcanic rows in Ecuador (Hall et al., 1999).

The modern volcano was formed by a sequentially construction of three major edifices on a basement of metamorphic rocks. It has a total diameter of 12 km. Tungurahua I was roughly located at the same place as today and was built up in the mid-Pleistocene, mainly by andesitic and dacitic lava flows as well as interbedded tephra. Tungurahua II was formed in the past 14,000 years as a result of the collapse of the initial edifice.

3000 years ago the Tungurahua II edifice collapsed. The collapse of Tungurahua II produced a large debris-avalanche deposit and a horseshoe-shaped caldera which is open to the west side. Tungurahua III the current glacier capped stratovolcano was

constructed in this caldera ([Glo](#)).

The current ongoing long term eruption started in October 1999. The eruptive phase was preceded by hydrothermal tremors between 1994 and 1997 (?). From September 1998 to July 1999 an increase of seismic activity like volcano tectonic earthquakes indicates the raising of magma. This eruptive phase is characterized by alternating periods of high and low volcanic activity.

At Tungurahua three instruments with data recorded in the time span from July in 2008 to August in 2009 are used in this thesis.

## Nevado Del Ruiz

Nevado Del Ruiz is a glacier-covered, subduction zone volcano which is located in the Central Cordillera of Colombia, 140 km west of Bogota (Lat: 4.892°N; Long:75.324°W). Nevado De Ruiz has a height of 5389 m and covers an area of more than 200 km<sup>2</sup>. Three major edifices have been constructed since the beginning of the Pleistocene, consisting of andesitic and dacitic lavas and pyroclastics ([Glo](#)). The current cone is built within the caldera of older edifice and consists of a cluster of lava domes. The crater on the summit the name is Arenas crater, with a diameter of 1 km and a depth of 240 m. The last big eruption was in 1985. This was South America's deadliest eruption.

In this thesis the data of two NOVAC Instruments in the time from the end of 2009 to the end of 2011 are used.

### 3 Remote sensing of volcanic gases

In this thesis we are interested in the volcanic trace gases SO<sub>2</sub> and BrO, both measured with the Differential Optical Absorption Spectroscopy (DOAS) a remote sensing technique proposed by [Platt and Stutz \(2008\)](#)

#### Beer-Lambert Law

The Lambert-Beer law describes the attenuation of light when traveling through a material.

This section will give an overview about the reasons for decreasing light intensity when going through a medium.

The Lambert-Beer law describes the attenuation of light when traveling through a material.

, Atoms and Molecules exists in several energy states, depending on the different electron configuration. Moreover Molecules have additionally rotation and vibration states, also enclose to the energy states. If a photon matches the energy gap between two possible energy states, this includes, that the lower energy state is occupied and the selection rules are fulfilled the molecule could absorb the photon, remaining in a higher energy state.

The additional photon energy could be loosed by collision with another molecule or by emission. But since the direction of the emitted photon is mostly not the same direction of the absorbed photon the intensity I<sub>0</sub> of the light before passing the medium is higher than the intensity I after traveling the distance L through the medium.

This can be described as:

$$I(L, \lambda) = I_0(\lambda) \cdot \text{expt} \left( - \int_0^L \sigma(\lambda, p, T) \cdot c(l) dl \right) \quad (3.1)$$

where  $c(l)$  is the location-dependent concentration of the trace gas of interest.  $\sigma(\lambda, p, T)$  is the absorption cross section,  $\sigma(\lambda, p, T)$  is unique for each molecule and depends on pressure p and on the temperature T.

An important quantity used in many optical remote sensing techniques is the optical density  $\tau$ . The optical density is a measure for the weakening of radiation when going through a material.  $\tau$  can be calculated using the lambert beer law:

$$\tau = -\ln \left( \frac{I(\lambda)}{I_0(\lambda)} \right) = \sigma \cdot S \quad (3.2)$$

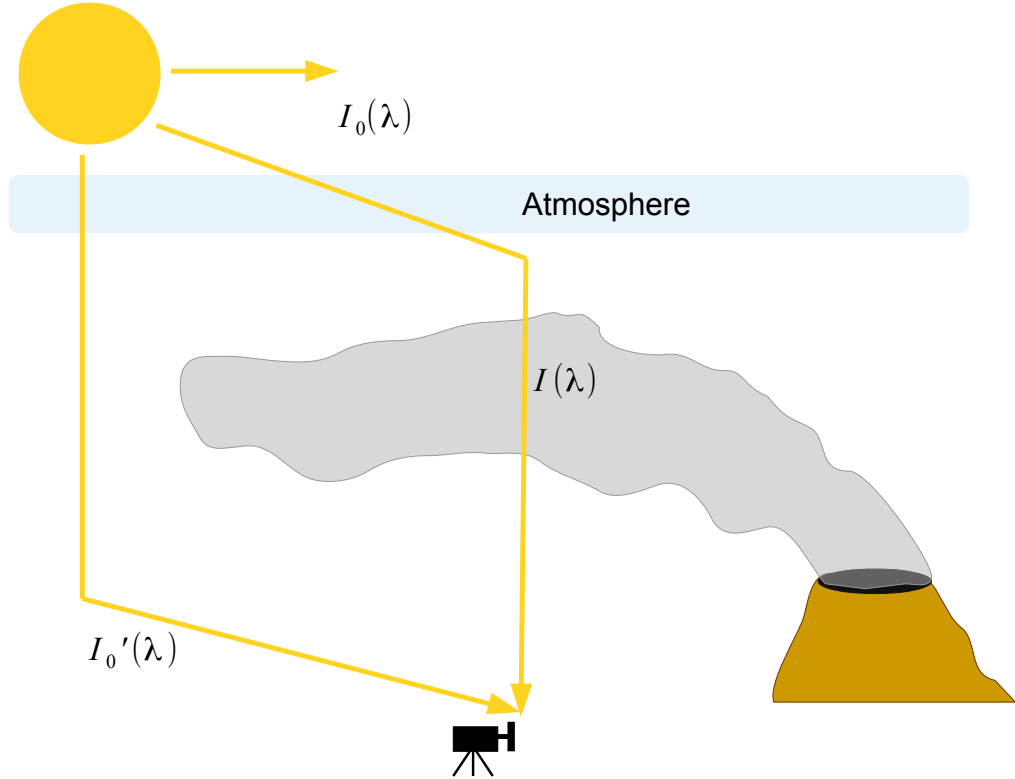


Figure 3.1:

Hereby is  $S$  the column density. The column density is the concentration of the trace when integrating along the light path, the dimension of  $S$  is therefore the number of molecules divided by an area:  $\frac{\text{molec}}{\text{cm}^2}$ .

$$S = \int_0^L c(l) dl \quad (3.3)$$

When measuring at a volcano, that means measuring in the atmosphere the situations gets more complex, since we need to deal with several absorbers and scattering processes have to be taken into account. One possibility is to treat scattering effects as pseudo absorbers with the respective extinction coefficients for Rayleigh ( $\epsilon_R$ ) and Mie ( $\epsilon_M$ ) scattering

$$I(L, \lambda) = I_0(\lambda) \cdot \text{expt} \left( - \int_0^L \sum_j \sigma_j(\lambda, p, T) \cdot c_j(l) + \epsilon_R(\lambda, l) + \epsilon_M(\lambda, l) dl \right) \quad (3.4)$$

The first term of Equation (3.4) in the exponential function, multiple absorbers  $j$  are considered, the corresponding concentration depends on the position  $l$  of the light path. The last two terms in describe the extinction due to Rayleigh and Mie scattering in the atmosphere.

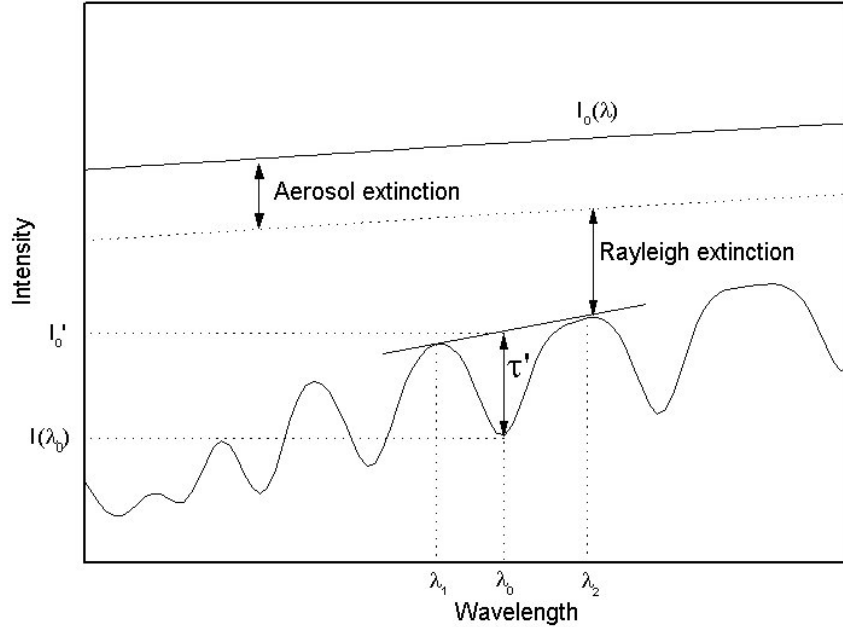


Figure 3.2: Basic idea of the DOAS principle: Light attenuate due to broad band and narrow band effects. The broad band extinction is caused by aerosols and Raylight scattering ( $I_0 \rightarrow I'$ ). The measured intensity  $I$  is formed by narrow band effects due to differential absorption structures by trace gases with the optical density  $\tau'$ . Adapted from Kern (2009)

Inelastic scattering (for example the Ring effect) and effects due to turbulences in the atmosphere are neglected here.

### 3.1 Differential Optical Absorption Spectroscopy (DOAS)

It is impossible to distinguish between various broad-band effects, like scattering in the atmosphere or instrument effects which influence the measured spectra (Lübcke, 2014). Therefore Equation (3.4) cannot be applied to real measurements.

Differential Optical Absorption Spectroscopy (DOAS) was invented in the late 1970s by Perner and Platt (1979). This section will give an overview about the DOAS technique. More detailed information can be found in the work of Platt and Stutz (2008)

Differential Optical Absorption Spectroscopy uses the fact, that absorption can be divided into broad-band parts and narrow-band parts. Broad band parts are effects that only changes weakly with the wavelength, i.e. scattering and instruments effects have a broad-band structure. The narrow band part includes effects that

strongly depends on the wavelength. Within the DOAS-Method only narrow-band absorption features of molecules are used to obtain their column densities. The absorption cross section of trace gases  $j$  have broad-band ( $\sigma_b(\lambda)$ ) and narrow band ( $\sigma'(\lambda)$ ) features, only the narrow-band structures are used in DOAS.

$$\sigma(\lambda) = \sigma_b(\lambda) + \sigma'(\lambda) \quad (3.5)$$

With this considerations the Lambert-Beer law Equation (3.4) can be rewritten dividing the exponential part into a narrow-band part and a broad-band part:

$$I(\lambda, L) = \overbrace{I_0(\lambda) \cdot \exp \left( - \int_0^L \sum_j \sigma_{b,j}(\lambda, p, T) \cdot c_j(l) + \epsilon_R(\lambda, l) + \epsilon_M(\lambda, l) dl \right)}^{=I'_0(\lambda)} \cdot \exp \left( - \int_0^L \sum_j \sigma'_j(\lambda, p, T) \cdot c_j(l) dl \right) \quad (3.6)$$

The so defined  $I'_0(\lambda)$  differs from  $I_0(\lambda)$  only by broad band effects. With  $I'_0(\lambda)$  a differential optical density  $\tau'$  can be defined:

$$\tau' = \ln \left( \frac{I'_0(\lambda)}{I(\lambda)} \right) = \int_0^L \sum_j \sigma'_j(\lambda) \cdot c_j(l) dl = \sum_j \sigma'_j(\lambda) \cdot S_j \quad (3.7)$$

The optical density can now be calculated by using the difference of the column density  $S_M$  in the measurement spectrum to the column density  $S_R$  of a reference spectrum. From Equation (3.6) we know:

$$I_{P,R} = I'_0 \cdot \exp(-S_{P,R} \cdot \sigma(\lambda)) \quad (3.8)$$

In general the obtained column density  $S_M$  is called differential slant column density: "dSCD". If the reference spectrum does not contain the trace gas of interest (is not contaminated with trace gases) that means  $S_R = 0$ ,  $S_M$  is called the slant column density (SCD). With Equation (3.8) the optical density can be derived by:

$$\tau(\lambda) = -\ln \left( \frac{I_M}{I_R} \right) = \sigma(\lambda) \cdot (S_M - S_R) \quad (3.9)$$

### 3.1.1 Technical implementation of the DOAS approach

The theory explained above only describes the ideally situation. In real measurements more problems occur due to instrument limitations inelastic scattering causing the Ring effect and due to impacts of external parameters like temperature.

In the following a short overview about these problems and their consequences for our retrieval is given. Further information can be found in Lübcke (2014).

## Optical and spectral resolution of the spectrometer

The resolution of the spectrometer is finite, thus, the detector receives a spectrum  $I^*(\lambda)$  which can be retrieved with a convolution of the incident spectrum  $I(\lambda)$  with the instrument function  $H(\lambda)$ :

$$I^*(\lambda) = I(\lambda) * H(\lambda) = \int I(\lambda - \lambda') \cdot H(\lambda - \lambda') d\lambda' \quad (3.10)$$

For the evaluation all  $\sigma_j$  of the trace gases of interest need to have the same spectral resolution as the instrument used for recording the spectra. In this work we will use high resolution cross sections and convolute them with the instrument function  $H$ :

$$\sigma^*(\lambda) = \sigma(\lambda) * H(\lambda) \quad (3.11)$$

The instrument function  $H$  can be approximated by using the spectral lines of a mercury lamp since the width of those lines is only a few pm, they could be treated as delta peaks when comparing it to the resolution of the spectrometers.

## Effects of the detector

The detector only has discrete pixels, therefore a wavelength interval is mapped to a pixel  $i$ .

$$I'(i) = \int_{\lambda(i)}^{\lambda(i+1)} I^*(\lambda'd) d\lambda' \quad (3.12)$$

For the retrieval the relationship between the detector channels and the wavelength of the spectrum need to be known. The wavelength to pixel mapping (WMP) for a detector with  $q$  channels can be calculated as:

$$\lambda(i) = \sum_{k=0}^{q-1} \gamma_k \cdot i^k \quad (3.13)$$

Hereby,  $\gamma_0$  is a shift of the spectrum and  $\gamma_1$  is a squeeze (respectively stretch) of the spectrum. The wavelength to pixel mapping can be discovered by using a mercury lamp again and compare pixel-position with the well known wavelength of the individual HG-lines of the mercury lamp.

The wavelength to pixel mapping depends on the instrument temperature as well as on the ambient pressure (Lübeck et al., 2014).

## **Ring effect**

As mentioned above inelastic scattering causes the Ring effect (named after Grainger and Ring, 1962). The Ring effect is observable through a filling of the Fraunhofer lines in spectra of scattered solar radiation, (e.g. if the sunlight travels through the earth atmosphere). When compared to direct sunlight measurements (e.g. outside of the earth atmosphere). ([Bussemer \(1993\)](#),[Solomon et al. \(1987\)](#)) proposes that the Ring effect is a result of rotational Raman scattering mainly of  $O_2$  and  $N_2$  in the atmosphere. [Solomon et al. \(1987\)](#) suggested to treat the Ring effect as a pseudo-absorber.

## **Part II**

### **Evaluation of the data of Tungurahua and Nevado Del Ruiz**

## 4 Network for Observation of Volcanic and Atmospheric Change



Figure 4.1: Global map of the volcanoes monitored by NOVAC. Used with friendly permission of Santiago Arellano.

The Network for Observation of Volcanic and Atmospheric Change (NOVAC) is a network of instruments monitoring volcanoes over the whole world. NOVAC was installed to gain another tool for risk assessment, for gas emissions and geophysical researches.

NOVAC was originally funded by the European Union on the first October in 2005. The aim of NOVAC is to establish a global network of stations for the quantitative measurement of volcanic gas emissions. At the beginning, NOVAC encompassed observatories of 15 volcanoes in Africa America and Europe, including some of the most active and strongest degassing volcanoes in the world. Although the EU-funding has stopped, the network has been constantly growing since it was founded. In 2017 more than 80 instruments are installed at over 30 volcanoes in more than 13 countries. Figure 4.1 shows a map, with all volcanoes of the Network for Observation of Volcanic and Atmospheric Change.

The great advantage of the data monitored in NOVAC is the fact that NOVAC provides continuous gas emission data over many years. This ensures statistically meaningful results for the data evaluation.

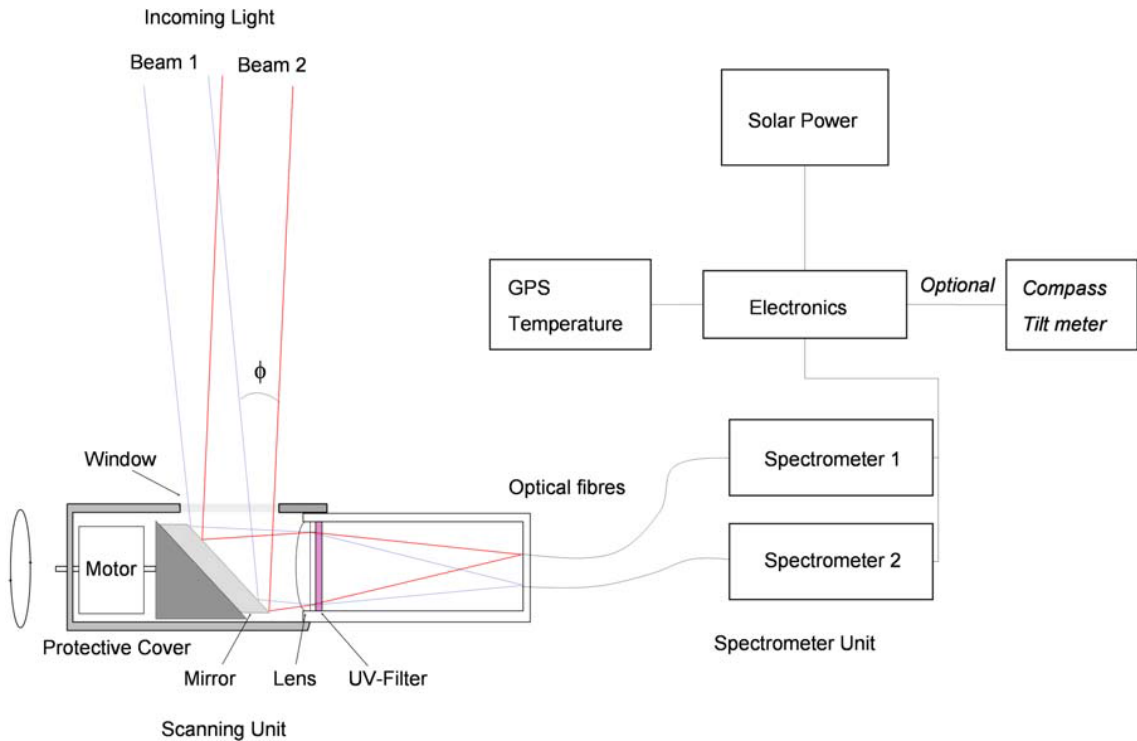


Figure 4.2: schematic sketch of a NOVAC instrument. From Galle et al. (2010)

The instruments used in NOVAC are scanning UV-spectrometer named Mini DOAS instruments.

The Mini DOAS instrument represents a major breakthrough in volcanic gas monitoring as it is capable of real-time semi-continuous unattended measurement of the total emission fluxes of SO<sub>2</sub> and BrO from a volcano. Semi-continues in this case means that the measurement is only possible during daytime and if the sunlight is sufficient.

The basic Mini DOAS system consists of a pointing telescope fiber-coupled to a spectrograph. Ultraviolet light from the sun, scattered from aerosols and molecules in the atmosphere, is collected by means of a telescope with a quartz lens defining a field-of-view of 12 mrad. NOV

The spectrometers measure in the UV region in a wavelength range of 280 to 420 nm. In this range the differential structures of SO<sub>2</sub> and BrO are dominant.

The NOVAC-instruments need to be very robust to stand the conditions around volcanoes. Therefore the design of the instruments is rather simple, this means the instruments do not have internal stabilisation features like temperature stabilization to keep the measurement independent of external parameters.

This comes with a reduced precision of the data, but the huge amount of data produced by NOVAC compensates for this limitation.

## 4.1 Measurement routine

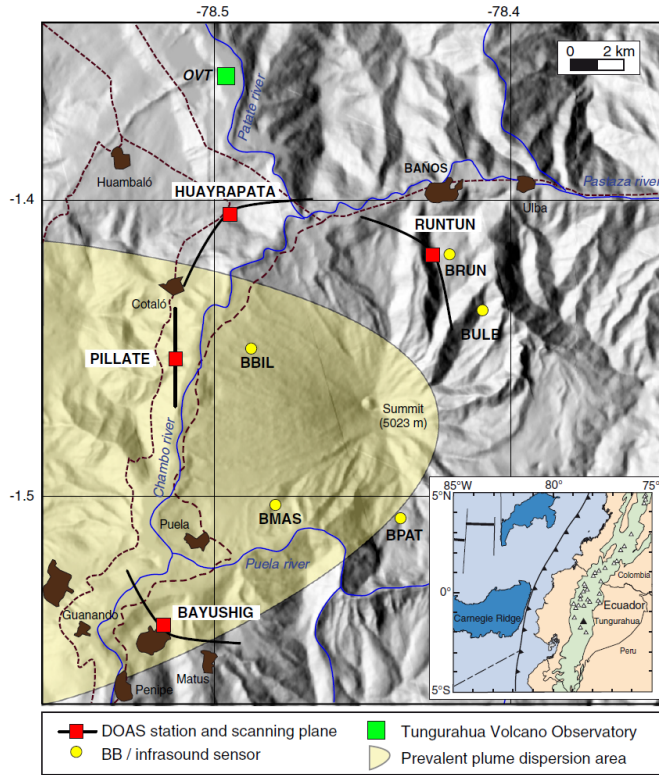


Figure 4.3: Topographic Map of the Tungurahua Volcano. The predominant plume direction is shaded in yellow. Four NOVAC stations are shown as red squares, the corresponding scanning geometry is sketched with black lines. From [Hidalgo et al. \(2015\)](#).

The instruments are set up five to ten km downwind of the volcano. To cover most of the occurring wind directions two to five instruments are installed at each volcano. Ideally, the measurement plane is orthogonal to the plume, to get the best measurement results. In reality, the measurement plane might be rotated.

For the calculations of gas data from the DOAS retrieval a scan of the Plume and a scan without any volcanic trace gases (reference spectrum) is needed. This is done without any knowledge of the plume location by scanning the whole sky. The measurement routine starts with a spectrum in zenith direction: the pre-reference. The exposure time of the pre-reference will be used for the whole scan. Afterwards, the dark current spectrum is recorded for the correction of the dark current and offset.

Then the instrument turns automatically to the side, recording spectra at the elevation angle from  $-90^\circ$  to  $90^\circ$  with steps of  $3.6^\circ$ .

The instruments records 53 spectra per Scan, the pre-reference, the dark current

spectrum and 51 spectra at different elevation angles. One hole measurement takes 6 to 15 minutes.

# 5 Evaluation routine

This chapter outlines the algorithm which is used for the evaluation of the spectroscopic data recorded in NOVAC. The problem of contamination of the reference is explained and possible solutions are presented.

## 5.1 Conventional evaluation routine

The fitting routine used for this thesis is based on the DOASIS software ([Kraus, 2006](#)). The equations of the DOAS retrieval of this work are slightly different from Equation (3.7). Equation (3.4) can be rewritten as:

$$\begin{aligned} \ln(I(\lambda, L)) &= \ln(I_0) + P(\lambda) - \int_0^L \sum_j \sigma_j(\lambda, p, T) \cdot c_j(l) dl \\ &= \ln(I_0) + P(\lambda) - \sum_j \sigma_j(\lambda, p, T) \cdot S_j \end{aligned} \quad (5.1)$$

The term  $P(\lambda)$  is a polynomial that accounts for all broad-band effects which approximates the scattering effects of the atmosphere.

The remaining task of the DOAS routine is to find a model function  $F(\lambda)$  that minimizes  $\chi^2$ :

$$\chi^2 = \sum_{i=\lambda_1}^{\lambda_2} (\ln(I(i)) - F(i))^2 \quad (5.2)$$

While  $F(\lambda)$  can be expressed on the basis of Equation (5.1):

$$F(\lambda) = \ln(I_0) + P(\lambda) - \sum_j \sigma_j(\lambda) \cdot S_j \quad (5.3)$$

The DOAS fitting routine uses a combination of a standard least-squares fit and a Levenberg-Marquardt algorithm to minimize  $\chi^2$

The SO<sub>2</sub> evaluation is performed for a wavelength range between 314.8 nm and 328 nm. Including a SO<sub>2</sub> absorption cross section recorded at a temperature of 298K ([Vandaele et al., 2009](#)) and a O<sub>3</sub> absorption cross section recorded at 221K ([Burrows et al., 1999](#)).

The BrO evaluation is performed for a wavelength range between 330.6 nm and 352.7 nm (found by [Vogel \(2011\)](#)). The sum in Equation (5.3) includes for the

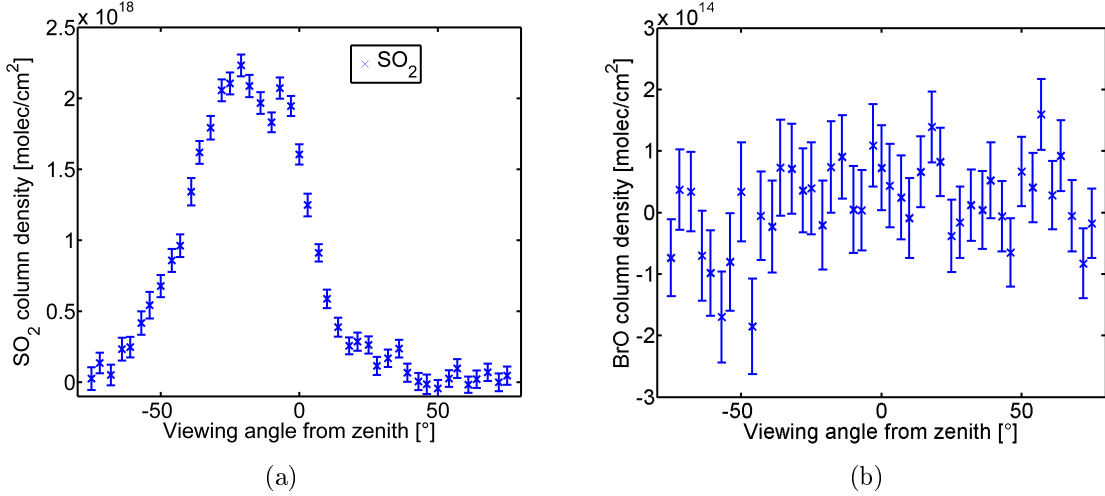


Figure 5.1: (a)  $\text{SO}_2$  SCD as a function of the elevation angle with error bars computed by the DOASIS fitting routine. (b) BrO SCD as a function of the elevation angle with error bars computed by the DOASIS fitting routine. Taken from [Warnach \(2015\)](#)

BrO evaluation the following absorption cross sections: BrO at 298K ([Fleischmann et al., 2004](#)), the  $\text{SO}_2$  and  $\text{O}_3$  absorption cross sections described above,  $\text{O}_4$  ([Hermans et al., 2003](#)),  $\text{NO}_2$  at 298K ([Vandaele et al., 1998](#)) and  $\text{CH}_2\text{O}$  at 298K ([Meller and Moortgat, 2000](#)).

NOVAC provides spectral data for roughly 50 different elevation angles. For the DOAS evaluation a reference and a measurement spectrum is needed. To get the SCD's the references need to be free of any volcanic trace gas of interest (this will be discussed more detailed in Section 5.2). With the  $F(\lambda)$  (Equation (5.3)) the column density of BrO and  $\text{SO}_2$  of the measurement spectrum relatively to the reference spectrum can be calculated using the calculations from above.

In the following we describe the technical implementation of the DOAS approach using the data of NOVAC instruments:

The first step is to correct each spectrum of the scan for dark current and offset using the dark current spectrum. The next task is to locate the measurement spectrum and the reference region in the volcano plume. To do so, the pre-reference (the spectrum recorded at an elevation angle of  $0^\circ$ ) is used to perform the evaluation of the scan spectra recorded at every elevation angle. For every spectrum of the scan the  $\text{SO}_2$  differential slant column density (dSCD) with respect to the pre-reference is calculated using Equation (5.3) by the DOASIS fit routine.

The result is  $\text{SO}_2$  dSCDs as a function of the elevation angle. This way the elevation angle corresponding to the maximum and the minimum of the  $\text{SO}_2$  column density can be determined. The location of the  $\text{SO}_2$  maximum defines the location of the plume. The assumption is that the minimum of the  $\text{SO}_2$  curve corresponds

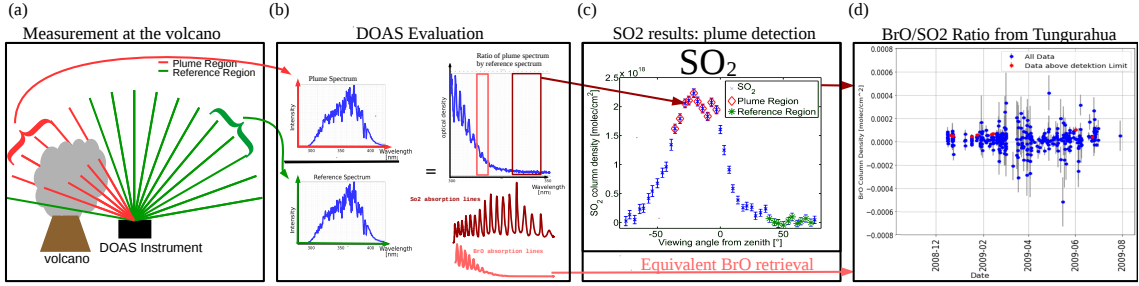


Figure 5.2: NOVAC Evaluation: (a) Measurement at the volcano (b) Evaluation of the spectral data with the DOAS routine using the absorption cross sections of BrO and SO<sub>2</sub>. (c) Finding the location of the plume and reference (d) (taken from [Warnach \(2015\)](#)) Computation of the ratios BrO/SO<sub>2</sub> at Tungurahua.

to a region outside of the plume which is true in most cases. The background SO<sub>2</sub> amount in the earth atmosphere around Tungurahua is negligible (see Section 2.4.1) so we take it as a region of zero SO<sub>2</sub>.

To detect the plume region we use a gauss fit of the SO<sub>2</sub>-elevation-angle-curve. To increase the quality and to get a more robust result the sum over several plume spectra is taken. If the gauss curve is too wide we use the 10 spectra with the highest SO<sub>2</sub> amount. As reference we use the sum of the 10 spectra with the lowest SO<sub>2</sub> amount.

The absolut slant column densities (SCD's) of BrO and SO<sub>2</sub> can now be calculated with the previously detected reference and plume spectrum. In Figure 5.1 (a) an example SO<sub>2</sub> SCD as a function of the elevation angle is shown. The SO<sub>2</sub> curve has a maximum at the position of the plume at an elevation angle of approximately -30° to 0° and a reference region at an elevation angle of 40° to 70°. The extrema of the BrO curve are not as distinct as it is the case for the SO<sub>2</sub> curve as it can be seen in Figure 5.1 (b). Since the BrO column density is much lower than the SO<sub>2</sub> column density, and just lies slightly above the detection limit, the plume is hard to detect using the BrO column density as it is shown in fig. 5.1 (b). Therefore we evaluate BrO only in the plume location found by using SO<sub>2</sub>.

To further increase the fit quality multiple reference and plume spectra of successive measurements are added. Figure 5.3 (b) shows the routine of adding multiple spectra of consecutive measuring times. In the following the spectra resulting from the multi adding technique will be referred to as "Multi Add Spectra" "Multi Add Spectra". The algorithm for co-adding is visualized in Figure 5.3 (b) was invented by [Vogel \(2011\)](#) and [Lübcke et al. \(2014\)](#).

Taking the BrO/SO<sub>2</sub> ratio if the column densities are close to zero yields unpredictable and unrealistic results. Thus, spectra measured outside of the volcano plume need to be excluded. This could be achieved by setting a BrO or/and an SO<sub>2</sub> threshold. A reasonable BrO threshold needs to be at least in the order of the

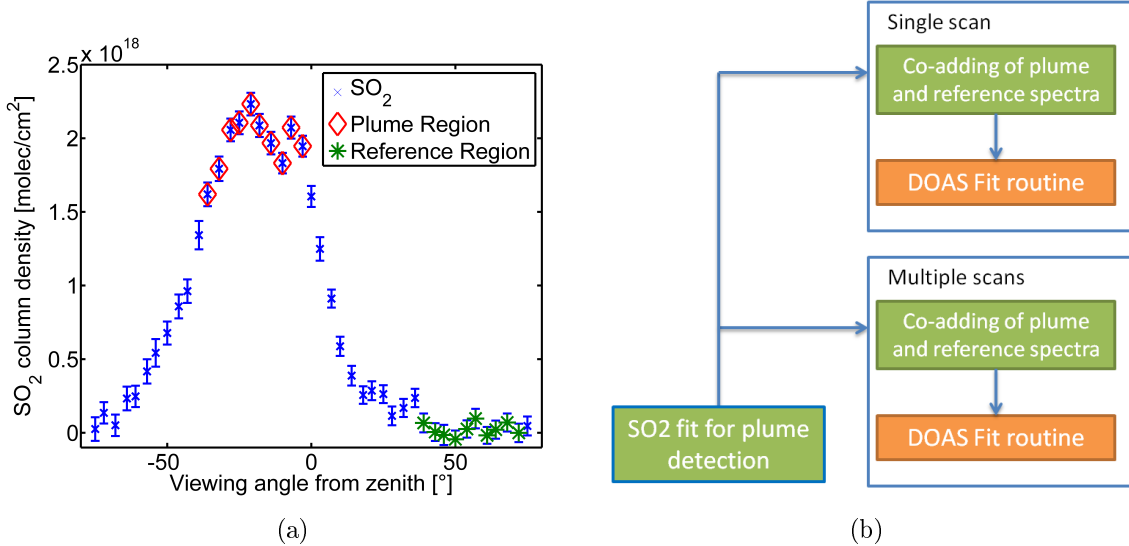


Figure 5.3: (a) SO<sub>2</sub> SCD as a function of the elevation angle. The co-added plume region is marked with red diamonds, and the co added reference region with green stars. From Warnach (2015). (b) Flow chart of the BrO and SO<sub>2</sub> evaluation. From Lübcke (2014).

DOAS fit error. However this could lead to elevated BrO/SO<sub>2</sub> ratios, since the BrO error is often close to the detection limit. Thus, all low BrO column densities are excluded from the evaluation (Lübcke et al., 2014). The other possibility is to set an SO<sub>2</sub> threshold. In this thesis an SO<sub>2</sub> threshold (plume limit) of  $7 \cdot 10^{17} \frac{\text{molec}}{\text{cm}^2}$  is used for the selection of spectra for the evaluation of the BrO/SO<sub>2</sub> ratio.  $7 \cdot 10^{17} \frac{\text{molec}}{\text{cm}^2}$  is a hight threshold for the column density. However, this this approach assures that only strongly significant gas amounts are accounted. This way, the BrO/SO<sub>2</sub> ratio will not be significantly influenced and that all utilized measurement spectra are inside of the volcano plume (Lübcke et al., 2014).

Increasing a plume limit leads to an decrease of usable data. The ratio of usable data as a function of the plume limit is shown in Figure 5.4. An exponential decrease of data can be observed. The plot is based on the data of Tungurahua. Plume limits below  $7 \cdot 10^{17}$  are shaded in yellow. A plume limit of  $7 \cdot 10^{17}$  leads to a ratio of usable data of approximately 10%.

## 5.2 Contamination problem

To assure that the reference is volcanic gas free a high resolution solar atlas spectrum (see below) is used to evaluate the reference. In some reference spectra an amount of SO<sub>2</sub> different from zero is found. Thus we can conclude, that there are some references which contain a non-negligible amount of volcanic trace gases. In rare (ca. 10% of the data) scenarios, the volcanic plume covers the whole scan region.

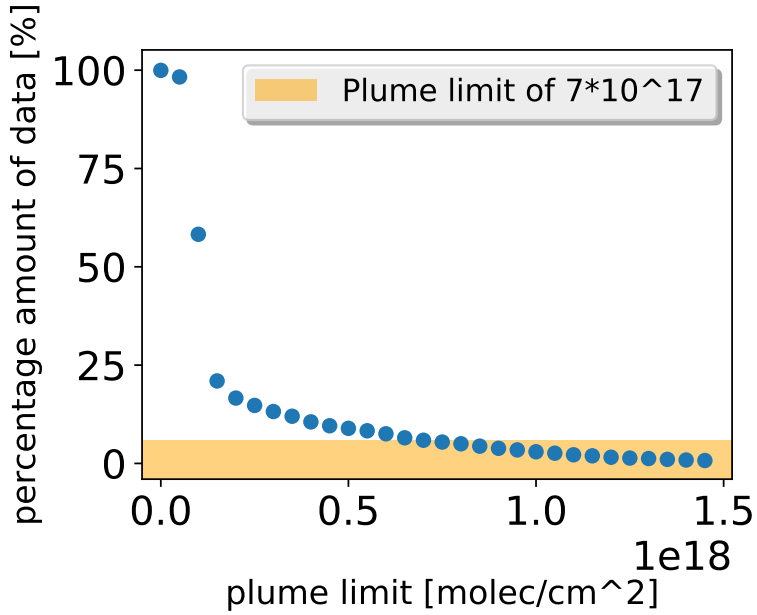


Figure 5.4: The decrease of the amount of data above the plume limit as a function of the plume limit. The plume limits below the actual plume limit of  $7 \cdot 10^{17}$  are marked with a yellow shade.

This could happen if for example the volcanic plume of the day before still extends over the hole scan area as a consequence of windless conditions. In consequence, the reference is contaminated with volcanic trace gases. Thus, the gas amount is underestimated by the NOVAC-evaluation: In Figure 5.5 we see an example from April 2011 (Tungurahua) where the reference region is contaminated by volcanic trace gases. The blue  $\text{SO}_2$  curve shows the calculations with the NOVAC-evaluation, but since there is still  $\text{SO}_2$  in the reference region, the assumption, that the  $\text{SO}_2$  amount could be set to zero in the reference region is wrong. The red curve shows the real  $\text{SO}_2$  curve, which lies significantly above the NOVAC -curve.

If the reference region for any reason is contaminated by volcanic trace gases, there are two possibilities: excluding the contaminated data from the evaluation or the reference spectrum has to be replaced by a volcanic-gas-free reference. Alternative spectra are a theoretical solar atlas spectrum or a volcanic-gas-free reference spectrum recorded by the same instrument.

In the following we will discuss the two alternative reference spectra.

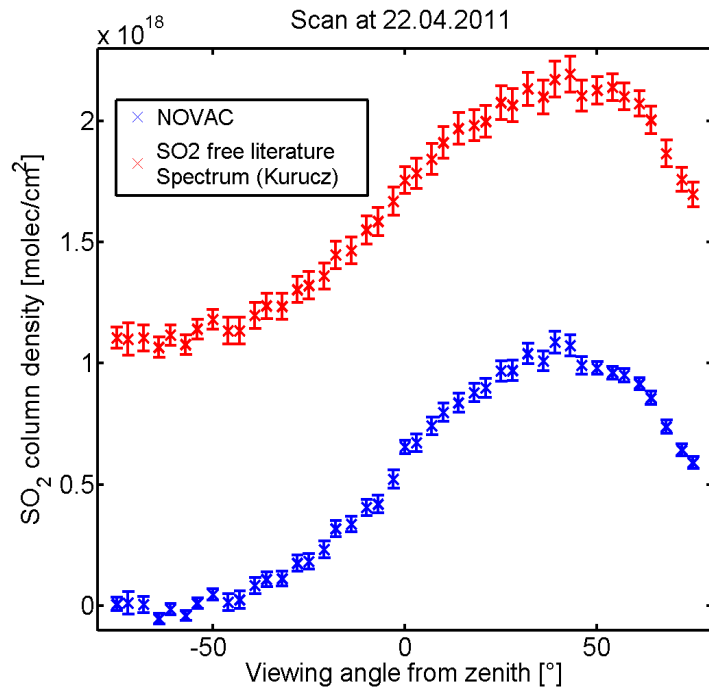


Figure 5.5: Scan with a contaminated reference spectrum from April 2011. From [Warnach \(2015\)](#)

## Evaluation using a Solar Atlas spectrum

An alternative for choosing the region with the lowest column density as reference region is to use a theoretical high resolution solar atlas spectrum as reference ([Chance and Kurucz, 2010](#)). The use of a theoretical solar atlas spectrum as a reference which is completely volcanic-trace-gases-free was first proposed by ([Lübcke et al., 2014](#)). The advantage of using a solar atlas spectrum as reference is, that we know that there are no volcanic trace gases and do not need to take this fact as a possibly inadmissible assumption. The disadvantage is, that using a solar atlas spectrum comes along with a drawback of precision: A theoretical solar atlas spectrum is far more precise than the spectra of the NOVAC instruments. Therefore the instrument functions need to be modeled and added to the retrieval.

The reduction of precision is acceptable for the SO<sub>2</sub> retrieval but not suitable for a BrO retrieval because then most data would be below the detection limit.

Possible contaminations can be checked by a theoretical solar atlas spectrum to evaluate the SO<sub>2</sub> amount in the reference.

## Evaluation using a spectrum of the same instrument

An alternative reference spectrum could be a volcanic-gas-free reference spectrum recorded by the same instrument at a different time. When using such a reference several problems occur:

As described in Chapter 4 the instruments used in NOVAC do not include features like temperature stabilization. Due to that the measurements are not independent of external parameters. So we need to choose a reference recorded at similar conditions with respect to meteorology and radiation as well as in the temporal proximity due to instrumental changes with time and ambient conditions. Ideally the external conditions should be equal to the conditions at the time when the plume was recorded.

In this work we combine both options in order to achieve both, enhanced accuracy but still maximum possible precision of the SO<sub>2</sub> and BrO retrievals. So we use the solar atlas spectrum to check for contamination and a reference spectrum recorded in temporal proximity by the same instrument as reference.

Thus, if contamination occurs it is possible to choose from a list of gas free alternative references. In theory, for ideal instruments all references should lead to the same results for the gas retrievals. But instruments are imperfect (see Chapter 4) thus the reference need to be chosen carefully in order to ensure reliable results.

As discussed above it might occur, that the reference is contaminated for example by the plume of the day before. If that happens, we underestimate the gas amount by using a contaminated reference. But another possibility is, that the plume itself is also contaminated. This might be the case if the volcanic gas of the volcano is not taken away by the wind, but accumulates at the instrument. If this is the case, using an other reference would lead to an overestimation of the column density of gases. With the data retrieved by the NOVAC instruments it is very difficult to discover whether the plume is contaminated or not.

Figure 5.6 shows the strength of contamination as function of the mean SO<sub>2</sub> amount of the day before. The strength of contamination is measured as the difference when perform the evaluation for SO<sub>2</sub> with the contaminated reference recorded as the same time as the plume spectrum was recorded and when using a gas free reference. The data where fitted with a linear function. The left plot shows data from the Tungurahua volcano. In the right plot the data of Nevado Del Ruiz are visualized. Even though both plots show a slight increase of contamination strength with the mean amount of SO<sub>2</sub> of the day before, the increase is not significant.

However this thesis is build on the assumption, that the plume is free of additional contamination. In the following we discuss how to find the an optimal reference from another scan automatically.

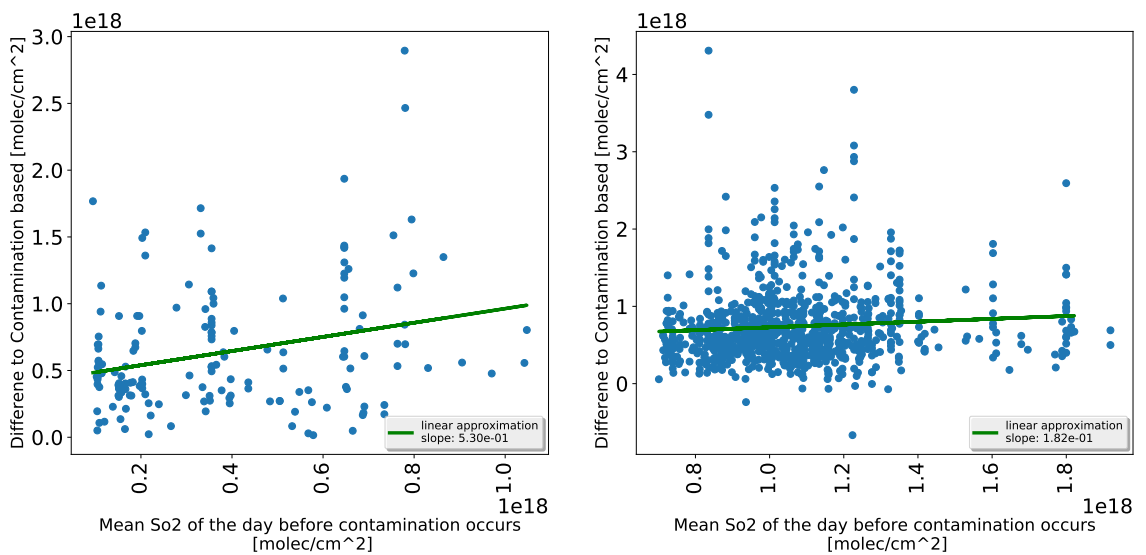


Figure 5.6: The strength of contamination as function of the mean SO<sub>2</sub> amount of the day before. The strength of contamination is defined as the difference in SO<sub>2</sub> SCD when evaluation with an alternative reference, or neglect the contamination. Left: data from Tungurahua. Right: data from Nevado Del Ruiz.

# 6 BrO Evaluation and its limitations

This chapter discusses the evaluation of BrO by spectroscopic instruments of NO-VAC.

The evaluation of the data from NOVAC is parted into the evaluation of SO<sub>2</sub> and the evaluation of BrO. While the retrieving of SO<sub>2</sub> is relatively easy due to the high amount of SO<sub>2</sub> (magnitude of SO<sub>2</sub> at Tungurahua  $\approx 1e^{18}$ ), the BrO evaluation is much more problematic (as it can be seen in Figure 5.1). The magnitude of BrO SCD is around  $\approx 1e^{14}$ . This results in a larger uncertainty of the BrO SCD. Most of the BrO data are below the detection limit of  $\text{BrO}_{err}/\text{BrO}_{value} < 1/4$ . In comparison SCDs of SO<sub>2</sub> are in almost all cases (99.5% of the data) above the detection limit. Choosing a different reference than the reference measured at the same time as the plume results in 99% of all data in an increasing absolute error. Thus an BrO error which is smaller than the "Same Time Error" is often not possible to retrieve. However, due to the large uncertainty of BrO relative to SO<sub>2</sub> this thesis will concentrate on BrO analysis. Thus, the reference is chosen with respect to the BrO error to maximise the quality of the BrO/SO<sub>2</sub> ratio. The amount of gas free alternative references is around 1500 per year. To make the best choice it is necessary to examine the conditions which influence the BrO retrieval.

Every spectrum is measured under certain conditions. These conditions in general are not the same when measuring the plume and the reference. References where the surrounding conditions e.g temperature or cloudiness are equivalent with the surrounding conditions of the plume measurement lead to a small error. In the following, we will take a closer look at the dependency of the BrO error on external parameters.

## Data used for the analysis

For this analysis every plume reference pair of the observed time span is used. Thus for 1000 recorded "multi add" spectra results in 1000<sup>2</sup> plume reference pairs and their corresponding differences in the external parameter and their associated BrO error.

## 6.1 BrO error dependence on external parameters

The measurement and evaluation depends on the surrounding conditions like temperature or cloudiness (Lübcke, 2014)

As a result the surrounding conditions need to be taken into account if choosing a new reference.

The better the surrounding conditions of the time where the reference is measured coincide with the conditions of the time when the plume is measured. The lower the time difference, the lower the expected BrO error.

The surrounding conditions that are considered in this thesis are:

- Temporal difference between measuring the plume and the reference.
- Temperature,
- Colorindex,
- Exposure time,
- Elevation angle,
- Daytime

The analysis of these external parameter is done for spectra recorded at Tungurahua and Nevado Del Ruiz (see section 2.5).

### 6.1.1 Temporal difference

Due to instrument drifts the fit quality decreases with the time difference between recording the plume and the reference. This could be a result of a wavelength shift over time which was observed by [Warnach \(2015\)](#). [Warnach \(2015\)](#) suggested that the drift is caused by a hysteresis effect. Figure 6.1 shows the wavelength shift as a function of the time for six NOVAC instruments located at Tungurahua in the time between 2008 to 2014. For the analysis in this thesis data of Tungurahua between 2008 to the mid of 2009 are used. Figure 6.1 shows a rather steep drift in this time interval. [Warnach \(2015\)](#) observed a decrease of the shift after initial negative drift after the first 2 years at Pillate. Thus, it could be that the temporal difference could become less important for old instruments. For the following discussions date of Pillate from 2008 to 2009 are used.

When using reference and plume spectra of the same time, these effects are cut out since the shift is equal for the plume and reference spectrum. For increasing temporal difference between reference and plume measurement time the fit quality decreases and thus the BrO error increases.

In Figure 6.2 the BrO error as a function of the time difference between recording the plume and the reference is shown. The running mean is drawn with a black line. In Figure 6.2 (a) it can be seen that a large temporal difference results in an increase of BrO error of more than 600%. BrO errors of such magnitudes are too large for our purposes therefore it is useful to define a maximal temporal difference.

The maximal temporal difference should be large enough to ensure an amount of references which is large enough to be able to pick a reference with similar conditions,

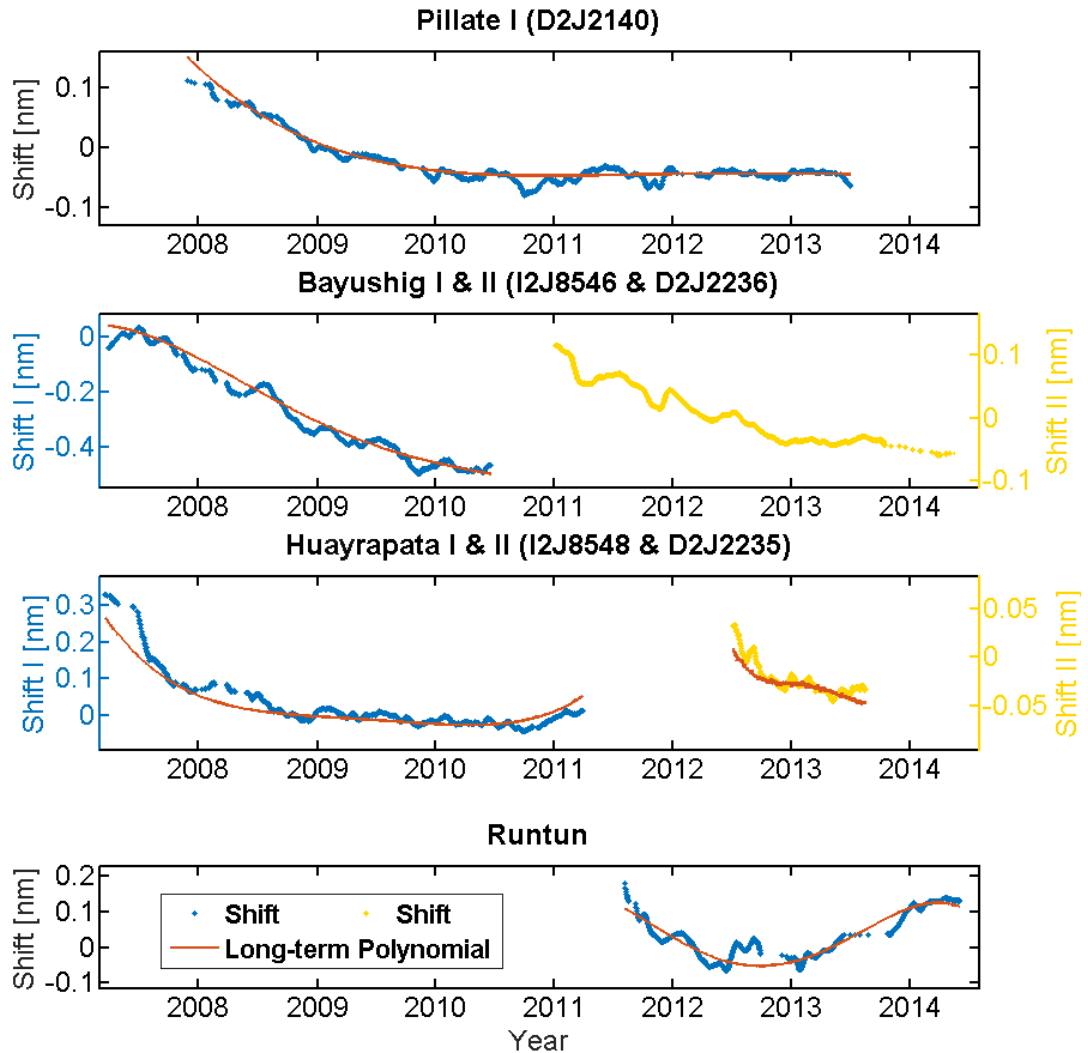


Figure 6.1: Wavelength shift over the time. The shift is shown for six NOVAC-instruments from Tungurahua. The red and yellow dots show the running mean about 20 days. Red line indicates a temperature independent long term polynomial. From Warnach (2015)

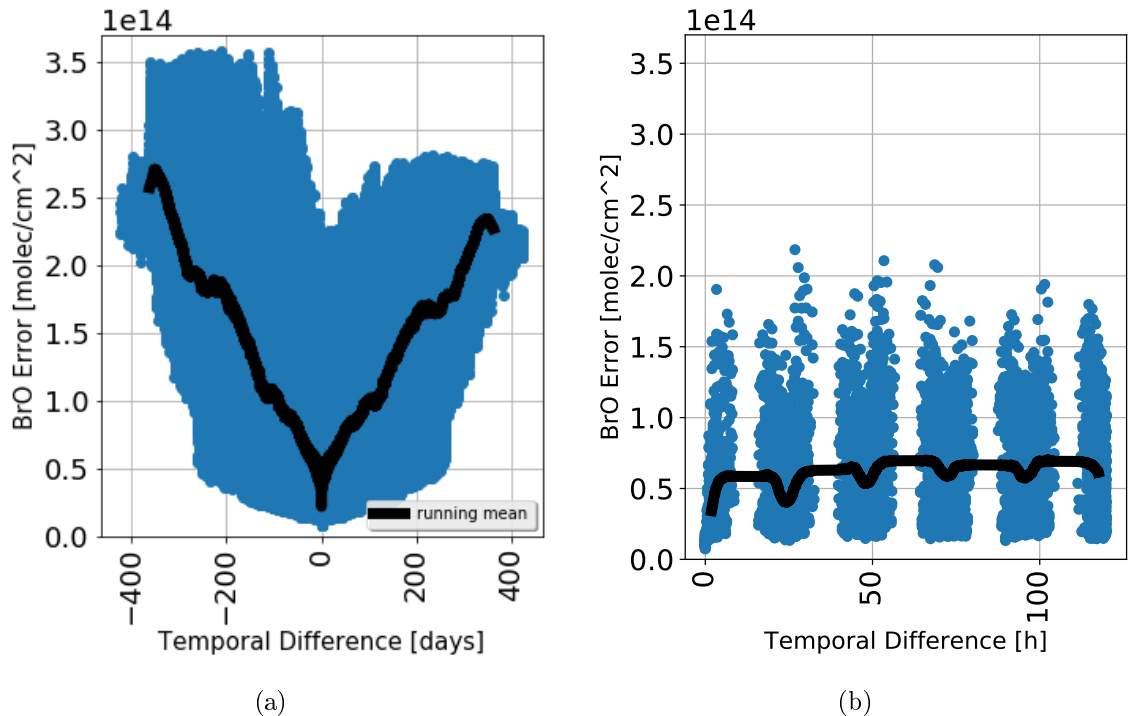


Figure 6.2: The BrO error as a function of the temporal difference shown for the Pillate instrument from Tungurahua (2008-2009). (a) Temporal differences up to 400 days are shown. (b) Temporal differences below 120h; periodical BrO error evolution indicates the impact of the daytime

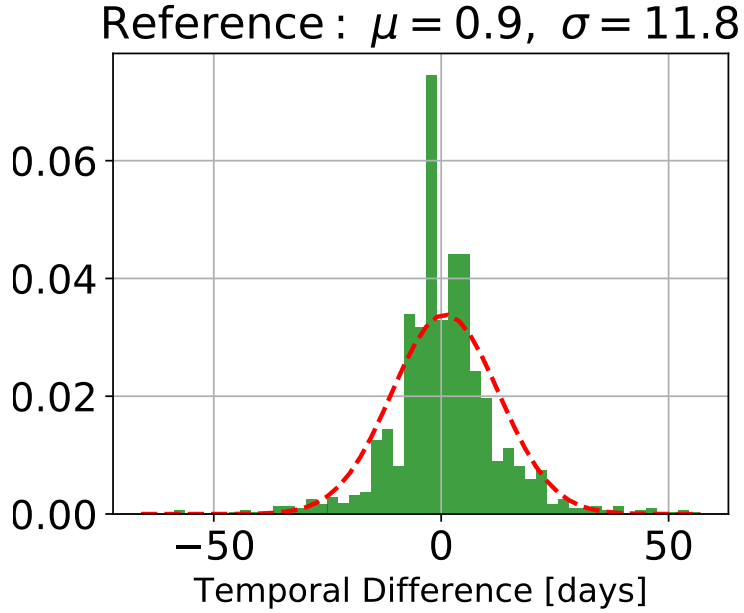


Figure 6.3: Histogram showing the frequency of getting the best reference as function of the temporal difference between plume and reference measuring.

but the maximal temporal difference should be small enough to prevent to large BrO errors due to long term shifts.

To evaluate the maximal time difference, for which we still get reliable results for all possible reference-plume pairs the corresponding BrO error was calculated. With this data for all plume spectra we are able to find the associated reference where the BrO error is minimal. In Figure 6.3 a histogram is plotted with the probability of picking the best reference as a function of the time difference. Obviously the best results are obtained in cases where the day of measuring the reference is the same day as measuring the reference. That means, if the time difference is smaller than one day. A gauss fit was used to fit the data of the histogram. We allow all time differences which are in two sigma area. Thus the maximal time difference is 14 days

Figure 6.2 (b) shows the evolution of the BrO error for a maximal temporal difference of 120 hours. It is only possible to record data during daytime. This causes the lack of data at some temporal differences. A periodic decrease of the BrO error can be seen. This is a result of a decrease of the BrO error when the surrounding conditions coincide. In this case the daytime coincidence causes the BrO error to decrease. For further discussion of the daytime see Section 6.1.3.

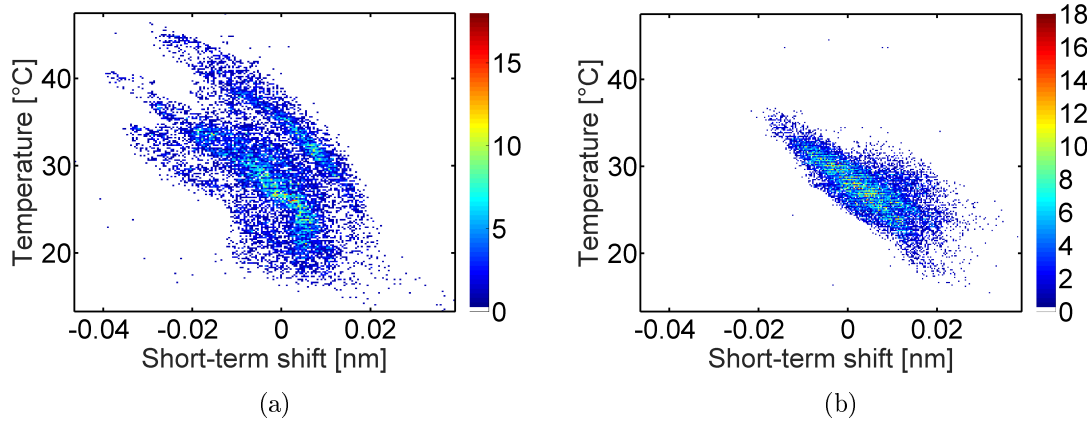


Figure 6.4: Short Term wavelength as a function of the instrument temperature for Pillate 1. (a) initial period prior to January 2010 (b) after 2010. From [Warnach \(2015\)](#)

By restricting the temporal difference to 14 days the amount of possible gas free references decreases on an average of 195 alternative references per contaminated plume (see table 6.1). Whereas none of the plumes do not have alternative references. The minimum amount of references is 8.

If a continuously evaluation is required, this means the spectra are evaluated directly after the recording, the number of suitable gas free references halves since only references recorded before the plume are available.

For the following analysis of external parameters all temporal differences are below 14 days.

Instrument	D2J2140_0	I2J8546_0	I2J8548_0	D2J2200_0	D2J2201_0
Mean	84.6 ≡ 100%	163.7 ≡ 100%	217.1 ≡ 100%	284.0 ≡ 100%	225.6 ≡ 100%
Std	35.8 ≡ 100%	29.9 ≡ 100%	64.8 ≡ 100%	69.5 ≡ 100%	41.2 ≡ 100%
Min	8 ≡ 100%	113 ≡ 100%	97 ≡ 100%	64 ≡ 100%	63 ≡ 100%
Max	169 ≡ 100%	214 ≡ 100%	399 ≡ 100%	433 ≡ 100%	297 ≡ 100%

Table 6.1: Amount of possible references while restricting the time span between plume and reference to two weeks.

Furthermore it can be seen that the evolution of the BrO error with the temporal difference is symmetric around zero, thus it is not necessary to distinguish between

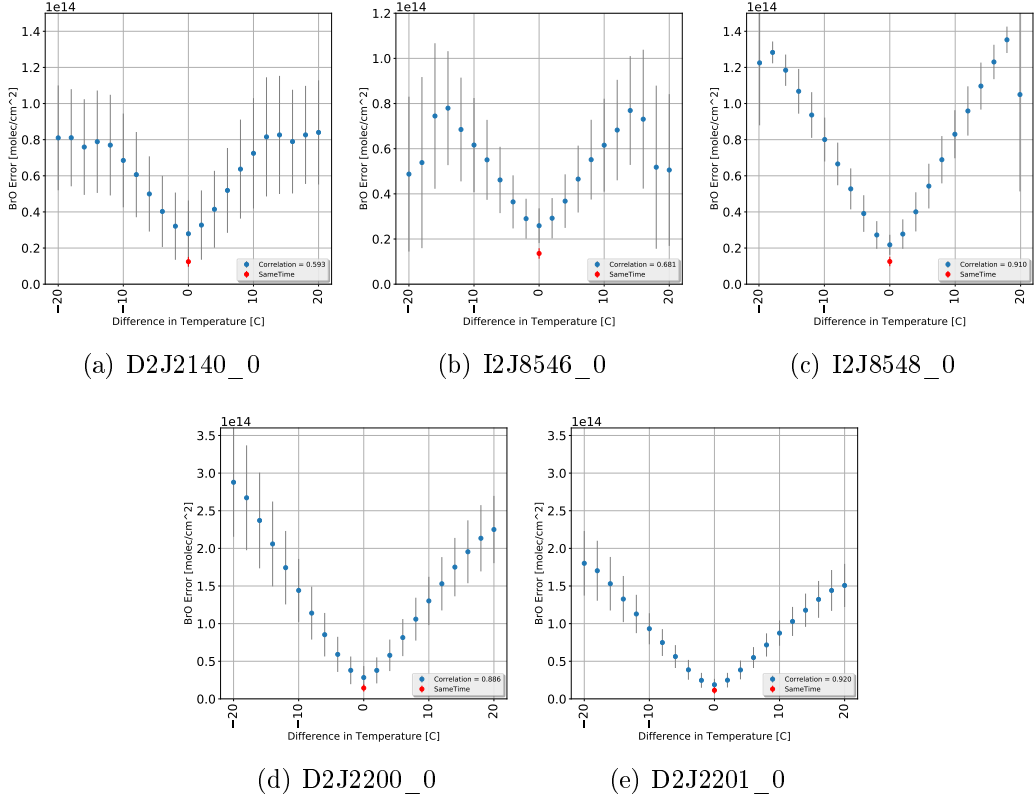


Figure 6.5: The BrO measurement error as a function of the difference of temperature between measuring the reference and the plume are shown. (a)-(c) show the data for the instruments at Tungurahua, (d)+(e) at Nevado Del Ruiz. To evaluate the plume spectra all reference spectra with a temporal distance of no longer than two weeks are used. A increase of the BrO error with the distance in temperature is observable.

positive or negative temporal differences.

### 6.1.2 Temperature

The instrument design of the NOVAC instruments compromise between accuracy and longevity as explained in Chapter 4. In particular there are no internal thermal stabilizations installed as an attempt to reduce the instruments power consumption. This can influence the recorded spectra.

Each pixel of the spectrometer, which is used for the DOAS experiment, collects photons of a certain wavelength range.

The calibration for the wavelength to pixel mapping (WMP) is commonly done with a Mercury lamp or by the comparison with the high defined Kuruz spectrum. As the WMP depends on the optical alignment of the spectrometer, which itself depends

on the temperature, it is not constant. Changes in the spectrometers temperature can cause changes in the instrument line function and shifts in the WMP (([Pinardi et al., 2007](#))). Moreover, [Warnach \(2015\)](#) show that, short term shifts are related to the instrument temperature (see Figure 6.4).

The above discussed temperature dependence of the WMP causes a reduction of the fitquality with increasing instrument temperature difference between plume and reference. Thus the BrO error increases as well with the temperature difference. To quantify the BrO error dependency on the temperature all plume spectra of Tungurahua from August 2008 to August 2009 (Nevado del Ruiz from end of 2009 to the end of 2011) are evaluated with respect to all plume spectra of the same time period. The BrO error as function of the temperature difference can be seen in Figure 6.5. The blue dots shows the mean BrO error at the specific temperature difference, the standard deviation is illustrated with gray bars.

The mean BrO deviation for the sametime evaluation is additionally added with a red point.

Instrument	D2J2140_0	I2J8546_0	I2J8548_0	D2J2200_0	D2J2201_0
Slope	4.10e+12	3.93e+12	6.50e+12	1.24e+13	8.17e+12
Correlation	0.593	0.681	0.910	0.886	0.920
Zero point	2.58e+13	2.23e+13	1.60e+13	1.38e+13	9.07e+12
$\Delta T_2$	6.3	5.7	2.5	1.1	1.1

When looking at all discussed external parameters, temperature has the strongest impact on the BrO error due to the strong impact on the WMP.

To quantify the degree of dependency between the BrO error and the difference in temperature the data are fitted with an polynomial of the first order. As a result of the symmetry around zero it is possible to not distinguish between positiv or negative temperature differences. Thus the absolute temperature difference was used for the calculations of the fit. The slope and zero point are calculated for each instrument and are shown in section 6.1.2. The zero points at Tungurahua vary

Instrument	D2J2140_0	I2J8546_0	I2J8548_0	D2J2200_0	D2J2201_0
Mean	39.6/46,8%	119.3/72,9%	158.2/72,9%	233.6/82,3%	151.6/67,2%
Std	24.66/68,9%	50.4/168,6%	75.97/117,2%	84.5/121,6%	72.6/176,2%
Min	1/12,5%	8/7,1%	12/12,4%	3/4,7%	6/9,5%
Max	130 /76,9%	213 /99,5%	386/96,7%	414 /95,6%	296 /99,7%

Table 6.2: Remaining amount of References if only time difference below  $3.358^{\circ}C$  are accepted. The percentages values refer to the decrease of the data relative to Table 6.1

from  $1.6 \cdot 10^{13}$  to  $.56 \cdot 10^{13}$ . The variation at Nevado Del Ruiz id from  $9.07 \cdot 10^{12}$  to  $1.38 \cdot 10^{13}$ .

Section 6.1.2 also shows the correlation between the BrO error and the absolute Temperature difference. The correlation is calculated using the python library Numpy. The correlation reaches from 0.593 at D2J2140\_0 to 0.92 at D2J2201\_0 and show a large variation between the instruments.

Furthermore, the table shows the temperature difference  $\Delta T_2$  for which the error doubles compared to a same-temperature-reference.

If restricting the temperature difference to the mean  $\Delta T_2$  of all instruments ( $Mean(\Delta T_2) = 3.3$ ) the amount of possible references decrease as it is shown in table 6.2.

The advantage of restricting the accepted temperature difference is more control about the choice of the best reference. The disadvantaged is that the amount of possible references decrease. Thus it could be that a reference is dismissed, which has a large temperature but the reference is equal in all other examined external references, thus it leads to a small BrO error.

### 6.1.3 Daytime

During the day a lot of external parameters like temperature, solar altitude etc. change. In particular the solar altitude could have an impact on the fit quality since the light path of the sun is much longer at the evening than at noon. Therefore the scattering effects and the fraunehofer structures is different for both spectra.

Figure 6.6 shows the dependency of the BrO error on the daytime. The data are calculated as described for the temperature.

Instrument	D2J2140_0	I2J8546_0	I2J8548_0	D2J2200_0	D2J2201_0
Slope	5.07e+12	1.40e+12	3.77e+12	2.04e+13	1.38e+13
Correlation	0.340	0.156	0.310	0.538	0.631
Zero point	3.43e+13	3.39e+13	3.28e+13	4.01e+13	2.24e+13
$\Delta DT_2$	6.8	24.2	8.7	1.9	1.62

Table 6.3: Results of fitting the dependence of the BrO error on the absolute difference in daytime with in one dimensional polynomial.  $\Delta DT_2$  is the daytime difference for which the error doubles compared to a same-time-reference. The results differ for every considered instrument.

Section 6.1.3 shows equivalent calculations as section 6.1.2. Since the BrO error plotted against the difference in daytime is symmetric around zero only the absolute differences in daytime are used. These data are fitted with a first order polynomial. The results can be seen in section 6.1.3. Furthermore, the correlations for each instruments and the the differences in daytime where the mean BrO error increases to

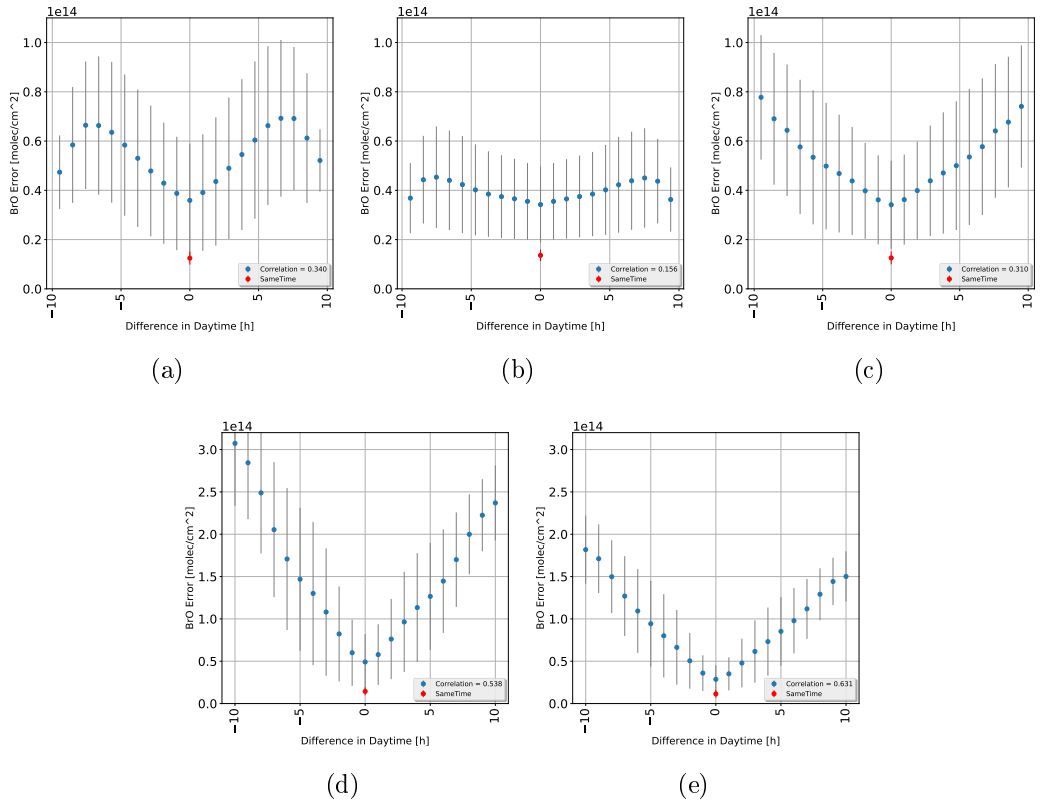


Figure 6.6: The BrO measurement error as a function of the difference of the day time between measuring the reference and the plume are shown. To evaluate the plume spectra all reference spectra with a temporal distance of no longer than two weeks are used. An increase of the BrO error with the distance in day time is observable.

Instrument	D2J2140_0	I2J8546_0	I2J8548_0	D2J2200_0	D2J2201_0
Mean	71.97 ≈ 85,1%	147.35 ≈ 90,0%	198.4 ≈ 91,4%	274.96 ≈ 96,8%	205.8 ≈ 91,2%
Std	31.87 ≈ 89,0%	31.98 ≈ 107,0%	70.96 ≈ 109,5%	70.78 ≈ 101,8%	50.08 ≈ 121,6%
Min	6 ≈ 75,0%	58 ≈ 51,3%	91 ≈ 93,8%	54 ≈ 84,4%	45 ≈ 71,4%
Max	160 ≈ 94,7%	214 ≈ 100,0%	399 ≈ 100,0%	433 ≈ 100,0%	297 ≈ 100,0%

Table 6.4: Remaining amount of References if the maximal accepted daytime difference is 4.75h. The percentages values refer to the decrease of the data relative to Table 6.1. 4.75h is the mean of the  $\Delta DT_2$ s in section 6.1.3 without I2J8546\_0 due to the large uncertainty at I2J8546\_0

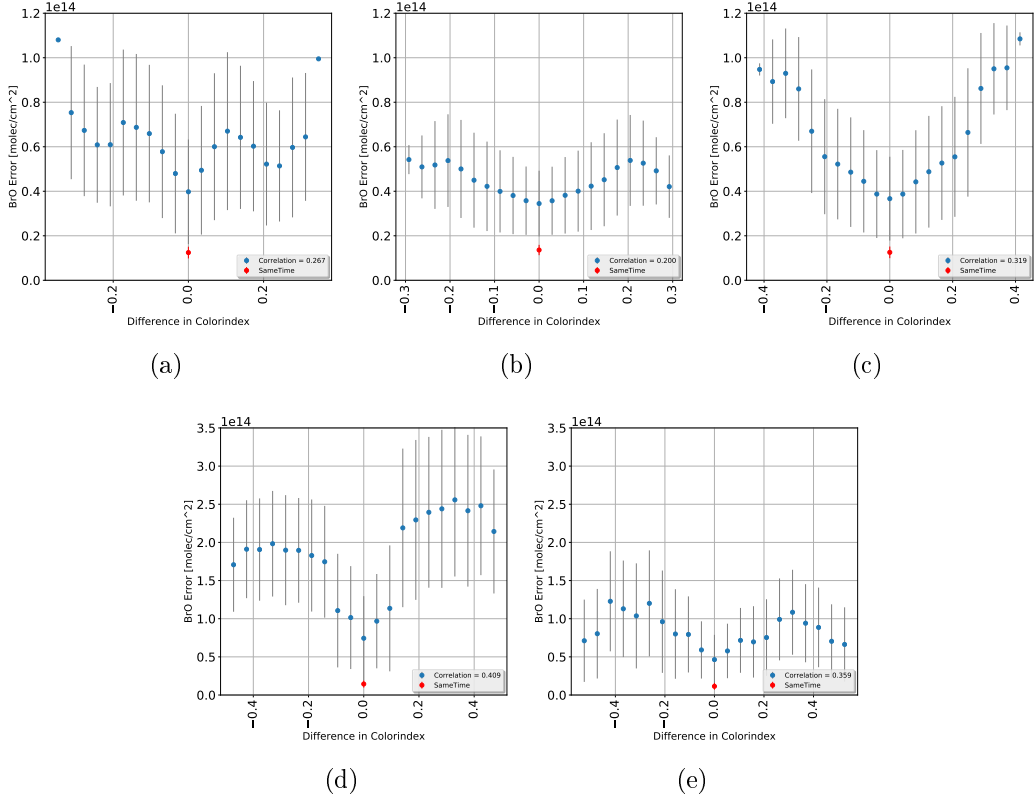


Figure 6.7: The BrO measurement error as a function of the difference of colorindex between measuring the reference and the plume are shown. To evaluate the plume spectra all reference spectra with a temporal distance of no longer than two weeks are used. A increase of the BrO error with the distance in colorindex is observably.

twice of the zero point ( $\Delta DT_2$ ) are shown. To gain more control about the algorithm a maximal daytime difference is defined where the corresponding references are still acceptable. The maximum daytime difference is defined as the mean  $\Delta DT_2$  of every instrument. Since the data from instrument I2J8546\_0 does not significantly depend on the daytime, this instrument was excluded for the calculation of the mean. Mean( $\Delta DT_2$ ) = 4.75. If restricting the data to only references with corresponding daytime of below Mean( $\Delta DT_2$ ) we get an averaged decrease of possible references of 9%. All decreases compared to table 6.1 are listed on table 6.4.

#### 6.1.4 Colorindex

Clouds have a strong influence on the atmospheric radiative transfer and thus affect the interpretation and analysis of DOAS - observations (Wagner et al., 2014).

Clouds can be identified by several measurement quantities that they influence. As Mie scattering is dominant in clouds the wavelength of the light that is scattered is

different than the Rayleigh sky. Thus, clouds can be easily identified by their white color. Therefore, the cloudiness of the sky can be quantified in a scalar measure defined by the ratio of the measured intensity at two wavelengths, the so-called colour index. Wagner et al. (2014) showed that for a zenith-looking instrument the measured radiation intensity is enhanced by clouds. Thus, clouds can cause large errors for the retrieved gas column density and the corresponding uncertainties. Cloud effects are especially severe if the cloudiness for the recorded plume and reference spectra strongly defer. Also for broken clouds the described effect can be observed as measurements at some elevation angles might be influenced by clouds while others are not. In this work the Colour Index (CI) is the ratio between the intensities at 320nm and 360 nm. These two wavelengths are as far apart as the filter used for stray-light prevention in the spectrometers allows. On the other hand, the lower wavelength avoids the deep UV range where SO<sub>2</sub> and O<sub>3</sub> absorption plays a dominant role. The Mie scattering in the clouds is responsible for the higher amount of radiation from larger wavelengths. This results in a decrease of the CI (Lübecke, 2014).

We evaluated the CI at the zenith, to increase the stability of the fit we added in each cases 10 intensities. Using always the zenith to evaluate the colour index makes the colour index more comparable, but if broken clouds occur, the CI of the reference and the plume could differ from the calculated CI of the zenith. This could be a reason for the large deviations of the mean BrO error as function of the colour index (see Figure 6.7)

- The BrO error as a function of the difference in colour index is also symmetric around zero for all observed instruments, thus the absolute difference in colour index is sufficient for the evaluating.
- The BrO error decreases for extreme differences in colour index for almost all instruments, the only exception is the I2J8548\_0 at Tungurahua. Especially at D2J2140\_0 the curve is not monotonically increasing with increasing difference in colorindex. Even though D2J2140\_0 is symmetric around zero.

Instrument	D2J2140_0	I2J8546_0	I2J8548_0	D2J2200_0	D2J2201_0
Slope	2.30e+14	7.92e+13	1.17e+14	5.42e+14	1.91e+14
Correlation	0.267	0.200	0.319	0.409	0.359
Zero point	4.01e+13	3.36e+13	3.47e+13	7.21e+13	4.74e+13
$\Delta CI_2$	0.174	0.424	0.297	0.133	0.248

As for the temperature and the daytime the BrO error was fitted on the absolute differences in colorindex with a polynomial of the first grad for each instrument. The absolute difference can be taken due to the symmetric around zero as it can be seen in fig. 6.7. The results including the slope, zero point, correlation and the

Instrument	D2J2140_0	I2J8546_0	I2J8548_0	D2J2200_0	D2J2201_0
Mean	84.6≡ 100,0%	163.7≡ 100,0%	215.6≡99,3% 100,9%	275.4≡97,0% 97,6%	219.4≡97,3% 121,0%
Std	35.8≡100,0% 100,0%	29.9≡ 100,0%	65.4≡ 100,9%	67.8≡ 97,6%	49.86≡ 121,0%
Min	8≡ 100,0%	113≡ 100,0%	97≡ 100,0%	61 ≡ 95,3%	28 ≡44,4% 100,0%
Max	169≡ 100,0%	214≡ 100,0%	399≡ 100,0%	421 ≡ 97,2%	297 ≡ 100,0%

Table 6.5: Amount of Possible references while restricting the difference in colorindex between plume and reference to differences above 0.2553.

Instrument	D2J2140_0	I2J8546_0	I2J8548_0	D2J2200_0	D2J2201_0
Mean	38.98	113.8	153.2	223.8	149.37
Std	24.47	50.6	76.78	82.5	72.41
Min	1	8	12	3	6
Max	130	213	386	399	296

Table 6.6: Amount of Possible references while restricting the difference in colorindex between plume and reference to differences above 0.2553. maximal Time difference is  $3.358^{\circ}C$ ,maximal daytime diff is 4.75h without

colorindex where the BrO error increases to twice of the zero point ( $\Delta CI_2$ ) are listed an section 6.1.4. The data were restricted to references where the corresponding colorindex difference is below the mean of the  $\Delta CI_2 = 0.256$ . The remaining number of references compared to table 6.1 can be found in table 6.5

### 6.1.5 Elevation Angle

The elevation angle describes the angle between the horizon and the zenith. When using the plume spectrum and the reference spectrum of the same time, the difference in elevation angle cannot be zero, since the location of the plume does not coincide with the location of the reference.

As can be seen in fig. 6.8 the BrO error does not depend significantly on the difference between the Elevation Angles. This could have several reasons. One problem is, that the Elevation Angle of Plume and Reference spectrum is not the same. This could also be a reason of uncertainty of the evaluations of the plume spectrum. Only the data of the D2J2200\_0 instrument vary with the elevation angle. The observable variation of the BrO error with the elevation angle differs from the symmetric

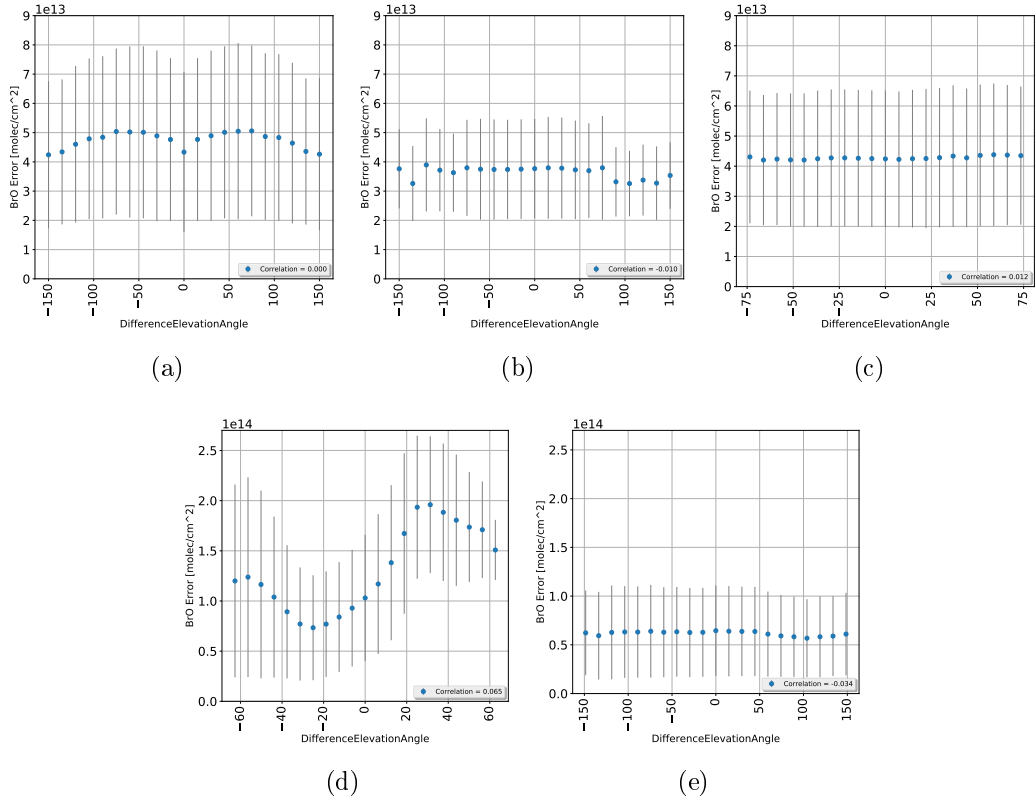


Figure 6.8: The BrO measurement error as a function of the Elevation Angle. To evaluate the plume spectra all reference spectra with a temporal distance of no longer than two weeks are used. We can't see any significant correlation.

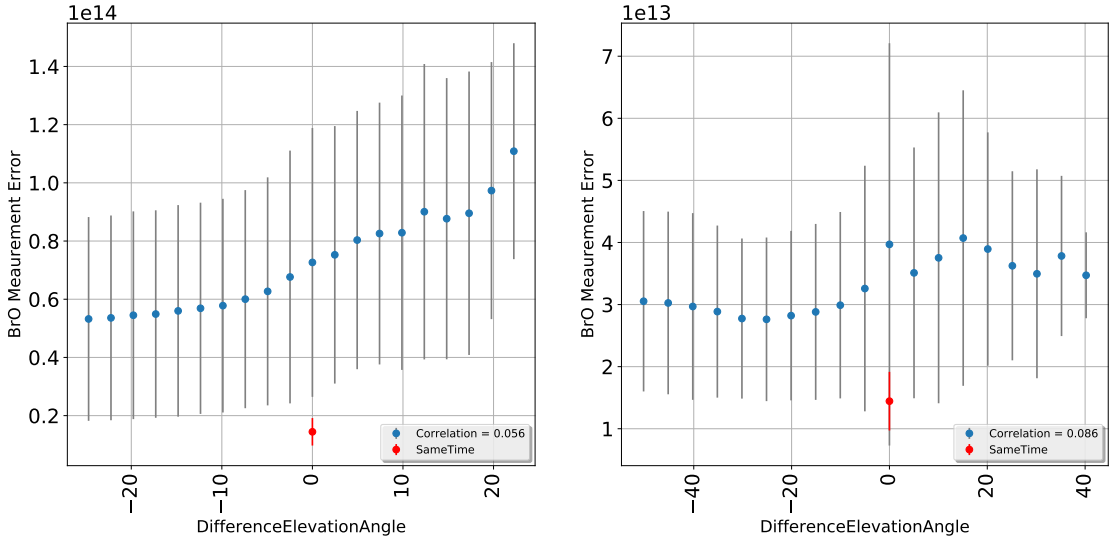


Figure 6.9: Left: constant daytime,right: constant temperature

dependence of all other external parameter, the minimum BrO error can be found at a difference in elevation angle of  $-20^\circ$ . This curve is a result of the solar altitude over the day which can be seen if we only use data of the same day time. Such a plot can be seen in ?.

- The BrO error as a function of the difference in colour index is also symmetric around zero for all instruments, except D2J2200\_0 at Nevado Del Ruiz.
- Only D2J2140\_0 shows a minimum of the BrO error at a difference in Elevation Angle of  $0^\circ$ . The BrO error curve from D2J2200\_0 shows a minimum at around  $-20^\circ$ .
- Because there is no significant dependence between BrO error and the difference in Elevation Angle it will not be considered in further analysis.

Instrument	D2J2140_0	I2J8546_0	I2J8548_0	D2J2200_0	D2J2201_0
Slope	1.73e+8	1.55e+10	-9.00e+9	2.92e+11	-3.96e+10
Correlation	0.000	-0.010	0.012	0.065	-0.034
Zero point	4.77e+13	4.23e+13	3.78e+13	8.37e+13	6.44e+13

Since the BrO error does not depend noticeable on the Elevation Angle no restriction on differences of the elevation angle are needed.

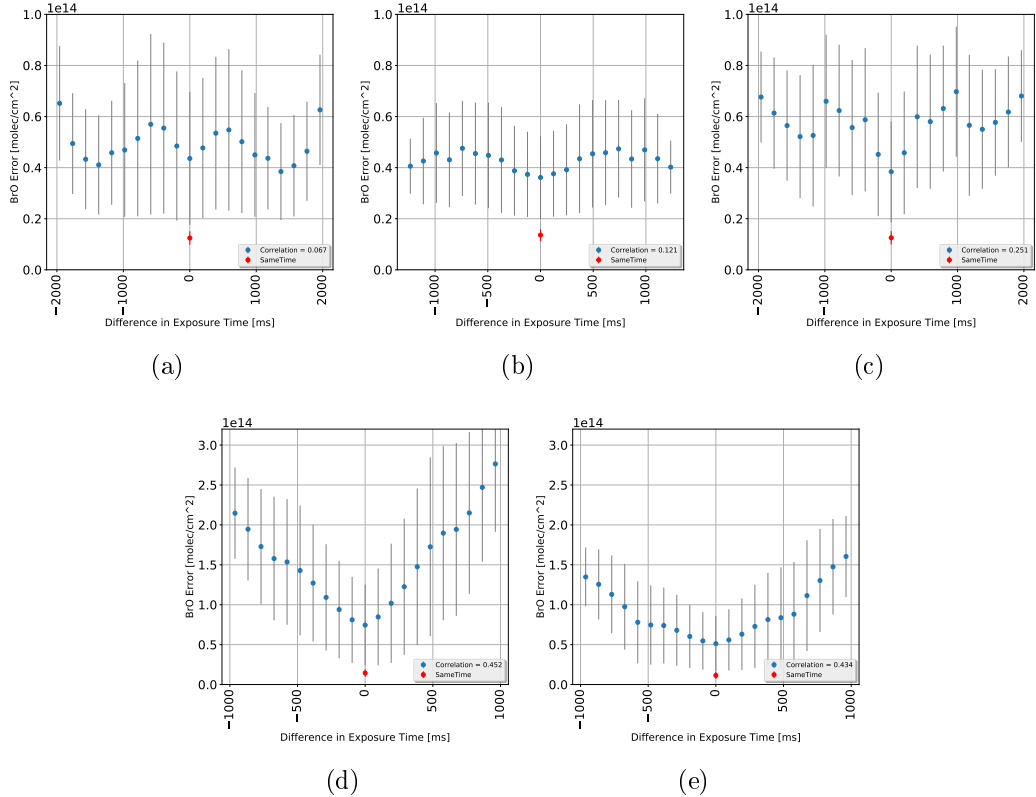


Figure 6.10: The BrO measurement error as a function of the difference of exposure time between measuring the reference and the plume are shown. To evaluate the plume spectra all reference spectra with a temporal distance of no longer than two weeks are used. A increase of the BrO error with the distance in exposure time is observably.

### 6.1.6 Exposure Time

The Exposure Time is a degree of sky lightness. The exposure time is the length of time the sensor of the NOVAC instrument is exposed to light. In one scan the exposure time is set constant to the exposure time of the first scan, the pre reference. The amount of light that reaches the film or image sensor is proportional to the exposure time. The exposure time is adjusted in the way that the maximum intensity does not overly the capacity of the sensor.

We can observe an small dependency of the BrO error on the Exposure time at Tungurahua and Nevado Del Ruiz as it is shown in Figure 6.10

- The BrO error as a function of the difference in Exposure Time is also symmetric around zero for all observed instruments, thus the absolute difference in the Exposure Time is sufficient for the evaluating.
- The instruments at Tungurahua does not show significantly dependence on the Exposure Time, even though there is always a minimum of the BrO error at a difference of the Exposure Time of 0ms.
- Nevado Del Ruiz shows a stronger correlation between the BrO error and the Exposure Time.

Instrument	D2J2140_0	I2J8546_0	I2J8548_0	D2J2200_0	D2J2201_0
Slope	5.54e+9	1.54e+10	3.04e+10	1.72e+11	9.37e+10
Correlation	0.067	0.121	0.251	0.452	0.434
Zero point	4.63e+13	3.58e+13	3.87e+13	6.88e+13	4.68e+13
$\Delta T_2$	8357	662	1273	95	499

Section 6.1.6 shows the slope, correlation, zero point and the  $\Delta ET_2$ s: the differences in Exposure time where the BrO error increases by a factor of two compared to the difference of exposure time of zero. Restrictions of the exposure Time to the mean of the  $\Delta ET_2$ s of all instruments which is 632.25 ms leads to an average decrease compared to table 6.1 of data of [hier den mittelwert](#). The results for each instrument can be found in table 6.7.

### Dependency of external parameters on each other

In all those discussions on the impact of the external parameter on the retrieved BrO error the dependency of the external parameter on each other were neglected. It is plausible that the temperature correlates with the cloudiness or the lightness due to sunlight. Therefore the correlation of the Exposure Time with the BrO error could be a result of the correlation of the Temperature with the BrO error. Figure 6.11 shows an example of the dependency of external parameters on each other. The

Instrument	D2J2140_0	I2J8546_0	I2J8548_0	D2J2200_0	D2J2201_0
Mean	81.67≡ 96,5%	162.79≡ 99,4%	212.78≡ 98,0%	283.99≡ 100,0%	225.59≡ 100,0%
Std	35.30 ≡ 98,6%	30.07 ≡ 100,6%	64.47 ≡ 99,5%	69.5 ≡ 100,0%	41.2≡ 100,0%
Min	8 ≡ 100,0%%	113≡ 100,0	95 ≡ 97,9%	64≡ 100,0%	63≡ 100,0%
Max	167≡ 98,8%	214 ≡ 100,0%	395 ≡ 99,0%	433 ≡ 100,0%	297 ≡ 100,0%

Table 6.7: Amount of Possible references while restricting the difference in Exposure Time between plume and reference to differences below 632.25ms

Instrument	D2J2140_0	I2J8546_0	I2J8548_0	D2J2200_0	D2J2201_0
Mean	36.0≡ 42,6%	112.9≡ 69,0%	148.88≡ 68,6%	217.0≡ 76,4%	140.38≡ 62,2%
Std	22.35 ≡ 62,4%	50.6 ≡ 169,2%	75.9 ≡ 117,1%	82.07 ≡ 118,1%	71.0 ≡ 172,3%
Min	1 ≡ 12,5%	8≡ 7,1%	12 ≡ 12,4%	3≡ 4,7%	6≡ 9,5%
Max	127≡ 75,1%	212≡ 99,1%	382≡ 95,7%	398 ≡ 91,9%	283≡ 95,3%

Table 6.8: Amount of Possible references while restricting the difference in colorindex between plume and reference to differences above 0.2553. maximal Time difference is 3.358°C,maximal daytime diff is 4.75h without Exposure Time between plume and reference to differences below 632.25ms

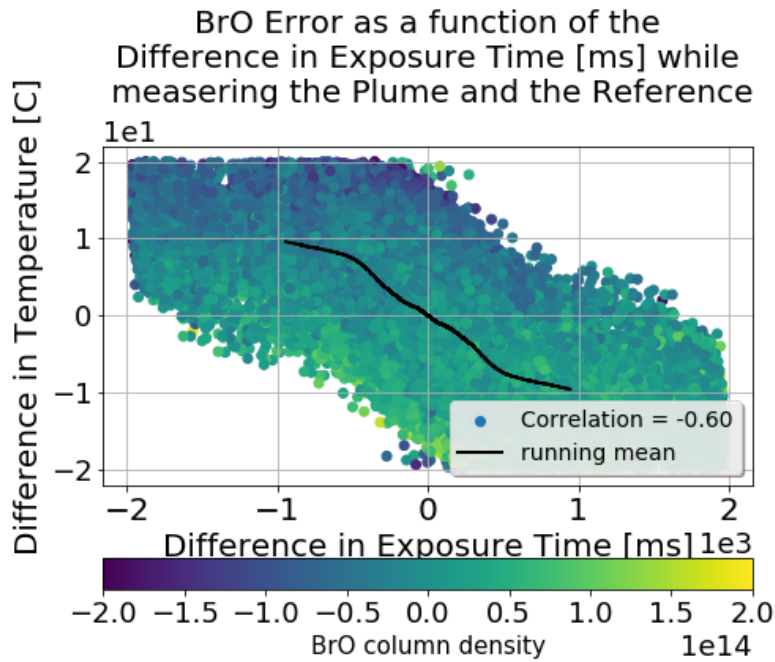


Figure 6.11: A example of the dependency of external parameters on each other. The difference in Temperature as a function of the Exposure Time. Data from Tungurahua

Difference in Temperature as a function of the Difference in Exposure Time. The BrO error is color-coded.

All correlations between the external parameters are shown in Figure 6.12. Figure 6.12 show discrete correlation values from 0.3 to 1. Correlations below 0.3 are ignored. Small plus and minus signs indicate whether the correlation is negative or positive. The difference in temperature correlates with the difference in daytime (Correlation of  $\approx 0.5$ ) with the difference in Exposure Time (Correlation of  $\approx 0.4$ ). The difference in temperature also slightly correlates with the difference in Colorindex (Correlation of  $\approx 0.3$ ) and the temporal difference (Correlation of  $\approx 0.3$ ) probably due to long term changes in Temperature. Furthermore the difference in Exposure Time correlates with the daytime and the colorindex (Correlation of  $\approx 0.4$ ).

To eliminate the correlation between the external parameters the BrO error dependency on one external parameter where calculated by keeping the differences in the other external parameters constant. The results can be seen in Figure 6.13 (Tungurahua) and Figure 6.14 (Nevado Del Ruiz). When comparing the correlations of the data from Figure 6.13 and Figure 6.14 to the correlations of Figure 6.5 to Figure 6.10 a large reduction of the correlation is obvious. Only the difference in Temperature still shows a significant correlation to the BrO error. However the minimal BrO error coincidence in almost all cases with a difference in external parameters of zero. An dependency of the BrO error on the external parameter can still be seen even

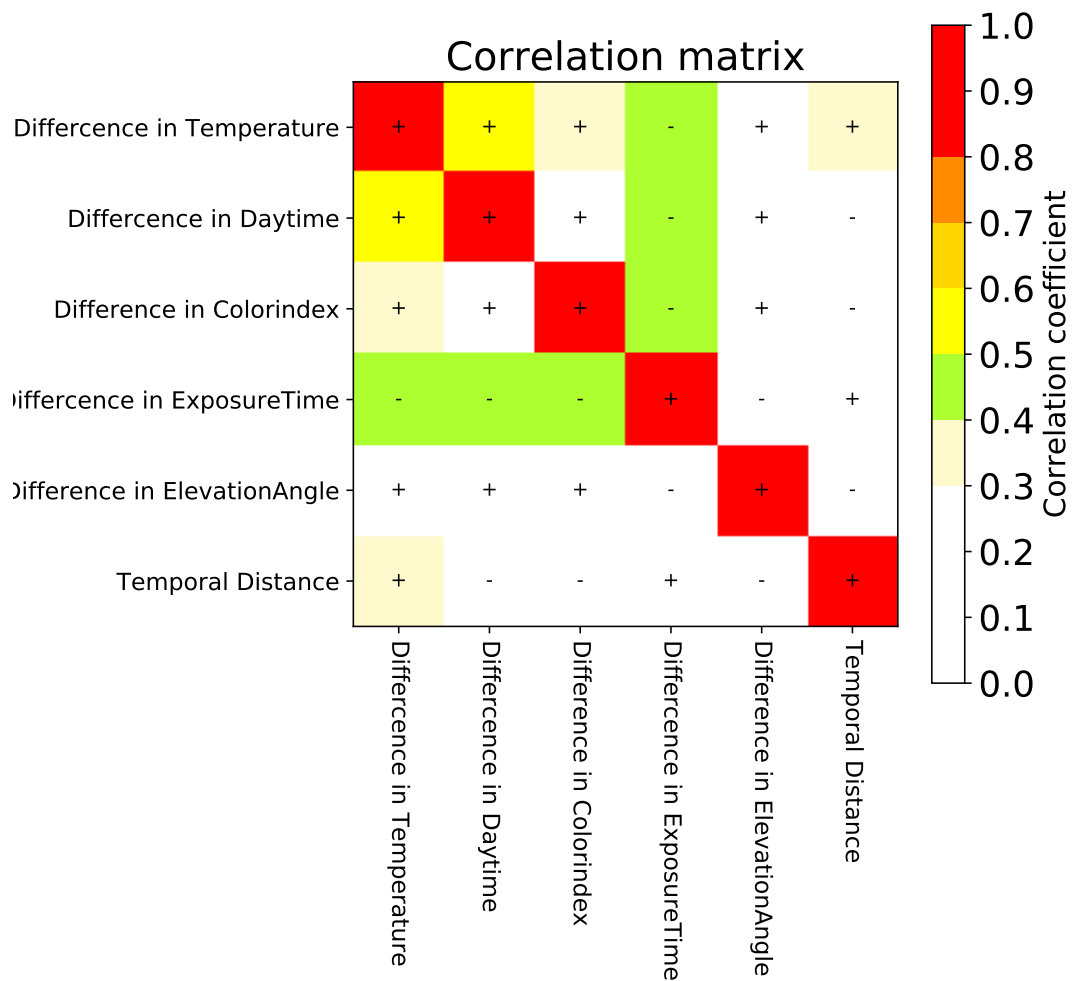


Figure 6.12: Correlation matrix of the external parameters. The correlation is discrete colour coded. Positive correlation is labeled with a plus whereas negative correlation is labeled with a minus.

tough the correlation is very small. And the variability (visualized as the length of the grey bars) increases with increasing difference in external parameters for almost all cases.

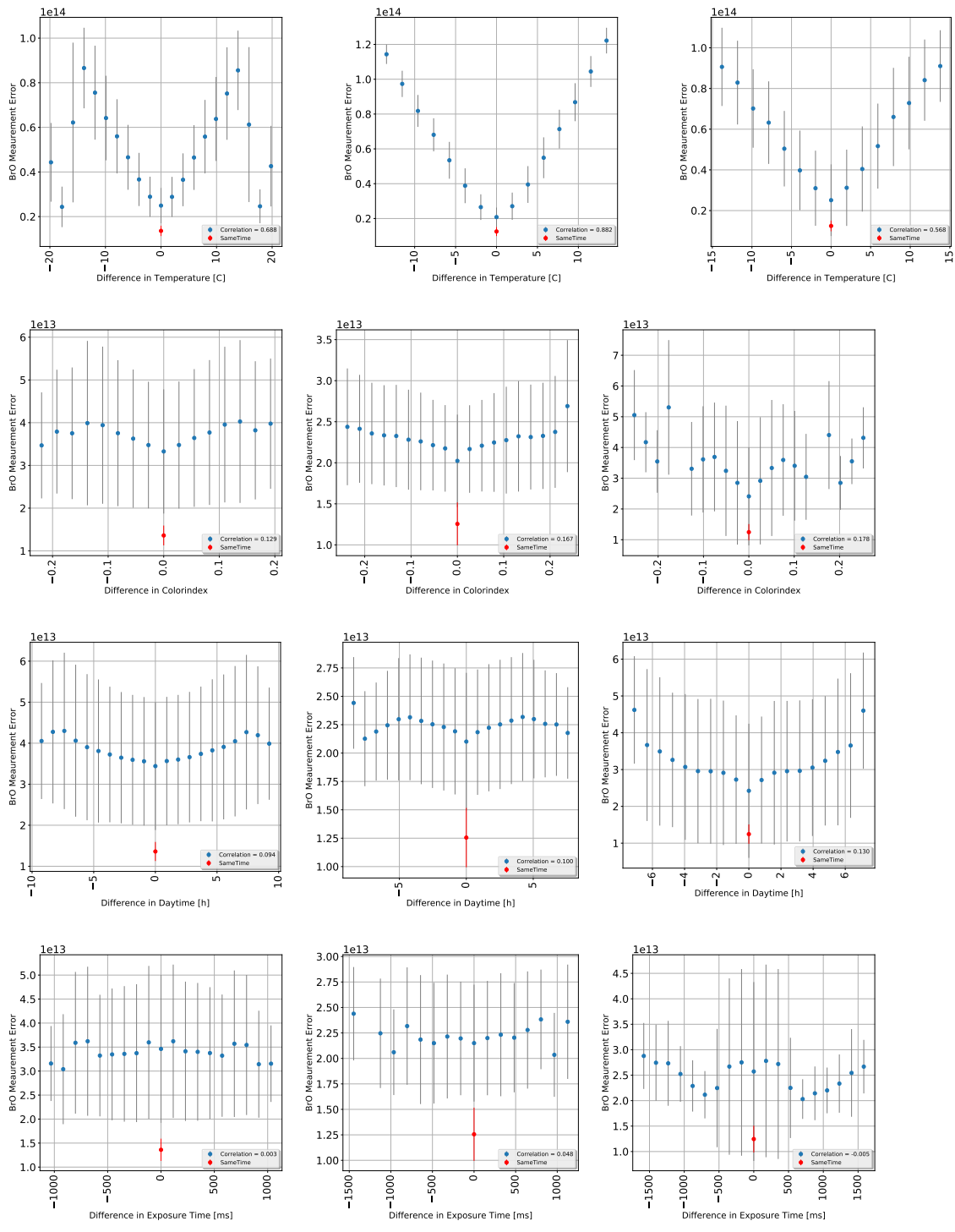
Excluding of the external parameters due to the rather low correlation lead to a worse quality of the results, since the effects of the single parameter add up to an not negligible amount. Although the added impact of all external parameter except for the temperature are less important than the temperature.

## Summary

This chapter examine the influence of external on the precision of the BrO evaluation. Herby the following parameter were considered: Temporal Difference, Temperature, Daytime, Colorindex, Elevation Angle, Exposure Time. The findings are based on the data of three instruments installed at the Tungurahua volcano and two instruments at the Nevado Del Ruiz volcano. The maximal temporal difference between measuring the plume and the reference was set two 14 days to prevent large uncertainties in the BrO evaluation. Due to the mechanical influence on the wavelength to pixel mapping the temperature has at all analysed instruments the most significant impact on the BrO evaluation of all considered external parameters. The Elevation Angle does not seem to influence the evaluation for all examined instruments thus the elevation is excluded from the evaluation. The influence of the other external parameter change at every instrument. So a relatively strong impact of the exposure time can be seen at the D2J2201\_0 instrument at Nevado Del Ruiz, while the exposure time does not seem to significantly influence the evaluation of the data from the I2J8548\_0 at Tungurahua. A large part of the impact of the external parameters results from the dependence on the temperature.

## 6.2 BrO dependence on external parameters

The external parameters not only influence the fit quality but also the evaluation of the gas amount. A high different in certain external parameter could distort the calculated BrO column density. Figure 6.15 shows the evaluation of one Plume with respect to different references. The temporal difference between the references and the plume do not exceed two weeks. In theory we expect that the choice of the reference should not make a difference, therefore all BrO column densities resulting from the evaluation should be equivalent. But we can see a high variation if choosing different references. The variability of the BrO column density depends as well on the external parameters, when looking at the temperature dependency a mean decrease of the BrO column density with the temperature can be seen. Figure 6.15 is a result of an exemplary evaluation of one plume. An examination of all several plumes evaluated by different references is shown in Figure 6.18. Here are equivalent plots shown as for the BrO error (see for example fig. 6.5). Figure 6.16 shows the exemplary evaluation of different plumes by on reference. Here we assume different



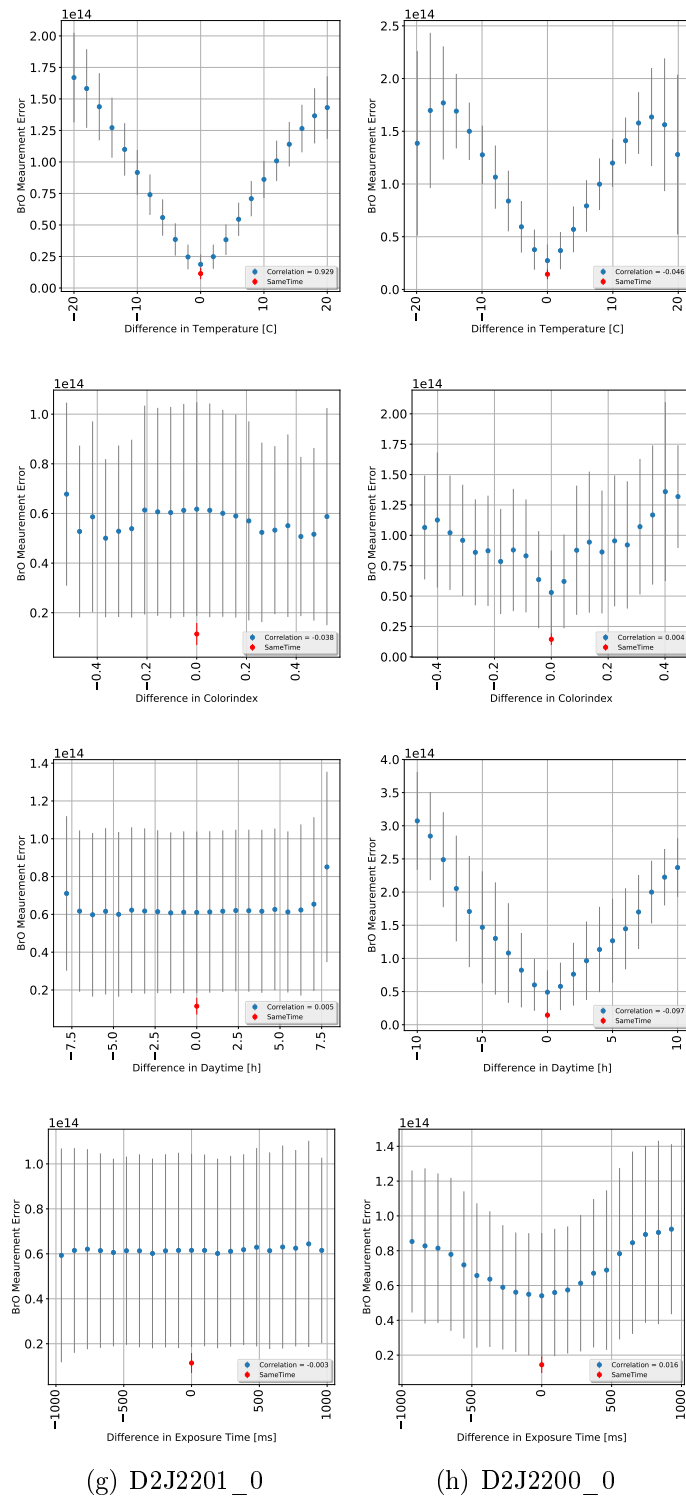
(j) I2J8546\_0

(k) I2J8548\_0

(l) D2J2140\_0

Figure 6.13: DiffExpTime at Tungurahua

Figure 6.14: BrO error as a function of the external while measering the Plume and the Reference at Nevado del ruiz



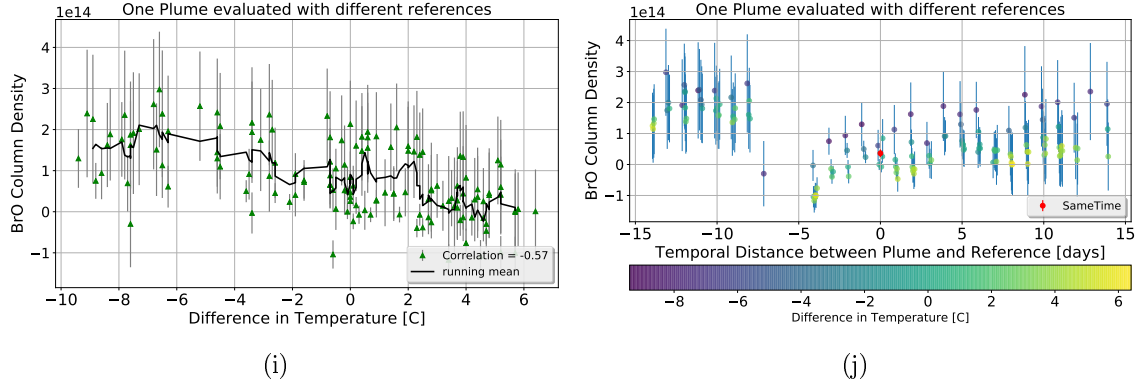


Figure 6.15: One Plume is evaluated by using different references. The plume was recorded at Tungurahua volcano with the D2J2140\_0 instrument. recording time was the 081203 at 1646 o clock. The y axis show the BrO column density differene between the NOVAC method and contamination based Method. (a) The difference in BrO is plotted as a function of the temperature difference between the plume and the references. Every data point indicates one reference. (b) The difference in BrO is plotted as a function of the temporal difference between the one plume and the different references

column densities, but this variability should be independent of the difference in the external parameters. But Figure 6.16 shows a clear dependence on the Temperature. The correlation for this example is -0.76, thus it can be concluded, that here is also a significant dependence. Examination of the Daytime

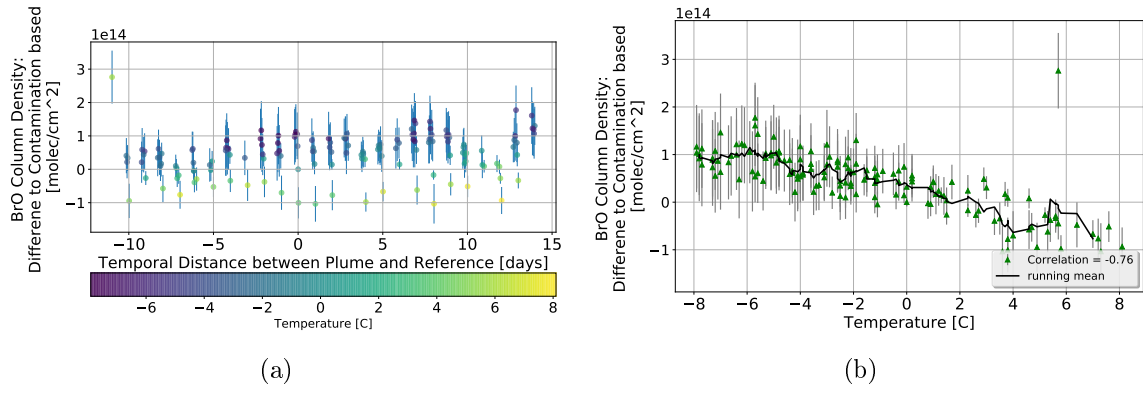


Figure 6.16: One Reference is used to evaluated different Plume spectra. The reference was recorded at Tungurahua volcano with the D2J2140\_0 instrument. recording time was the 081115 at 1337 o clock. The y axis show the BrO column density. (a) The BrO is plotted as a function of the temporal difference between the one reference and the plumes (b) The BrO is plotted as a function of the temperature difference between the plume and the references. Every data point stands for another plume evaluated with the same reference.

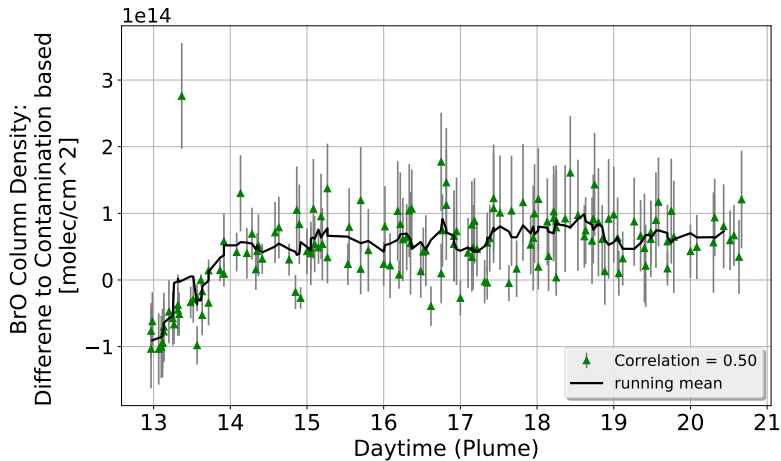


Figure 6.17: The difference of BrO when performing the evaluation with The NO-VAC Method minus the contamination based method as a function of the Daytime when measuring the plume. The recording time of the reference was 081115 at 1337 o clock

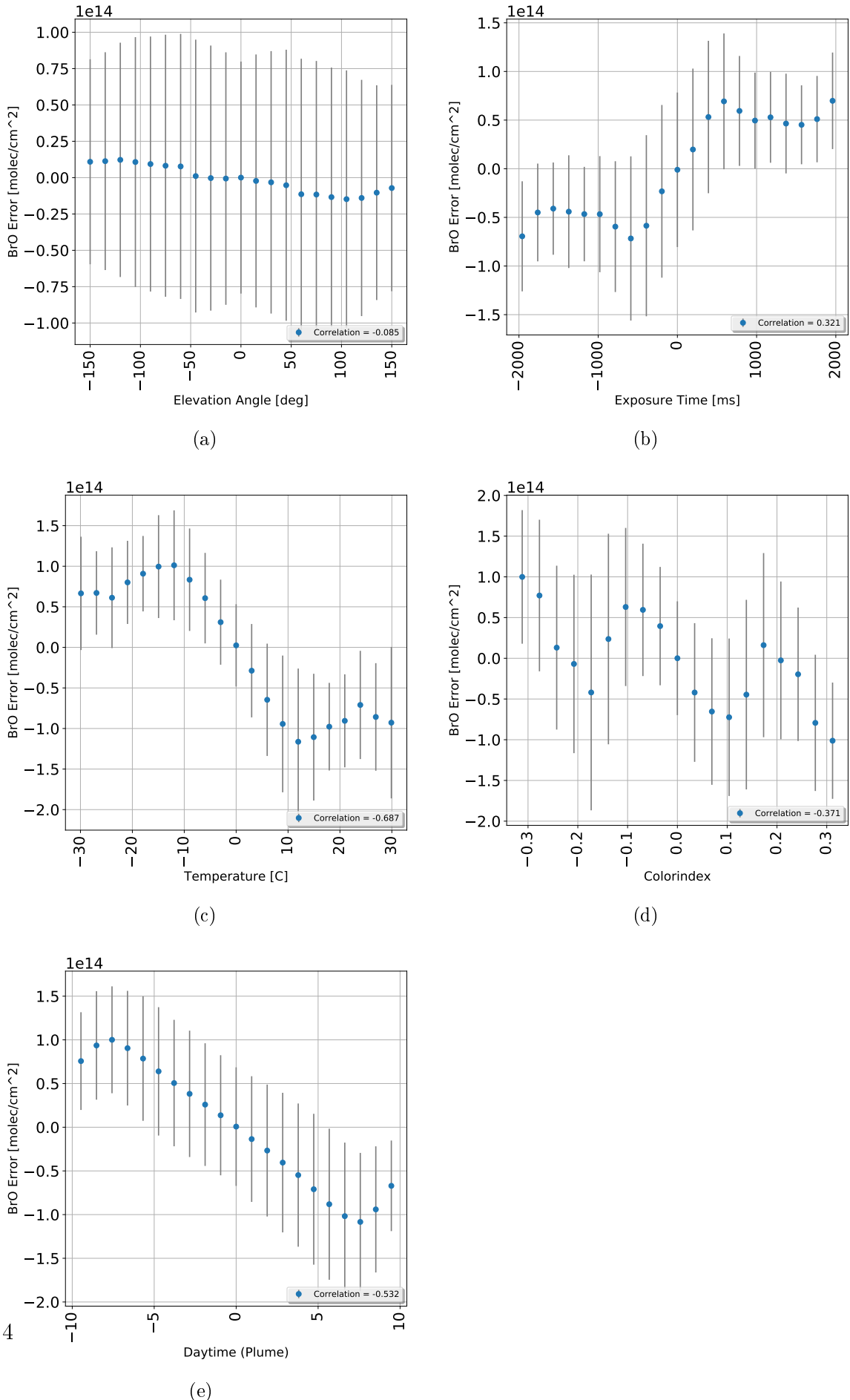


Figure 6.18: The Dependence of the BrO evaluation on external parameter is shown.

## 7 Contamination based method

Based on the findings about the influence of external parameters on the BrO error we developed an algorithm which is able to pick an appropriate volcanic-trace-gas free reference.

The first step is, to evaluate every reference with solar atlas spectrum, to check for contamination.

If the reference is contaminated:

- We have a list of possible references where all references are not contaminated and the temporal distance to the plume date is no longer than 14 days.
- we calculate of all possible references the differences in the external parameters
- We use the analysis of external parameters described above to estimate the BrO error of all references
- We choose the reference with the smallest estimated BrO error as new reference
- We evaluate the plume spectra with the new reference.

The assumption is, that the BrO error  $\epsilon_{BrO}$  can be described as the sum of  $\epsilon_0$  and the deviation of  $\epsilon_{BrO}$  with respect to all external parameters.  $\epsilon_0$  is the BrO error when evaluate the plume spectrum with the "same-time-reference", it is determined due to the accurateness of the NOVAC-instruments.

$$\epsilon_{BrO} = \epsilon_0 + \frac{d\epsilon}{dt} + \frac{d\epsilon}{d^\circ} + \frac{d\epsilon}{dT} + \frac{d\epsilon}{dt} + \frac{d\epsilon}{dc} + \mathcal{O}(OE) \quad (7.1)$$

$$\rightarrow \Delta\epsilon_{BrO} = \epsilon_{BrO} - \epsilon_0 = \underbrace{\frac{d\epsilon}{dt}}_{=0} + \frac{d\epsilon}{d^\circ} + \frac{d\epsilon}{dT} + \frac{d\epsilon}{dt} + \frac{d\epsilon}{dc} + \mathcal{O}(OP) \quad (7.2)$$

With  $\epsilon_{BrO}$  describes the BrO error, t: time between plume-time and reference-time, T, temperaure; dt: daytime, c: colorindex, OP: other excluded external parameters  
The task occurring at this stage is to find the best representation for the deviations.  
An then find the reference which minimize  $\Delta\epsilon_{BrO}$

The easiest way is to just calculate the BrO error of all possible references for every plume. Using this method we would be able to just choose the reference where the BrO error is minimal. But this takes to much time since the evaluation time would be proportional to the number of possible references because the evaluation need

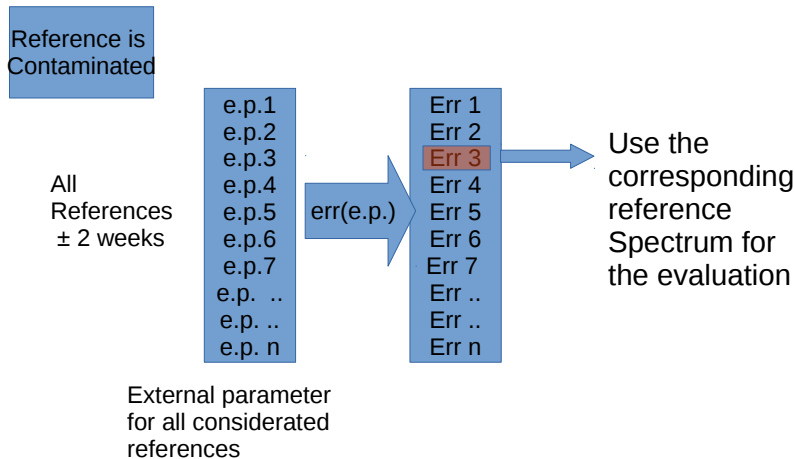


Figure 7.1: Visualization of the contamination based Method. If the reference is contaminated a list of possible references is available, where the temporal difference between the plume and the reference is not longer than two weeks. For every possible reference, the estimated BrO error is calculated by considering the corresponding difference in important external parameters. The reference with the so calculated minima BrO error is used for the evaluation.

to be done for every plume-reference pair. Doing the evaluation for every plume-reference pair would make it impossible to do the evaluation in real, or near real time.

But we use this optimal evaluation to rate our model and compare them among each other. The optimal evaluation always choose the reference with the smallest absolute error. We don't use the relative error due to his vulnerability. Using the relative error could lead to a less precisionness since the references with the highest BrO column density would be preferred.

The results of the algorithm which chooses the reference automatically are described relative to an optimal evaluation. If the relative error is larger than 5 the data are excluded from the evaluation.

We tried several methods for choosing the best reference based on the analysis of external parameters. Fitting the data with a first order polynomial brought the best results.

## 7.1 Fit data

The following chapter analyses the possibility of fitting the data by a first order polynom. Figure 6.5-Figure 6.10 show the BrO error as a function of external parameters. Hereby are the curves symmetric around zero differences in the respective

external parameter. Therefore it is not necessary to distinguish between positive or negative deviations from the equal surrounding conditions. Thus the absolute differences can be taken.

A linear approximation of the BrO error as function of the considered external parameter leads to a variation of Equation (7.2) : With linear differentiations of the BrO error with respect to the respective external parameters Equation (7.2) can be written as:

$$\Delta\epsilon_{BrO} = a_t \cdot \Delta t + a_{ET} \cdot \Delta ET + a_T \cdot \Delta T + a_{dt} \cdot \Delta dt + a_c \cdot \Delta c + \mathcal{O}(OP) \quad (7.3)$$

To determine the coefficients  $a_x$  (Equation (7.3)) the data as from Figure 6.5-6.10 where used. The fitting was done with an ordinary least square linear regression. In particular we used the python function Linear Regression from the library sklearn (SKI).

As can be seen in Section 6.1 the impact of the different external parameters change for every instrument depending on the location and the instrument themselves. Whereas the BrO error not show any dependence on some external parameter at some instrument the error has very strong dependence on the same external parameter at another instrument. An example is the correlation between BrO error of 0.6 at D2J2201\_0 (Nevado Del Ruiz) and a correlation of 0.16 at I2J8546\_0 at the Tungurahua volcano. To get a more stable algorithm less external parameter are preferable. Thus we need to distinguish between the stability of the fit, which favours less external parameters and quality of the fit, which favours more external parameters. A preferable solution is, to find a solution which is valid for all instruments at the same time to save calculation time. One possibility is to use all external parameter where the correlation is above a certain number, since we want to get a selection valid for all instruments there are two possibilities: The first one is we decide by using the mean correlation of all instruments, the second option is to use the highest correlation

	Mean Correlation	Highest Correlation
Temperature	0.798	0.92
Colorindex	0.3108	0.409
Exposure Time	0.265	0.452
Elevation Angle	0.02	0.067
Daytime	0.395	0.631

To answer this question quantitatively for the fitting routine we evaluated data of Tungurahua and Nevado Del Ruiz with different combinations of the external

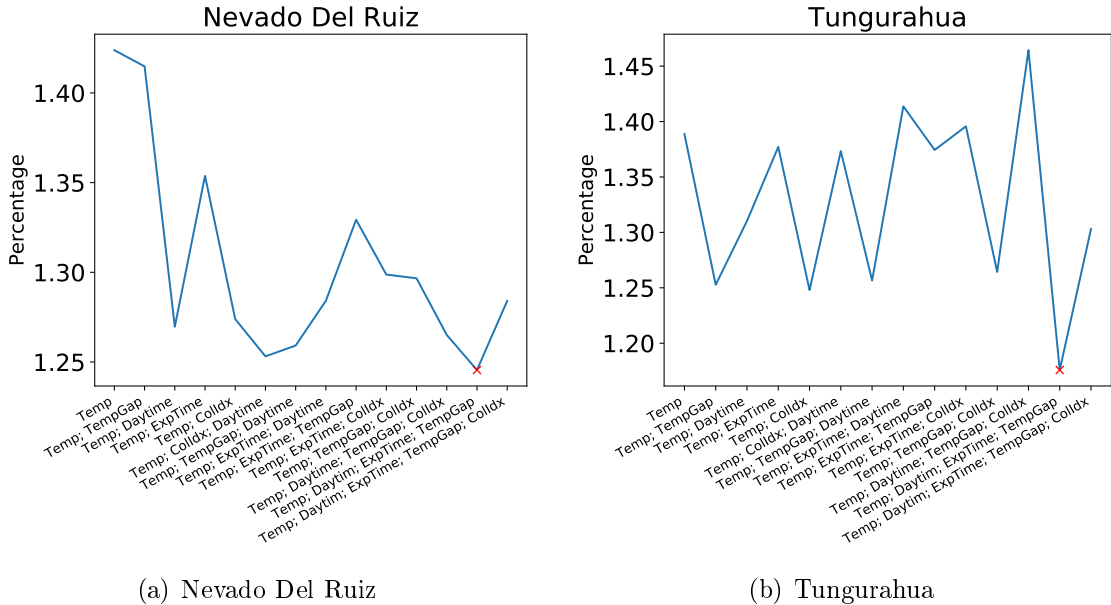


Figure 7.2: Deviation from the "optimal evaluation" as a function of the selection of differences in external parameters which are used for the evaluation

parameter described in Section 6.1. Since we could not observe any correlation between the BrO error and the Elevation angle the external parameter elevation angle was neglected in this analysis. To rate the results for the single instruments (three at Tungurahua and two at Nevado Del Ruiz) the difference to the "optimal evaluation" (explained in ??) was used. Hereby the factor x, a quantity which describes the distinction between the optimal-Method and the contamination based method serves as indicator:

$$X = \frac{1}{n} \sum_k^n \frac{EContBased_k}{EOpt_k} \quad (7.4)$$

$n$  is the total amount of contaminated spectra,  $EOpt$  is the BrO error, in the optimal-evaluation,  $EContBased$  is the BrO error, in the contamination based-evaluation. Figure 7.2 shows the calculations of the x factor for the Tungurahua and the Nevado Del Ruiz volcano. The x-axis shows the external parameter used for the factor X. The y-axis shows the added factors x for every instrument at the volcanoes. The x factors were weighted with the percentage amount of data. The factors X change from instrument to instrument. The results for every instrument can be seen in the appendix (Figure .1). The factors X range from 1.18 to 1.42.

Single references-plume pars result in an very high BrO error, which has a very high impact on the calculation of the X factors. If using the median and not the mean as described in Equation (7.4) our method is mostly better than the "optimal method". As in Figure 7.2 can be seen for both volcanoes the x factor is minimal for the combination of the following external parameters:

- Temperature
- Daytime
- Colorindex
- Temporal Difference

For the final algorithm this combination of external parameters is used. The coefficients  $a_x$  were calculated for each instrument at Nevado Del Ruiz and Tungurahua. Furthermore the coefficients  $a_x$  are calculated with the combined data from all instruments installed at one volcano. The results for the Nevado Del Ruiz volcano can be found in Table 7.1 and for the Tungurahua volcano in Table 7.2.

As it can be concluded from Figure 7.2 The best results are found if all parameters are used with a mean correlation above 0.3 (see Section 7.1)

## 7.2 Other approaches

Fitting is not the only possibility of finding the optimal reference out of the list of all possible references.

Also other possibilities were tried to find the best algorithm. In the following two additionally possibilities are presented. Both are based on the findings in section 6.1.

### 7.2.1 Nearest neighbor approach

Beside linear regression also the nearest neighbor approach can be utilized to estimate the BrO error for the evaluation with a potential reference spectrum. The nearest neighbor search describes an optimization problem for a given point  $m \in \mathbb{R}^n$  and a set  $S \subset \mathbb{R}^n$ :

$$\bar{s}(m) = \min_{s \in S} d(m, s) \quad (7.5)$$

Here  $d(\cdot, \cdot)$  is a distance function that computes the dissimilarity between the two input arguments. Typical distance metrics are the L1 distance  $d_{L1}(m, s) = \|m - s\|$  or the L2 (also euclidean) distance function  $d_{L2}(m, s) = \|m - s\|^2$ .

In many cases not only one nearest neighbor but a set  $M$  of  $k$  nearest neighbors is of interest. In this case the optimization problem of Eq. 7.5 must be modified to

$$\bar{S}_k(m) = \min_{S_k \subset S} \sum_{s \in S_k, m \in M} d(s, m) \quad (7.6)$$

In many cases the nearest neighbor search is used to estimate a target variable  $y_m$  for a feature vector  $m \in \mathbb{R}^n$ . This method assumes a given set feature vectors  $S$  for which the target variables  $y_S$  are known. Then the target variable  $y_m$  for a given  $m$  can be estimated by:

	(b) Data of Nevado Del Riz D2J2201_0		(c) Data of Nevado Del Riz D2J2200_0		(d) Data of Nevado Del Both Instruments	
Constant	value	import	value	import	value	import
$a_T$	7.505e+12	0.866	1.179e+13	0.925	1.07e+13	0.973
$a_{CI}$	3.482e+13	0.048	1.024e+14	0.046	3.48e+10	0.070
$a_t$	-3.2e+09	0.0	-1.6e+09	0.0	-9.1e+08	0.0
$a_{dt}$	1.869e+12	0.095	1.054e+12	0.033	1.52e+11	0.006
					-6.81e+13	-0.047

Table 7.1: (a)Data from Nevado Del Ruiz from the D2J2201\_0 instrument. All external parameter where taken into account.  $\epsilon_0 == 5.404e + 12$  (b)Data from Nevado Del Ruiz from the D2J2200\_0 instrument. All external parameter where taken into account.  $\epsilon_0 == 1.105e + 13$  (c) Data from Nevado Del Ruiz from both instrument. All external parameter where taken into account.  $\epsilon_0 = 1.260e + 13$

$$y_m = \frac{1}{k} \sum y_s \quad (7.7)$$

## Advantages of the Nearest Neighbor approach

The main advantage of the nearest neighbor method is that there is no need for a pre-assumption of a fitting method. The fitting method is presupposing that the BrO error depends linear on the external parameter. As it can be seen in fig. 6.5-fig. 6.10 this do not need to be tha case. Thus the nearest neighbor method is able to approximate the BrO error as a function of the external data in a more variable way.

## Disadvantages of the Nearest Neighbor approach

Compared to fitting the data, the nearest neighbor is much slower. This is a result of the need for a complex calculation for every checked reference plume pair. Thus, the calculation time increases with the amount of learning data.

To normalize the distances d, the normalization function need to be choose and therefore pre-assumptions about feature importance are required. Including the fact, that the results of the nearest neighbor method a little worse compared to the fitting method, the disadvantages of the nearest neighbor method outweigh the advantages.

	(b) Data of Tungurahua D2J2140_0		(c) Data of Tungurahua I2J8548_0		(d) Data of Tungurahua I2J8546_0	
Constant	value	import	value	import	value	import
$a_T$	3.732e+12	0.664	6.459e+12	0.920	3.939e+12	0.850
$a_{CI}$	6.982e+13	0.078	2.760e+13	0.066	-1.521e+13	-0.042
$a_t$	3.5e+10	0.2	1.2e+10	0.13	2.0e+10	0.2
$a_{dt}$	7.797e+11	0.069	-6.049e+11	-0.055	1.158e+11	0.017

(e) Data of Tungurahua I2J8546_0	
value	import
5.055e+12	0.838
2.534e+13	0.057
1.8e+10	0.117
-1.109e+11	-0.012

Table 7.2: (a)Data from Tungurahua from the instrument. All external parameter where taken into account.  $\epsilon_0 = 5.404e + 12$  (b)Data from Tungurahua from the instrument. All external parameter where taken into account.  $\epsilon_0 = 1.105e + 13$  (c) Data from Tungurahua from all instrument. All external parameter where taken into account.  $\epsilon_0 = 1.260e + 13$ , both instruments Tungurahua zero point =  $1.610e+13$

### 7.2.2 Iterative approach

The idea of the iterative method is, that the importance of the individual external parameters are very different, that means if we have the list of possible references, we took all referenes where the temperature difference is minimal, so we get a new, much smaller list of possible referenecs. From this list we choose all references where the next external parameter for example the daytime is minimal and get again a new list. We proceed this way with the following external parameters. We experiment with the sequence of the parameters, to increase the success of the method. The final sequence was:

$$Temperature \bullet Daytime \bullet Colorindex \bullet TemporalDifference \bullet ExposureTime$$

## 8 Comparison with NOVAC evaluation

This chapter shows and discuss the difference of the BrO, SO<sub>2</sub> and BrO/SO<sub>2</sub> ratio data when evaluating with the NOVAC-Method, or with the contamination based method. The aim is to discover the systematic differences between the different retrievals and to discuss the reliability of the data.

To obtain the reference with minimal expected BrO error the calculation of Equation (7.3) and the corresponding coefficients from Table 7.2 (Tungurahua) and Table 7.1 (Nevado Del Ruiz) were used. For the retrieval only "Multi Add" data were used. The maximal temporal difference between measuring the reference and the plume is two weeks.

We restricted non of the external parameter due to the higher x factor as it can be seen in ...

Furthermore we do not distinguish between the individual instruments. ????????????

Figure 8.1 shows a comparison of the results of contaminated data for performing the evaluation with the NOVAC-method and the contamination based method. The x-axis shows the column density of BrO respectively SO<sub>2</sub> calculated with NOVAC-method, the y-axis shows the column density calculated with the contamination based method. Only data are used where the corresponding SO<sub>2</sub> column density lies above the plume limit ( $SO_2\_SCD > 7 \cdot 10^{17}$ ). Meaning the column densities evaluated with the contamination based method. The corresponding SO<sub>2</sub> SCD's evaluated with NOVAC could be below  $7 \cdot 10^{17}$ . The plots at the left side (Figure 8.1(a) and 8.1(c)) show the results from the Tungurahua volcano while the plots at the right side (Figure 8.1(b) and 8.1(d)) show the results from Nevado Del Ruiz volcano. The black solid line shows a linear fit of the data, the dotted line indicates where the both evaluation are equivalent.

Figure 8.1(a) respectively 8.1(b) show the results for the BrO retrieval:

- The BrO column densities retrieved due to the contamination based method have become larger on average compared to the NOVAC method.
- An almost constant offset of  $1.2 \cdot 10^{13}$  (Tungurahua) and  $2.0 \cdot 10^{13}$  (Nevado Del Ruiz) can be seen.

The constant offset between the results from the contamination based method and the NOVAC-method leads to the assumption, that ..... (Erklärung)

Figure 8.1(c) respectively 8.1(d) show the results for the SO<sub>2</sub> retrieval:

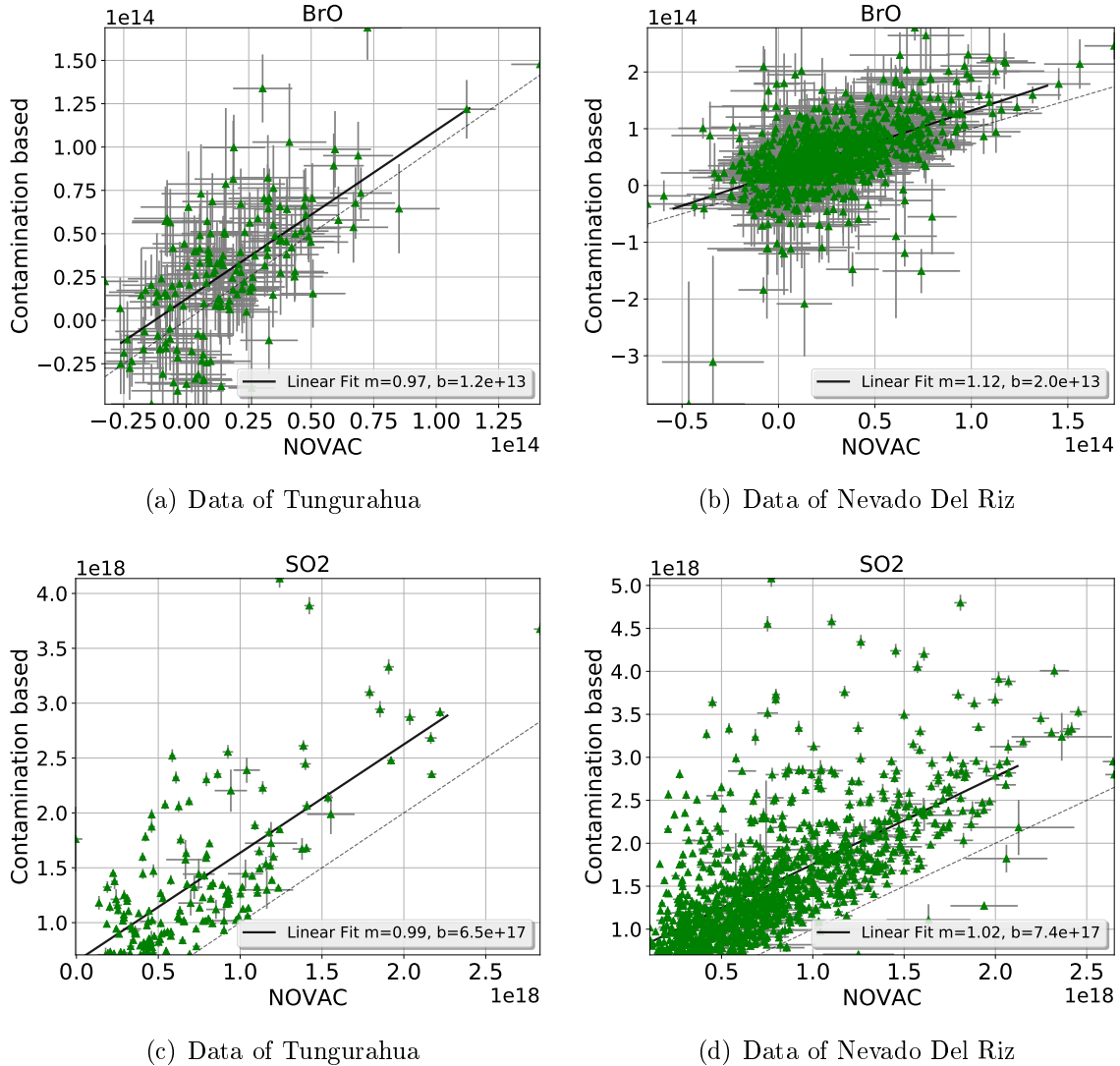


Figure 8.1: Comparison of the results of contaminated data for performing the evaluation with the NOVAC-method and the contamination based method. Only data are used where the corresponding SO<sub>2</sub> column density (retrieved from the contamination based method) lies above the plume limit of  $SO_2\_SCD > 7 \cdot 10^{17}$ . The black solid line shows a linear fit of the data, the dotted line indicates where the both evaluation are equivalent. (a) Results for the BrO column densities from Tungurahua; (b) Results for the BrO column densities from Nevado Del Ruiz; (c) Results for the SO<sub>2</sub> column densities from Tungurahua; (d) Results for the SO<sub>2</sub> column densities from Nevado Del Ruiz

- The SO<sub>2</sub> column densities retrieved due to the contamination based method have become larger for almost every measurement compared to the NOVAC

method.

- An almost constant offset of  $6.5 \cdot 10^{17}$  (Tungurahua) and  $7.4 \cdot 10^{17}$  (Nevado Del Ruiz) can be seen.

Figure 8.2 shows the difference of the ratio when performing the evaluation with the NOVAC method or the contamination based method. The results for Tungurahua are visualized at the left side (Figure 8.2(a), 8.2(c)) and the results for Nevado Del Ruiz are shown at the right side (Figure 8.2(b), 8.2(d)). Figure 8.2(a) and 8.2(b) show the results of the contamination based method plotted against the results of the NOVAC method. Figure 8.2(c) and 8.2(d) show the actual difference between both methods. The column density calculated with NOVAC was subtracted from the corresponding column density retrieved with the contamination based method. The black valid line indicates a linear fit of the data, the dotted grey line shows where the difference is zero, that means both evaluations lead to the same ratio.

- For low BrO/SO<sub>2</sub> ratios approximately below zero, the ratios calculated with the contamination based method are higher than the ratios retrieved with the NOVAC method. For higher BrO/SO<sub>2</sub> ratios (approximately above zero) the ratios calculated with the NOVAC method are larger.
- The absolute difference between both evaluation methods increases with the increase of the absolute ratio

Due to the increase of the SO<sub>2</sub> column density when performing the evaluation with the contamination based method more SO<sub>2</sub> SCD lie above the plume limit of  $7 \cdot 10^{17} \frac{\text{molec}}{\text{cm}^2}$ . This leads to an increase of the amount of reliable data.

In the following we will discuss the results for the Tungurahua volcano and the Nevado Del Ruiz.

## 8.1 Tungurahua

In total in the timespan from June 2008 to August 2009, 6500 multi add spectra were recorded. When performing the evaluation using the NOVAC-Method 6.7 percent of the SO<sub>2</sub> column densities are in the plume limit. Thus 6.7 percentage of the data can be used for the examination of the volcanic gas emissions in this timespan. 6.0 percentage of all spectra are found as contaminated. If the contaminated spectra would be excluded, only 5.5 percent of the SO<sub>2</sub> column densities are above the plume limit (see Table 8.2).

A higher amount of spectra within the SO<sub>2</sub> limits can be found in the contaminated data. Here the percentage of data in the plume-limit is: 19.2 . Therefore the contaminated data are 2.86 times more frequently above the detection limit. This lead to the presumption, that the possibility of getting contaminated data increases with the gas amount leaving the volcano.

When performing the evaluating of the contaminated data with the contamination based method 41.9 percent of the resulting SO<sub>2</sub> column densities are in the plume limit. Thus the reliable amount of contaminated data increase by 118.7 percentage while the total amount of data increase by 45.2 percent.

Due to using trace gas free references instead of contaminated references about 45.2 percent more data are available.

Due to the very small amount of BrO column densities above the detection limit often the daily mean of the BrO/SO<sub>2</sub> ratios is used. Hereby at least tree to four "Multi Adds" per day in the plume limit need to be recorded. Thus performing the evaluation of contaminated data with the contamination based method leads to more data. Some days which had less than tree to four valid data points could then have four or more multi adds. 12.5 percent more daily mean data can be retrieved when using the contamination based method. The amount of daily means increases less than the total amount of data, this effect can be explained due to a higher occurrence of contamination if the SO<sub>2</sub> column densities are high, thus more data are retrieved for days with high SO<sub>2</sub> amount.

## 8.2 Nevado Del Ruiz

At Nevado Del Ruiz a larger time span where examined thus there is a higher amount of "Multi Add" Data of: 14005. Using the NOVAC-evaluation 12.8 percentage of the SO<sub>2</sub> data are above the detection limit and 9.9 percentage of all the data are contaminated (see Table 8.2). 77.9 percentage of the contaminated data have a SO<sub>2</sub> column density above  $7 \cdot 10^{17} \frac{\text{molec}}{\text{cm}^2}$ . Thus we have as well a higher occurrence of the data above the plume limit within the contaminated data. The reliable amount of contaminated data increase by 95 percentage while the total amount of data increase by xy percent.

Due to using trace gas free references instead of contaminated references about 87.6 percent more data are available.

In total we get 22.6 percent more daily means in the TimeSpan at Nevado Del Ruiz.

## 8.3 BrO/SO<sub>2</sub> time series

The final time series of BrO/SO<sub>2</sub> for Tungurahua and Nevado Del Ruiz are shown Figure 8.5 (Nevado Del Ruiz) and Figure 8.4 (Tungurahua). Interpretation of the BrO/SO<sub>2</sub> ratio time-series

	Tungurahua	Nevado Del Ruiz		
Total Amount of Data	6500	14005		
Total amount of Data above Plume Limit	6.7%	12.8%		
Contaminated Data	0.060	0.099		
Contaminated data		Not contaminated data		
Within Plume-limit	Tungu rahua NOVAC Cont based	Nevado Del Ruiz 0.399 0.779	Tungu rahua Within Plume-limit	Nevado Del Ruiz 0.055 0.088
not analysable	0.025	0.078		

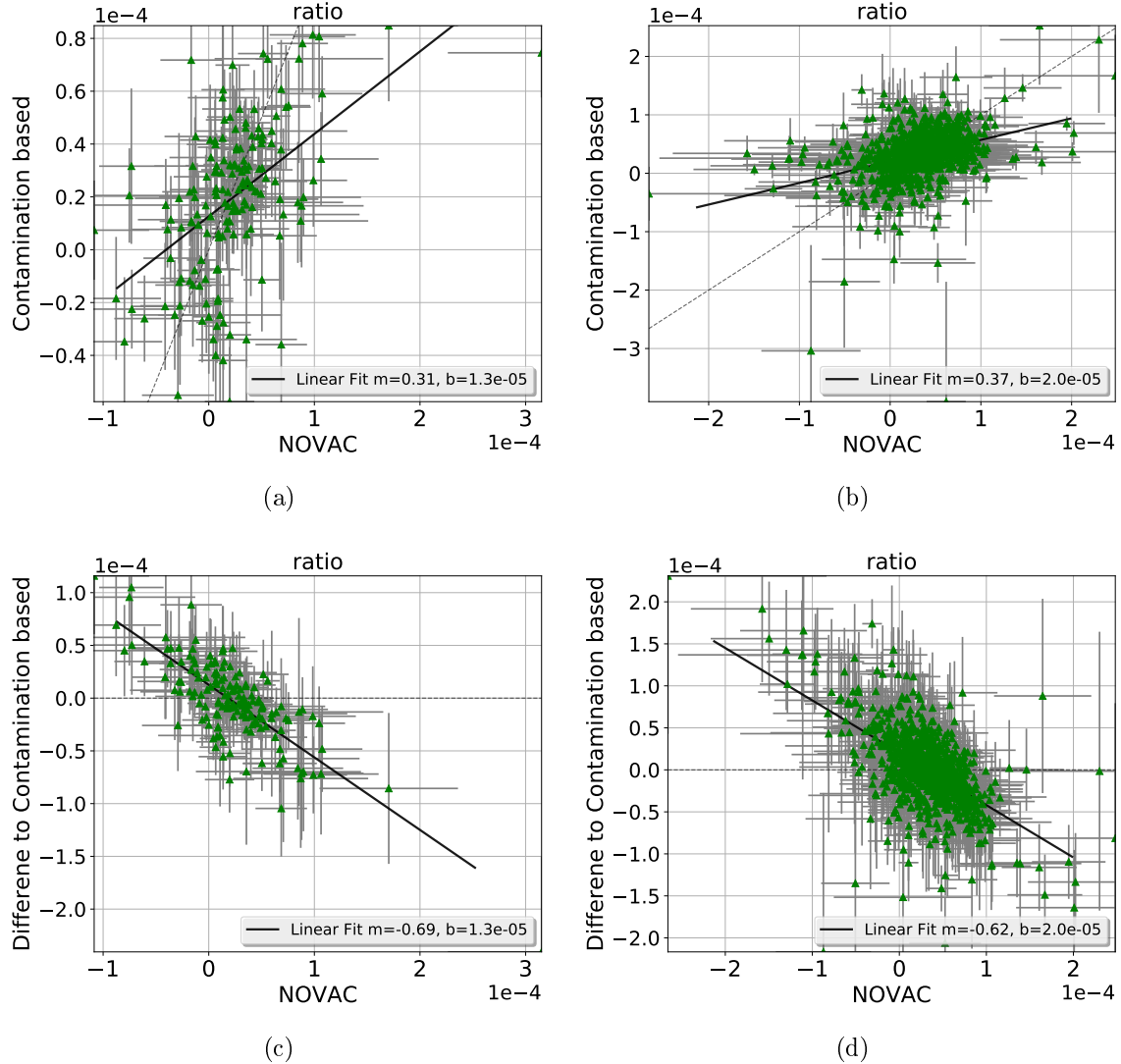


Figure 8.2: Comparison of the results of contaminated data for performing the evaluation with the NOVAC-method and the contamination based method. Only data are used where the corresponding SO<sub>2</sub> column density (retrieved from the contamination based method) lies above the plume limit of  $SO_2\_SCD > 7 \cdot 10^{17}$ . (a)+(b): The black solid line shows a linear fit of the data, the dotted line indicates where the both evaluation are equivalent. (a) Results for the BrO /SO<sub>2</sub> column densities from Tungurahua; (b) Results for the BrO /SO<sub>2</sub> column densities from Nevado Del Ruiz. (c) +(d) The column density calculated with NOVAC was subtracted from the corresponding column density retrieved with the contamination based method. The black valid line indicates a linear fit of the data, the dotted grey line shows where the difference is zero, that means both evaluations lead to the same ratio. (c) Tungurahua (d) Nevado Del Ruiz

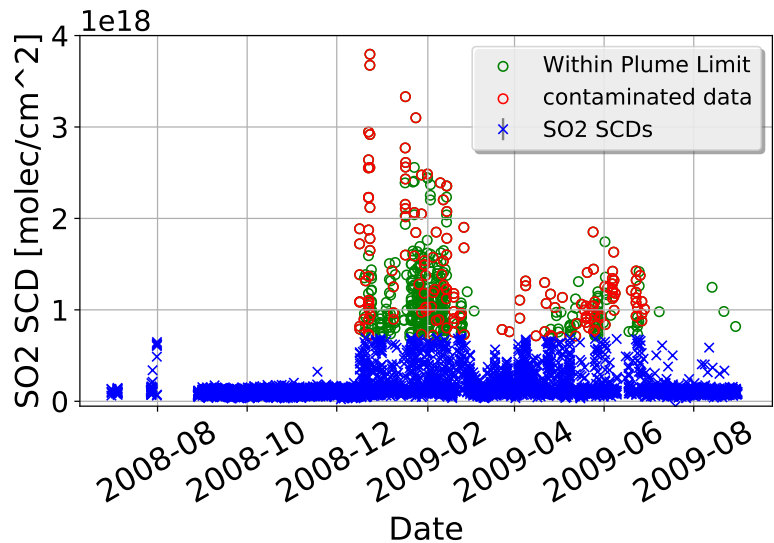


Figure 8.3: Time series of  $\text{SO}_2$  column densities at Tungurahua. Blue data points are below the detection limit, green data points are not contaminated, valid  $\text{SO}_2$  SCDs. Red data points are contaminated data, evaluated with the contamination based method.

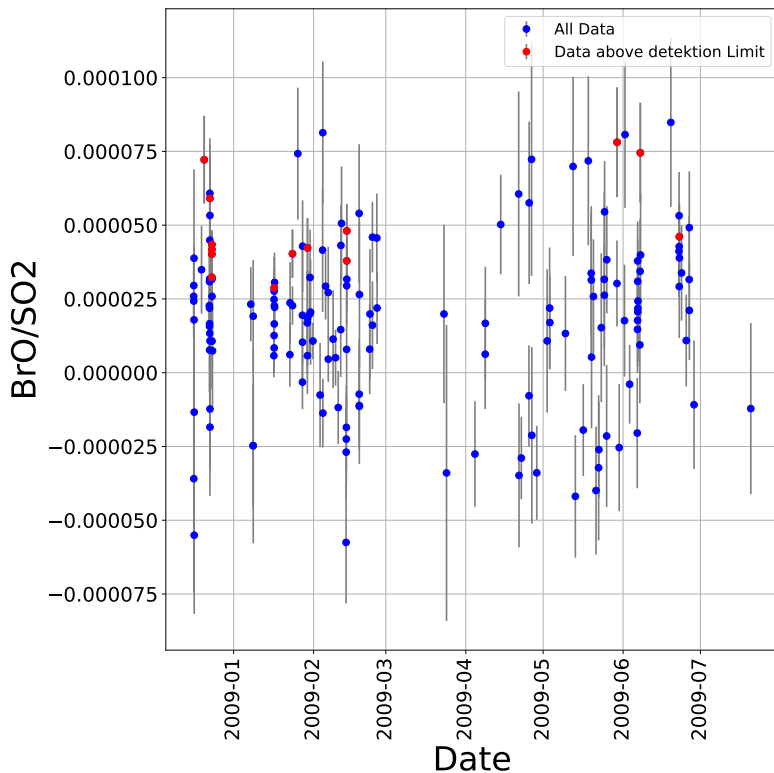


Figure 8.4:

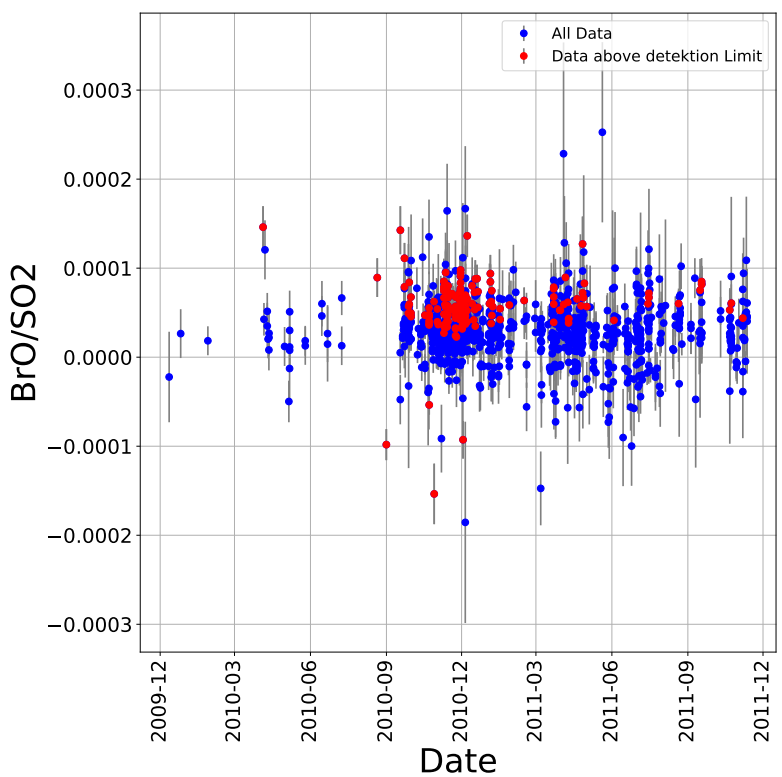


Figure 8.5:

## 9 Issues of our method

The presented method is questionable since we did not consider contamination of the plume due to a lack of information. And we did not consider the different lifetimes of SO<sub>2</sub> and BrO. This leads to a faster

### 9.1 Contamination of the plume

As discussed above it might occur, that, the plume is contaminated as well. This might be the case if the volcanic gas of the volcano is not taken away by the wind, but accumulates at the instrument. If this is the case, using an contamination free reference of another time would lead to an overestimation of the column density of gases.

The contamination of the plume is visualized in Figure 9.1. This is one possible occurrence of contamination. As it can be seen gas of the old plume affected the measurement of the reference and the plume. However for this example the influence on the measurement of the reference is much larger since the light path trough the old plume (coloured orange in Figure 9.1) is longer for the reference than for the measurement of the volcanic plume. Thus we underestimate the Gas amount if we do not use an gas free reference, but overestimate if we do so. The real gas amount might be between the measured amount with and without using a reference measured at another time.

The contamination set up could differ from Figure 9.1. This would lead to different results. However the reference region is in most of the time at a larger elevation angle than the plume, thus, the assumption that the light pass trough the old plume is on the average longer for the reference, of both reference and plume are contaminated.

With the data retrieved by the NOVAC instruments it is very difficult up to impossible to discover whether the plume is contaminated or not.

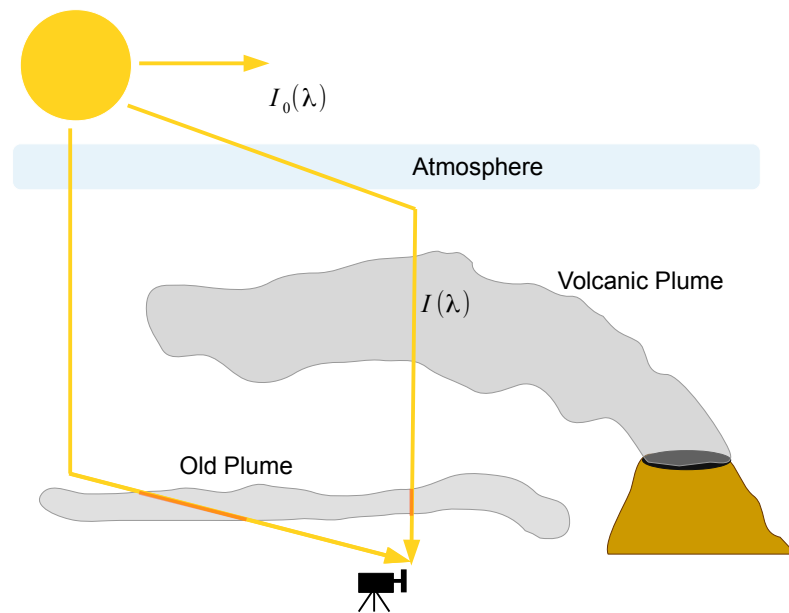


Figure 9.1: Visualization of the contamination of the plume. An old plume of the day before. Due to a lack of wind the plume sinks down and accumulates above the instrument. The light path through the old plume is longer when recording the reference spectra (orange).

## 10 Conclusion

In this thesis we made investigations on the contamination of the plume. We found a significant increase of the SCDs of SO<sub>2</sub> and BrO while the conatmination based evaluation leads to a higher increase of the SO<sub>2</sub> amount compared to the BrO evaluation. Thus the BrO/SO<sub>2</sub> ratio decreases for values above zero.

?? made investigations on the lifetime of SO<sub>2</sub> and BrO. The lifetime of SO<sub>2</sub> can reach to several weeks, while the decay of BrO proceed in faster times. As a result we should observe a lower contamination of BrO. This could be observed in our results. In theory it could be that due to the smaller lifetimes of BrO contamination only influences the SO<sub>2</sub> evaluation, if that is the case, the best option would be to use a high defined solar atlas spectrum as reference for the SO<sub>2</sub> evaluation, but an reference recorded with the same instrument at the same time for the BrO evaluation, since BrO could not be retrieved using an high defined

# Part III

## Appendix

## **Dependency external parameters on each other**

**Difference of Temperature on Difference of Exposure Time**

$$\Delta T = -26.32 \cdot \Delta ExpTime + 2 \cdot 10^{-15} \quad (.1)$$

**Difference of Temperature on Difference of colorindex**

$$\Delta T = 0.0022 \cdot \Delta ColIdx + 2 \cdot 10^{-19} \quad (.2)$$

**Difference of Temperature on Difference of Day time**

$$\Delta T = 0.262 \cdot \Delta daytime - 4 \cdot 10^{-17} \quad (.3)$$

**Difference of Temperature on Difference of Elevation angle**

$$\Delta T = 1.08 \cdot \Delta ElevAngle - 1 \cdot 10^{-16} \quad (.4)$$

**Difference of Exposure on Difference of Col Idx**

$$\Delta Exposure = -6.22 \cdot 10^{-5} \Delta ColIdx + 1 \cdot 10^{-18} \quad (.5)$$

**Difference of Exposure on Difference of Day time**

$$\Delta Exposure = -0.004 \cdot \Delta daytime - 1 \cdot 10^{-17} \quad (.6)$$

**Difference of Exposure on Difference ofElevation angle**

$$\Delta Exposure = -0.047 \cdot \Delta ElevAngle + 3 \cdot 10^{-16} \quad (.7)$$

**Difference of Colorindex on Difference of Day time**

$$\Delta ColIdx = 4.51 \cdot \Delta daytime - 1.2 \cdot 10^{-15} \quad (.8)$$

**Difference of Colorindex on Difference of Elevation angle**

$$\Delta ColIdx = -52 \cdot \Delta ElevAngle + 1.45 \cdot 10^{-14} \quad (.9)$$

**Difference of Colorindex on Difference of Elevation angle**

$$\Delta ColIdx = 3.5 \cdot \Delta ElevAngle - 6 \cdot 10^{-16} \quad (.10)$$

## **Figures to more plumes to one ref**

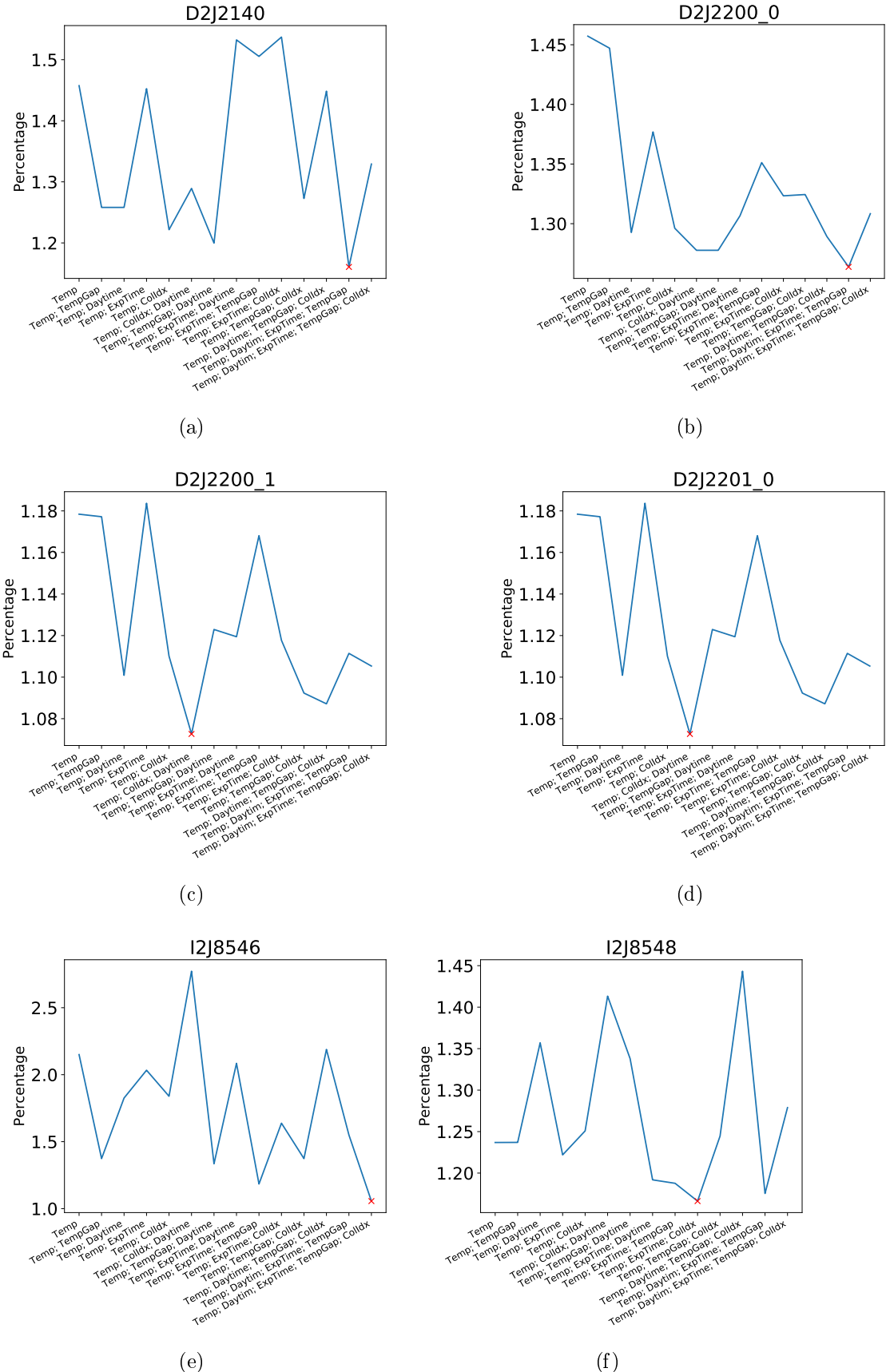


Figure .1:

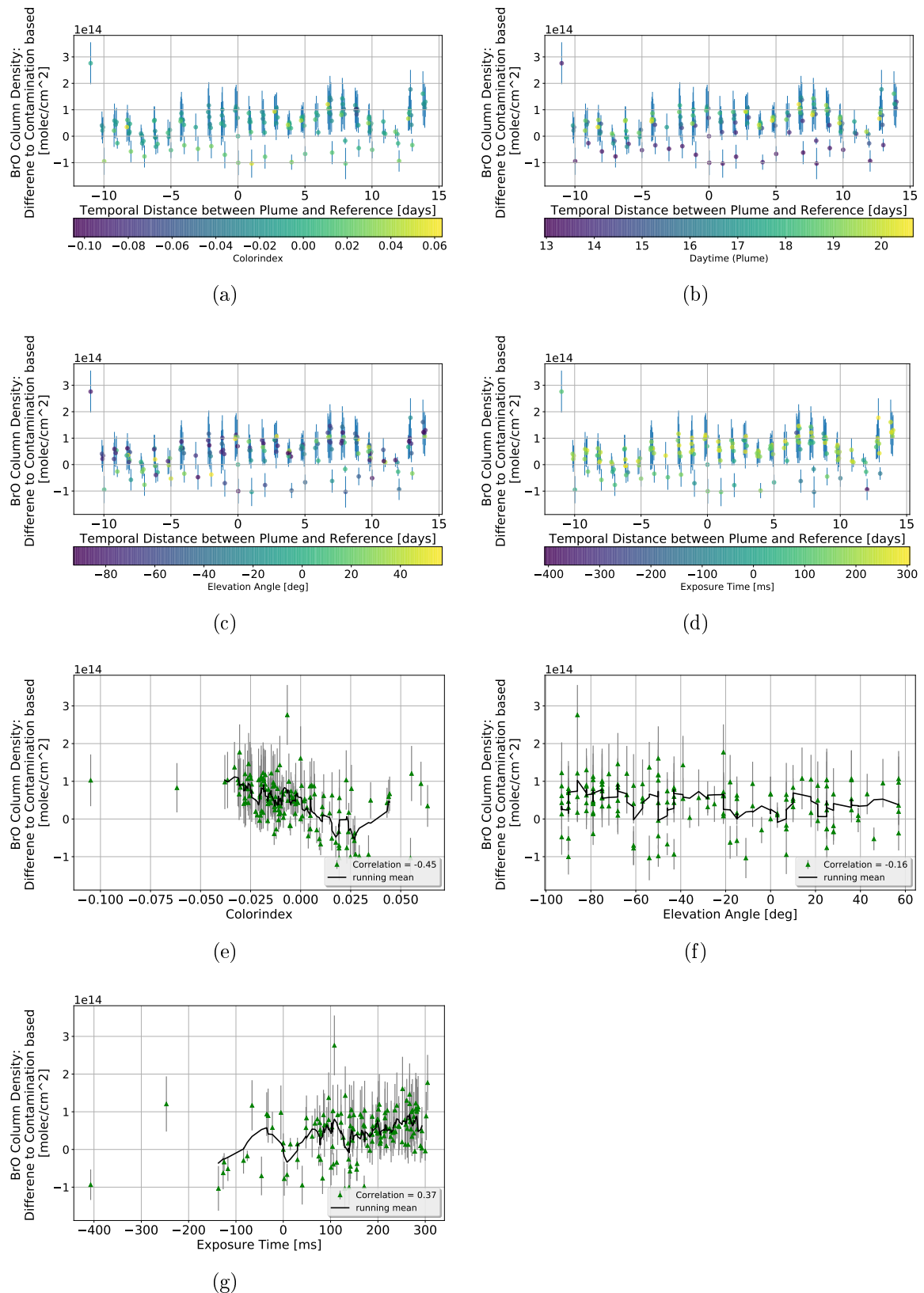


Figure .2:

# A Lists

## A.1 List of Figures

2.1	Influence of volcanic eruptions and quiet degassing on earth climate. Redrawn on the basis of Robock (2000) . . . . .	11
2.2	schematic sketch of a Bromine Explosion. Release of HBr at the volcanic vent. Mixing with ambient air in the effective source region leads to Br formation. This resulting Bromine species react to BrO with ozone from the plume. Adapted from Bobrowski et al. (2007) . . .	14
2.3	BrO/So <sub>2</sub> ratio as a function of the distance from the volcanic vent with a constant wind speed of 10 m/s. From Lübcke (2014) . . . . .	15
2.4	Bromine reactions inside of a volcanic vent. The release of Hbr at the volcaninc vent is drawn in orange. Inside of aerosols heterogeneous dissociation with HOBr forms Br <sub>2</sub> . Then Br <sub>2</sub> splits photolytically into single Br radicals. BrO results through a reaction with O <sub>3</sub> upon mixing with ambient air. Reactions with H <sub>2</sub> O forms HOBr creating an autocatalytic cycle. The reaction cycle along the blue lines are called Bromine explosion. From Warnach (2015) . . . . .	16
2.5	Dependency of the ratios of different volcanic trace gases on depth. Data originate from Stromboli volcano. From Lübcke (2014) repro- duced from Burton et al. (2007) . . . . .	17
3.1	. . . . .	21
3.2	Basic idea of the DOAS principle: Light attenuate due to broad band and narrow band effects. The broad band extinction is caused by aerosols and Raylight scattering ( $I_0 \rightarrow I'$ ). The measured intensity $I$ is formed by narrow band effects due to differential absorption struc- tures by trace gases with the optical density $\tau'$ . Adapted from Kern (2009) . . . . .	22
4.1	Global map of the volcanoes monitored by NOVAC. Used with friendly permission of Santiago Arellano. . . . .	27
4.2	schematic sketch of a NOVAC instrument. From Galle et al. (2010) .	28
4.3	Topographig Map of the Tungurahua Volcano. The predominant plume direction is shaded in yellow. Four NOVAC stations are shown as red squares, the corresponding scanning geometry is sketched with black lines. From Hidalgo et al. (2015). . . . .	29

5.1	(a) SO <sub>2</sub> SCD as a function of the elevation angle with error bars computed by the DOASIS fitting routin. (b) BrO SCD as a function of the elevation angle with error bars computed by the DOASIS fitting routine. Taken from Warnach (2015)	32
5.2	NOVAC Evaluation: (a) Measurement at the volcano (b) Evaluation of the spectral data with the DOAS routine using the absorption cross sections of BrO and SO <sub>2</sub> . (c) Finding the location of the plume and reference (d) (taken from Warnach (2015)) Computation of the ratios BrO/SO <sub>2</sub> at Tungurahua.	33
5.3	(a) SO <sub>2</sub> SCD as a function of the elevation angle. The co-added plume region is marked with red diamonds, and the co added reference region with green stars. From Warnach (2015). (b) Flow chart of the BrO and SO <sub>2</sub> evaluation. From Lübecke (2014).	34
5.4	The decrease of the amount of data above the plume limit as a function of the plume limit. The plume limits below the actual plume limit of $7 \cdot 10^{17}$ are marked with a yellow shade.	35
5.5	Scan with a contaminated reference spectrum from April 2011. From Warnach (2015)	36
5.6	The strength of contamination as function of the mean SO <sub>2</sub> amount of the day before. The strength of contamination is defined as the difference in SO <sub>2</sub> SCD when evaluation with an alternative reference, or neglect the contamination. Left: data from Tungurahua. Right: data from Nevado Del Ruiz.	38
6.1	Wavelength shift over the time. The shift is shown for six NOVAC-instruments from Tungurahua. The red and yellow dots show the running mean about 20 days. Red line indicates a temperature independent long term polynomial. From Warnach (2015)	41
6.2	The BrO error as a function of the temporal difference shown for the Pillate instrument from Tungurahua (2008-2009). (a) Temporal differences up to 400 days are shown. (b) Temporal differences below 120h; periodical BrO error evolution indicates the impact of the daytime	42
6.3	Histogram showing the frequency of getting the best reference as function of the temporal difference between plume and reference measuring.	43
6.4	Short Term wavelength as a function of the instrument temperature for Pillate 1. (a) initial period prior to January 2010 (b) after 2010. From Warnach (2015)	44
6.5	The BrO measurement error as a function of the difference of temperature between measuring the reference and the plume are shown. (a)-(c) show the data for the instruments at Tungurahua, (d)+(e) at Nevado Del Ruiz. To evaluate the plume spectra all reference spectra with a temporal distance of no longer than two weeks are used. A increase of the BrO error with the distance in temperature is observable.	45

6.6	The BrO measurement error as a function of the difference of the day time between measuring the reference and the plume are shown. To evaluate the plume spectra all reference spectra with a temporal distance of no longer than two weeks are used. An increase of the BrO error with the distance in day time is observable. . . . .	48
6.7	The BrO measurement error as a function of the difference of colorindex between measuring the reference and the plume are shown. To evaluate the plume spectra all reference spectra with a temporal distance of no longer than two weeks are used. A increase of the BrO error with the distance in colorindex is observably. . . . .	49
6.8	The BrO measurement error as a function of the Elevation Angle. To evaluate the plume spectra all reference spectra with a temporal distance of no longer than two weeks are used. We can't see any significant correlation. . . . .	52
6.9	Left: constant daytime,right: constant temperature . . . . .	53
6.10	The BrO measurement error as a function of the difference of exposure time between measuring the reference and the plume are shown. To evaluate the plume spectra all reference spectra with a temporal distance of no longer than two weeks are used. A increase of the BrO error with the distance in exposure time is observably. . . . .	54
6.11	A example of the dependency of external parameters on each other. The difference in Temperature as a function of the Exposure Time. Data from Tungurahua . . . . .	57
6.12	Correlation matrix of the external parameters. The correlation is discrete colour coded. Positive correlation is labeled with a plus whereas negative correlation is labeled with a minus. . . . .	58
6.13	DiffExpTime at Tungurahua . . . . .	60
6.14	BrO error as a function of the external while measering the Plume and the Reference at Nevado del ruiz . . . . .	61
6.15	One Plume is evaluated by using different references. The plume was recorded at Tungurahua volcano with the D2J2140_0 instrument. recording time was the 081203 at 1646 o clock. The y axis show the BrO column density differene between the NOVAC method and contamination based Method. (a) The difference in BrO is plotted as a function of the temperature difference between the plume and the references. Every data point indicates one reference. (b) The difference in BrO is plotted as a function of the temporal difference between the one plume and the different references . . . . .	62

6.16 One Reference is used to evaluated different Plume spectra. The reference was recorded at Tungurahua volcano with the D2J2140_0 instrument. recording time was the 081115 at 1337 o clock. The y axis show the BrO column density. (a) The BrO is plotted as a function of the temporal difference between the one reference and the plumes (b) The BrO is plotted as a function of the temperature difference between the plume and the references. Every data point stands for another plume evaluated with the same reference. . . . .	63
6.17 The difference of BrO when performing the evaluation with The NO-VAC Method minus the contamination based method as a function of the Daytime when measuring the plume. The recording time of the reference was 081115 at 1337 o clock . . . . .	63
6.18 The Dependence of the BrO evaluation on external parameter is shown. . . . .	64
7.1 Visualization of the contamination based Method. If the reference is contaminated a list of possible references is available, where the temporal difference between the plume and the reference is not longer than two weeks. For every possible reference, the estimated BrO error is calculated by considering the corresponding difference in important external parameters. The reference with the so calculated minima BrO error is used for the evaluation. . . . .	66
7.2 Deviation from the "optimal evaluation" as a function of the selection of differences in external parameters which are used for the evaluation	68
8.1 Comparison of the results of contaminated data for performing the evaluation with the NOVAC-method and the contamination based method. Only data are used where the corresponding SO <sub>2</sub> column density (retrieved from the contamination based method) lies above the plume limit of $SO2\_SCD > 7 \cdot 10^{17}$ . The black solid line shows a linear fit of the data, the dotted line indicates where the both evaluation are equivalent. (a) Results for the BrO column densities from Tungurahua; (b) Results for the BrO column densities from Nevado Del Ruiz; (c) Results for the SO <sub>2</sub> column densities from Tungurahua; (d) Results for the SO <sub>2</sub> column densities from Nevado Del Ruiz . . .	73

8.2 Comparison of the results of contaminated data for performing the evaluation with the NOVAC-method and the contamination based method. Only data are used where the corresponding SO <sub>2</sub> column density (retrieved from the contamination based method) lies above the plume limit of $SO_2\_SCD > 7 \cdot 10^{17}$ . (a)+(b): The black solid line shows a linear fit of the data, the dotted line indicates where the both evaluation are equivalent. (a) Results for the BrO /SO <sub>2</sub> column densities from Tungurahua; (b) Results for the BrO /SO <sub>2</sub> column densities from Nevado Del Ruiz. (c) +(d) The column density calculated with NOVAC was subtracted from the corresponding column density retrieved with the contamination based method. The black valid line indicates a linear fit of the data, the dotted grey line shows where the difference is zero, that means both evaluations lead to the same ratio. (c) Tungurahua (d) Nevado Del Ruiz . . . . .	77
8.3 Time series of SO <sub>2</sub> column densities at Tungurahua. Blue data points are below the detection limit, green data points are not contaminated, valid SO <sub>2</sub> SCDs. Red data points are contaminated data, evaluated with the contamination based method. . . . .	78
8.4 . . . . .	78
8.5 . . . . .	79
9.1 Visualization of the contamination of the plume. An old plume of the day before. Due to a lack of wind the plume sinks down and accumulates above the instrument. The light path through the old plume is longer when recording the reference spectra (orange). . . . .	81
.1 . . . . .	85
.2 . . . . .	86

## A.2 List of Tables

2.1 Volcanic gas constituents at the emission vent and global estimated source strength. Adapted from <a href="#">Textor et al. (2004)</a> . . . . .	12
6.1 Amount of possible references while restricting the time span between plume and reference to two weeks. . . . .	44
6.2 Remaining amount of References if only time difference below $3.358^{\circ}C$ are accepted. The percentages values refer to the decrease of the data relative to Table 6.1 . . . . .	46
6.3 Results of fitting the dependence of the BrO error on the absolute difference in daytime with in one dimensional polynomial. $\Delta DT_2$ is the daytime difference for which the error doubles compared to a same-time-reference. The results differ for every considered instrument. 47	

6.4	Remaining amount of References if the maximal accepted daytime difference is 4.75h. The percentages values refer to the decrease of the data relative to Table 6.1. 4.75h is the mean of the $\Delta DT_2$ s in section 6.1.3 without I2J8546_0 due to the large uncertainty at I2J8546_0	48
6.5	Amount of Possible references while restricting the difference in colorindex between plume and reference to differences above 0.2553. . . . .	51
6.6	Amount of Possible references while restricting the difference in colorindex between plume and reference to differences above 0.2553. maximal Time difference is $3.358^{\circ}C$ ,maximal daytime diff is 4.75h without . . . . .	51
6.7	Amount of Possible references while restricting the difference in Exposure Time between plume and reference to differences below 632.25ms . . . . .	56
6.8	Amount of Possible references while restricting the difference in colorindex between plume and reference to differences above 0.2553. maximal Time difference is $3.358^{\circ}C$ ,maximal daytime diff is 4.75h without Exposure Time between plume and reference to differences below 632.25ms . . . . .	56
7.1	(a)Data from Nevado Del Ruiz from the D2J2201_0 instrument. All external parameter where taken into account. $\epsilon_0 == 5.404e + 12$ (b)Data from Nevado Del Ruiz from the D2J2200_0 instrument. All external parameter where taken into account. $\epsilon_0 == 1.105e + 13$ (c) Data from Nevado Del Ruiz from both instrument. All external parameter where taken into account. $\epsilon_0 = 1.260e + 13$ . . . . .	70
7.2	(a)Data from Tungurahua from the instrument. All external parameter where taken into account. $\epsilon_0 == 5.404e + 12$ (b)Data from Tungurahua from the instrument. All external parameter where taken into account. $\epsilon_0 == 1.105e + 13$ (c) Data from Tungurahua from all instrument. All external parameter where taken into account. $\epsilon_0 = 1.260e + 13$ , both instruments Tungurahua zero point = $1.610e+13$	71

## B Bibliography

Smithsonian Institution global volcanism program. <https://volcano.si.edu/>. Accessed: 2018-03-20.

NOVAC novac-site. <http://www.novac-project.eu/>. Accessed: 2018-01-29.

Python scikit-learn.org. [http://scikit-learn.org/stable/modules/generated/sklearn.linear\\_model.LinearRegression.html](http://scikit-learn.org/stable/modules/generated/sklearn.linear_model.LinearRegression.html). Accessed: 2018-01-19.

N Bobrowski and G Giuffrida. Bromine monoxide/sulphur dioxide ratios in relation to volcanological observations at mt. *Etna*, 2009:433–445, 2006.

N Bobrowski and U Platt. So<sub>2</sub>/bro ratios studied in five volcanic plumes. *Journal of Volcanology and Geothermal Research*, 166(3-4):147–160, 2007.

N Bobrowski, G Hönninger, B Galle, and U Platt. Detection of bromine monoxide in a volcanic plume. *Nature*, 423(6937):273, 2003.

Nicole Bobrowski, R Von Glasow, A Aiuppa, S Inguaggiato, I Louban, OW Ibrahim, and U Platt. Reactive halogen chemistry in volcanic plumes. *Journal of Geophysical Research: Atmospheres*, 112(D6), 2007.

JP Burrows, A Richter, A Dehn, B Deters, S Himmelmann, S Voigt, and J Orphal. Atmospheric remote-sensing reference data from gome—2. temperature-dependent absorption cross sections of o<sub>3</sub> in the 231–794 nm range. *Journal of quantitative spectroscopy and radiative transfer*, 61(4):509–517, 1999.

Mike Burton, Patrick Allard, Filippo Muré, and Alessandro La Spina. Magmatic gas composition reveals the source depth of slug-driven strombolian explosive activity. *Science*, 317(5835):227–230, 2007.

Markus Bussemer. Der ring-effekt: Ursachen und einfluß auf die spektroskopische messung stratosphärischer spurenstoffe. *Diplomathesis, University of Heidelberg*, 1993.

K Chance and RL Kurucz. An improved high-resolution solar reference spectrum for earth's atmosphere measurements in the ultraviolet, visible, and near infrared. *Journal of quantitative spectroscopy and radiative transfer*, 111(9):1289–1295, 2010.

Oliver C Fleischmann, Matthias Hartmann, John P Burrows, and Johannes Orphal. New ultraviolet absorption cross-sections of bro at atmospheric temperatures measured by time-windowing fourier transform spectroscopy. *Journal of Photochemistry and Photobiology A: Chemistry*, 168(1-2):117–132, 2004.

Bo Galle, Mattias Johansson, Claudia Rivera, Yan Zhang, Manne Kihlman, Christoph Kern, Thomas Lehmann, Ulrich Platt, Santiago Arellano, and Silvana Hidalgo. Network for observation of volcanic and atmospheric change (novac)—a global network for volcanic gas monitoring: Network layout and instrument description. *Journal of Geophysical Research: Atmospheres*, 115(D5), 2010.

TM Gerlach. Volcanic sources of tropospheric ozone-depleting trace gases. *Geochemistry, Geophysics, Geosystems*, 5(9), 2004.

Hans-F Graf, Johann Feichter, and Bärbel Langmann. Volcanic sulfur emissions: Estimates of source strength and its contribution to the global sulfate distribution. *Journal of Geophysical Research: Atmospheres*, 102(D9):10727–10738, 1997.

Minard L Hall, Claude Robin, Bernardo Beate, Patricia Mothes, and Michel Monzier. Tungurahua volcano, ecuador: structure, eruptive history and hazards. *Journal of Volcanology and Geothermal Research*, 91(1):1–21, 1999.

Martina M Halmer, H-U Schmincke, and H-F Graf. The annual volcanic gas input into the atmosphere, in particular into the stratosphere: a global data set for the past 100 years. *Journal of Volcanology and Geothermal Research*, 115(3-4): 511–528, 2002.

C Hermans, AC Vandaele, S Fally, M Carleer, R Colin, B Coquart, A Jenouvrier, and M-F Merienne. Absorption cross-section of the collision-induced bands of oxygen from the uv to the nir. In *Weakly interacting molecular pairs: unconventional absorbers of radiation in the atmosphere*, pages 193–202. Springer, 2003.

Silvana Hidalgo, Jean Battaglia, Santiago Arellano, Alexander Steele, Benjamin Bernard, Julie Bourquin, Bo Galle, Santiago Arrais, and Freddy Váscone. So<sub>2</sub> degassing at tungurahua volcano (ecuador) between 2007 and 2013: Transition from continuous to episodic activity. *Journal of Volcanology and Geothermal Research*, 298:1–14, 2015.

IPCC. *Summary for Policymakers*, book section SPM, page 1–30. Cambridge University Press, Cambridge, United Kingdom and New York, NY, USA, 2013. ISBN ISBN 978-1-107-66182-0. doi: 10.1017/CBO9781107415324.004. URL [www.climatechange2013.org](http://www.climatechange2013.org).

Christoph Kern. *Spectroscopic measurements of volcanic gas emissions in the ultraviolet wavelength region*. PhD thesis, 2009.

Stefan Kraus. *DOASIS: A framework design for DOAS*. Shaker, 2006.

Peter Lübcke. *Optical remote sensing measurements of bromine and sulphur emissions: Investigating their potential as tracers of volcanic activity.* PhD thesis, 2014.

Peter Lübcke, Nicole Bobrowski, S Arellano, Bo Galle, G Garzón, Leif Vogel, and U Platt. Bro/so 2 molar ratios from scanning doas measurements in the novac network. *Solid Earth*, 5(1):409, 2014.

Richard Meller and Geert K Moortgat. Temperature dependence of the absorption cross sections of formaldehyde between 223 and 323 k in the wavelength range 225–375 nm. *Journal of Geophysical Research: Atmospheres*, 105(D6):7089–7101, 2000.

Kimio Noguchi and Hiroshi Kamiya. Prediction of volcanic eruption by measuring the chemical composition and amounts of gases. *Bulletin Volcanologique*, 26(1): 367–378, 1963.

Maddalena Pennisi and Marie-Françoise Le Cloarec. Variations of cl, f, and s in mount etna’s plume, italy, between 1992 and 1995. *Journal of Geophysical Research: Solid Earth*, 103(B3):5061–5066, 1998.

D Perner and U Platt. Detection of nitrous acid in the atmosphere by differential optical absorption. *Geophysical Research Letters*, 6(12):917–920, 1979.

G Pinardi, MV Roozendael, and C Fayt. The influence of spectrometer temperature variability on the data retrieval of so2. *NOVAC second annual activity report, NOVAC consortium*, 44:48, 2007.

U Platt and N Bobrowski. Quantification of volcanic reactive halogen emissions. *Volcanism and Global Change*, eds A. Schmidt, K. Fristad, L. Elkins-Tanton, Cambridge University Press, Cambridge, UK, ISBN, 1466525386, 2015.

Ulrich Platt and Jochen Stutz. Differential absorption spectroscopy. *Differential Optical Absorption Spectroscopy*, pages 135–174, 2008.

Alan Robock. Volcanic eruptions and climate. *Reviews of Geophysics*, 38(2):191–219, 2000.

A Schmidt and A Robock. Volcanism, the atmosphere and climate through time. *Volcanism Glob. Environ. Chang*, pages 195–207, 2015.

Anja Schmidt, Kirsten Fristad, and Linda T Elkins-Tanton. Volcanism and global environmental change, 2015.

Hans-Ulrich Schmincke. *Vulkanismus*. Wissenschaftliche Buchgesellschaft, 3 edition, 2000.

S Solomon, RW Portmann, RR Garcia, W Randel, F Wu, R Nagatani, J Gleason, L Thomason, LR Poole, and MP McCormick. Ozone depletion at mid-latitudes: Coupling of volcanic aerosols and temperature variability to anthropogenic chlorine. *Geophysical research letters*, 25(11):1871–1874, 1998.

Susan Solomon, Arthur L Schmeltekopf, and Ryan W Sanders. On the interpretation of zenith sky absorption measurements. *Journal of Geophysical Research: Atmospheres*, 92(D7):8311–8319, 1987.

Christiane Textor, Hans-F Graf, Claudia Timmreck, and Alan Robock. Emissions from volcanoes. In *Emissions of Atmospheric Trace Compounds*, pages 269–303. Springer, 2004.

Thorvaldur Thordarson and Stephen Self. Atmospheric and environmental effects of the 1783–1784 laki eruption: A review and reassessment. *Journal of Geophysical Research: Atmospheres*, 108(D1), 2003.

S Twomey. Pollution and the planetary albedo. *Atmospheric Environment (1967)*, 8(12):1251–1256, 1974.

Ann Carine Vandaele, Christian Hermans, Paul C Simon, Michel Carleer, Réginald Colin, Sophie Fally, Marie-France Merienne, Alain Jenouvrier, and Bernard Coquart. Measurements of the no<sub>2</sub> absorption cross-section from 42 000 cm<sup>-1</sup> to 10 000 cm<sup>-1</sup> (238–1000 nm) at 220 k and 294 k. *Journal of Quantitative Spectroscopy and Radiative Transfer*, 59(3-5):171–184, 1998.

Ann Carine Vandaele, Christian Hermans, and Sophie Fally. Fourier transform measurements of so<sub>2</sub> absorption cross sections: II.: Temperature dependence in the 29 000–44 000 cm<sup>-1</sup> (227–345 nm) region. *Journal of Quantitative Spectroscopy and Radiative Transfer*, 110(18):2115–2126, 2009.

Leif Vogel. *Volcanic plumes: Evaluation of spectroscopic measurements, early detection, and bromine chemistry*. PhD thesis, 2011.

T Wagner, A Apituley, S Beirle, S Dörner, U Friess, J Remmers, and R Shaiganfar. Cloud detection and classification based on max-doas observations. *Atmospheric Measurement Techniques*, 7(5):1289–1320, 2014.

Simon Warnach. Improvements of bro and so<sub>2</sub> retrievals of novac data - tungurahua volcano as a case study. Master's thesis, 2015.

Erklärung:

Ich versichere, dass ich diese Arbeit selbstständig verfasst habe und keine anderen als die angegebenen Quellen und Hilfsmittel benutzt habe.

Heidelberg, den (Datum) .....